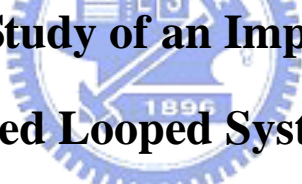


國立交通大學

機械工程學系

碩士論文

改善毛細泵吸迴路系統在電子冷卻上之實驗研究



**Experimental Study of an Improved Capillary  
Pumped Looped System for  
Electronics Cooling**

研究生：洪義祥

指導教授：林清發博士

中華民國九十五年六月

# 改善毛細泵吸迴路系統在電子冷卻上之實驗研究

Experimental Study of an Improved Capillary Pumped Looped System  
for Electronics Cooling

研究生：洪義祥

Student : Yi- Hsiang Hung

指導教授：林清發

Advisor : Tsing-Fa Lin

國立交通大學

機械工程學系

碩士論文

A Thesis

Submitted to Institute of Mechanical Engineering

College of Engineering

National Chiao Tung University

In Partial Fulfillment of the Requirements

For the degree of

Master of Science

In

Mechanical Engineering

June 2006

Hsinchu, Taiwan, Republic of China

中華民國九十五年六月

# 國立交通大學

## 論文口試委員會審定書

本校 機械工程 學系碩士班 洪義祥 :

所提論文(中文) 改善毛細泵吸迴路系統在電子冷卻上之實驗  
研究

(英文) Experimental Study of an Improved Capillary  
Pumped Looped System for Electronic Cooling

合於碩士資格水準、業經本委員會評審認可。

口試委員：

何清波

潘欽

洪義祥

指導教授：

林清俊

系主任：

傅武雄

教授

中華民國 95 年 6 月 9 日

## 誌 謝

時光飛逝，回首在新竹這幾年來的點點滴滴，與當年隻身到交大求學的我相比，在交大這充滿學術氣息的环境下似乎讓我在知識上成長茁壯許多。本論文之所以可以順利完成，首先要感謝的是指導老師 林清發 教授嚴謹及殷切的指導，使學生能培養出獨立思考、釐清並自行解決問題的能力；更在學生撰寫論文時，不辭辛勞逐字斧正文稿，在此獻上最高謝意。在研究所期間，要特別感謝工研院 劉家宏 博士和 張文瑞 學長在實驗設備設計、架設上的協助指導，亦要感謝博士班 郭威伸、賴佑民、陳尚緯、謝汎鈞 等博士班學長在生活及課業上指導與建議，使我受益匪淺，謝謝你們。

建安、君達、宇歆 這群不只是求學中的同學，更是生活上的好朋友。研究所之所以能在緊湊忙碌又充滿歡樂中的氣氛中度過，即是靠這些同學兼好友的夥伴們相互協助幫忙，令我永生難忘。另外也要感謝 峻樟、政陞、凱文、奎銘 等一群努力的學弟幫忙及合作，希望你們能繼續保持實驗室優良傳統，並帶著實驗室進步。

最後更要感謝我的奶奶默默的庇佑我，還有陪我二十幾年的父母及姊姊和弟弟對於我無怨無悔付出及支持，使我可以無後顧之憂的專注於研究，並且可無憂無慮過求學生活。並特別要感謝我大學老師 張財壽 的支持與指導，讓我順利的考上研究所，不管在課業上或生活上的關心與支持使我有勇氣面對一切的困難挑戰。

最後，僅以本文獻給我所關心的人和所有關心我的人。

今日我以交大為榮 願他日交大以我為榮

義祥 謹致

2006/6/30 于風城交大

# 改善毛細泵吸迴路系統在電子冷卻上之實驗研究

研究生：洪義祥

指導教授：林清發 博士

國立交通大學機械工程學系

## 摘要

本論文主要是改善毛細泵迴路系統在電子冷卻上之實驗研究，使用一溝槽外形的銅塊放置在蒸發器內部，其截面積尺寸為  $30\text{mm} \times 30\text{mm} \times 10\text{mm}$ ，並且此溝槽是由 5 個平行的矩形的通道構成用以提供蒸發器內的蒸氣流往蒸氣線，其每一個通道的尺寸為長  $30\text{mm}$  和寬為  $2.4\text{mm}$ 、高為  $3\text{mm}$ ，並且在溝槽的上方和一多孔性材質緊密接觸，其尺寸為  $30\text{mm} \times 30\text{mm} \times 3\text{mm}$  且平均孔隙半徑為  $21\mu\text{m}$ 。冷凝器是由水冷式的雙套管來達到冷卻的目地。另外，選用直徑為  $4.5\text{mm}$  光滑的鐵氟龍管來當作蒸氣線和液態線並且選用去離子水來當作實驗的工作流體，而在改善 CPL 系統的部份，我們將利用純棉的薄紗布去覆蓋在溝槽通道的側面和底面，用以增加蒸發器的蒸發面積。實驗的目的探討在不同輸入功率、冷凝器的冷卻溫度、工作流體的填充量、蒸發器和冷凝器之間的高度差及覆蓋在溝槽表面的紗布對熱傳性能的影響。在實驗參數的範圍上，加熱功率從 5 到 260 W、冷卻溫度從 20 到 40 度、流體填充量從 50 到 75% 及蒸發器和冷凝器的高度差從 0 到 10 公分，此實驗的操作中止是以蒸發器的平均溫度到達 80 度為限。

由實驗結果可以發現工作流體的填充量會影響到整個系統的熱傳能力，且在最高的散熱功率以及最低的熱阻值會發生在一最佳的填充量，而系統的熱傳能力僅稍微被冷卻水溫度所影響，並且蒸發器的操作溫度會隨著冷卻水溫度增加而提高。接著，當提高蒸發器和冷凝器的相對高度有助於改善 CPL 的熱傳能力。對於覆蓋一純棉的紗布在溝槽的側面和底面並且在可靠條件下也可以大大地改善熱傳的能力，但是在其它的條件下則影響不顯著。

最後，將提供有覆蓋紗布和沒覆蓋紗布之下的最大的散熱功率和最小的熱阻值的經驗公式以供設計 CPL 冷卻的設計者參考，而所有的實驗結果在本篇的論文中最高的散熱能力約為 255W。



# **Experimental Study of an Improved Capillary Pumped Looped System for Electronics Cooling**

**Student : Yi- Hsiang Hung**

**Advisor : Prof. Tsing-Fa Lin**

**Institute of Mechanical Engineering  
National Chiao Tung University**

## **ABSTRACT**

An experiment is carried out in the present study to investigate an improved design of a CPL (Capillary Pumped Loop) system for electronic cooling. The evaporator of the CPL system is modeled by a grooved square copper plate of size  $30\text{mm} \times 30\text{mm} \times 10\text{mm}$  glued onto another heated rectangular copper plate of the same size. The grooved copper plate contains five parallel rectangular open channels for the vapor generated in the evaporator to flow into a vapor transport line. Each channel is characterized by 30 mm in length, 2.4 mm in width, and 3 mm in height. A porous wick made from open-cell blowing foam of polyvinyl alcohol with a mean pore radius of  $21 \mu\text{m}$  and having a size of  $30 \times 30 \times 3 \text{mm}^3$  is placed on the grooved copper plate. The condenser is made of a double-pipe heat exchanger with liquid water flowing in the outer pipe. Besides, smooth teflon tubes of inside diameter 4.5 mm are chosen for the vapor and liquid transport lines. The deionized water is selected as the working fluid. Moreover, a thin cotton gauze layer of  $150 \mu\text{m}$  in thickness is covered on the side and bottom walls of the grooved channels to provide more surface area for liquid vaporization. Tests are conducted for the liquid inventory varied from 50% to 75%, cooling water temperature in the condenser from 20 to 40 , condenser-evaporator relative height from 0 to 10 cm. The test is terminated when the mean evaporator temperature exceeds 80 . In the study how the liquid

inventory, cooling water temperature in the condenser, relative height between the condenser and evaporator, and cotton gauze layer covering affect the CPL performance is investigated in detail.

The experimental results show that the liquid inventory significantly affects the heat transfer performance of the system. An optimal liquid inventory exists at which the maximum power input to the evaporator is the highest and the minimum thermal resistance of the CPL is the lowest. The CPL heat transfer capability is only slightly affected by the cooling water temperature in the condenser. But the evaporator temperature is noticeably higher for a higher cooling water temperature in the condenser. An increase in the relative height between the condenser and evaporator results in a significant improvement in the CPL performance. Besides, for a larger relative condenser-evaporator height the influences of the liquid inventory on the performance of the CPL are milder. Covering a thin cotton gauze layer on the side and bottom surfaces of the grooved channels can substantially improve the heat transfer performance of the CPL system under certain conditions. For other conditions the improvement is comparatively smaller.

Finally, empirical correlations for the  $Q_{e,max}$  and  $R_{th,min}$  are proposed for the CPL with and without cotton gauze covering for thermal design of CPU cooling. For all cases tested in the present CPL system the highest  $Q_{e,max}$  is 255W.



# TABLE OF CONTENTS

<b>ABSTRACT</b>	i
<b>TABLE OF CONTENTS</b>	iii
<b>LIST OF FIGURES</b>	v
<b>LIST OF TABLE</b>	xii
<b>NOMENCLATURE</b>	xiii
<b>CHAPTER 1 INTRODUCTION</b>	1
1.1 Motive	1
1.2 Literature Review	2
1.3 Objective	7
<b>CHAPTER 2 EXPERIMENTAL APPARATUS AND PROCEDURES</b>	14
2.1 CPL Loop	14
2.2 Fluid Inventory Unit	15
2.3 Cold-Water Loop	16
2.4 Measurement Unit	16
2.5 Equipment	17
2.6 Experimental Procedures	17
2.7 Experimental Parameters	18
<b>CHAPTER 3 DATA REDUCTION AND SIMPLE ANALYSIS</b>	31
3.1 Date Reduction	31
3.2 Thermodynamic States and Heat transfer Limitation	33
3.3 System Pressure Drop Analysis	35
3.3.1 Maximum capillary pressure	35
3.3.2 Pressure drop in transport lines	35
3.3.3 Pressure drop in grooved channels	36
3.3.4 Pressure drop in wick structure	36
3.3.5 Pressure drop due to gravity	37
3.4 Estimate of Mass Flow Rate	37
3.5 Uncertainty Analysis	38

<b>CHAPTER 4 RESULTS AND DISCUSSION</b>	44
4.1 Effects of Liquid Inventory	44
4.2 Effects of the Cooling Water Temperature in the Condenser	46
4.3 Effects of the Relative Height between the Evaporator and Condenser	47
4.4 Effects of Covering Cotton Gauze Layer on Grooved Channel Surfaces	48
4.5 Correlation Equations	50
<b>CHAPTER 5 CONCLUDING REMARKS</b>	105
<b>REFERENCES</b>	107



## LIST OF FIGURES

Fig 1.1	Schematic of a Capillary Pumped Loop -----	12
Fig 1.2	Schematic of a typical evaporator design-----	13
Fig 2.1	Schematic diagram of experimental apparatus -----	21
Fig 2.2	Three-dimensional plots illustrating the CPL test loop -----	22
Fig 2.3	The detailed of structure evaporator -----	23
Fig 2.4	A cutaway view of evaporator -----	24
Fig 2.5	Dimension of heater base-----	25
Fig 2.6	Photographs of the Polyvinyl Alcohol -----	26
Fig 2.7	Photographs of the pure cotton gauze-----	27
Fig 2.8	Schematic of enhance grooved of the evaporator design -----	28
Fig 2.9	Locations of the thermocouples and dimension of grooved copper block -----	29
Fig 2.10	Locations of the thermocouples of the outer wall of the adiabatic cotton -----	30
Fig 3.1	Schematics of a typical CPL system (a) and the corresponding P-T diagram at various locations (b)-----	43
Fig 4.1	Variations of the temperature at various locations in the CPL (a) and thermal resistance of the CPL (b) with the input power to the evaporator for the cooling water temperature in the condenser $T_{\text{cold}} = 25$ , liquid inventory of 50% and relative height between condenser and evaporator of 0 cm -----	59
Fig 4.2	Variations of the temperature at various locations in the CPL (a) and thermal resistance of the CPL (b) with the input power to the evaporator for the cooling water temperature in the condenser $T_{\text{cold}} = 25$ , liquid inventory of 57% and relative height between condenser and evaporator of 0 cm -----	60
Fig 4.3	Variations of the temperature at various locations in the CPL (a) and thermal resistance of the CPL (b) with the input power to the evaporator for the cooling water temperature in the condenser $T_{\text{cold}} = 25$ , liquid inventory of 62% and relative height between condenser and evaporator of	

0 cm ----- 61

Fig 4.4 Variations of the temperature at various locations in the CPL (a) and thermal resistance of the CPL (b) with the input power to the evaporator for the cooling water temperature in the condenser  $T_{\text{cold}} = 25$  , liquid inventory of 70% and relative height between condenser and evaporator of 0 cm ----- 62

Fig 4.5 Variations of the temperature at various locations in the CPL (a) and thermal resistance of the CPL (b) with the input power to the evaporator for the cooling water temperature in the condenser  $T_{\text{cold}} = 25$  , liquid inventory of 75% and relative height between condenser and evaporator of 0 cm ----- 63

Fig 4.6 Variations of the mean evaporator temperature (a) and thermal resistance of the CPL (b) with the input power to the evaporator for various liquid inventory for cooling water temperature in the condenser  $T_{\text{cold}} = 25$  and relative condenser-evaporator height of 0 cm----- 64

Fig 4.7 Variations of the temperature at various locations in the CPL (a) and thermal resistance of the CPL (b) with the input power to the evaporator for the cooling water temperature in the condenser  $T_{\text{cold}} = 20$  , liquid inventory of 62% and relative height between condenser and evaporator of 0 cm ----- 65

Fig 4.8 Variations of the temperature at various locations in the CPL (a) and thermal resistance of the CPL (b) with the input power to the evaporator for the cooling water temperature in the condenser  $T_{\text{cold}} = 25$  , liquid inventory of 62% and relative height between condenser and evaporator of 0 cm ----- 66

Fig 4.9 Variations of the temperature at various locations in the CPL (a) and thermal resistance of the CPL (b) with the input power to the evaporator for the cooling water temperature in the condenser  $T_{\text{cold}} = 30$  , liquid inventory of 62% and relative height between condenser and evaporator of 0 cm ----- 67

Fig 4.10 Variations of the temperature at various locations in the CPL (a) and

thermal resistance of the CPL (b) with the input power to the evaporator for the cooling water temperature in the condenser  $T_{\text{cold}} = 40$  , liquid inventory of 62% and relative height between condenser and evaporator of 0 cm ----- 68

Fig 4.11 Variations of the mean evaporator temperature (a) and thermal resistance of the CPL (b) with the input power to the evaporator for various cooling water temperatures in the condenser for the liquid inventory of 62% and relative condenser-evaporator height of 0 cm----- 69

Fig 4.12 Variations of the temperature at various locations in the CPL (a) and thermal resistance of the CPL (b) with the input power to the evaporator for various relative condenser-evaporator height for the cooling water temperature in the condenser  $T_{\text{cold}} = 25$  and liquid inventory of 50% ----- 70

Fig 4.13 Variations of the mean evaporator temperature (a) and thermal resistance of the CPL (b) with the input power to the evaporator for various relative condenser-evaporator heights for cooling water temperature in the condenser  $T_{\text{cold}} = 25$  and liquid inventory of 50% ----- 71

Fig 4.14 Variations of the temperature at various locations in the CPL (a) and thermal resistance of the CPL (b) with the input power to the evaporator for various relative condenser-evaporator height for the cooling water temperature in the condenser  $T_{\text{cold}} = 25$  and liquid inventory of 57% ----- 72

Fig 4.15 Variations of the mean evaporator temperature (a) and thermal resistance of the CPL (b) with the input power to the evaporator for various relative condenser-evaporator heights for cooling water temperature in the condenser  $T_{\text{cold}} = 25$  and liquid inventory of 57% ----- 73

Fig 4.16 Variations of the temperature at various locations in the CPL (a) and thermal resistance of the CPL (b) with the input power to the evaporator for various relative condenser-evaporator height for the cooling water temperature in the condenser  $T_{\text{cold}} = 25$  and liquid inventory of 62% ----- 74

Fig 4.17 Variations of the mean evaporator temperature (a) and thermal resistance of the CPL (b) with the input power to the evaporator for various relative condenser-evaporator heights for cooling water temperature in the

	condenser $T_{\text{cold}} = 25$ and liquid inventory of 62% -----	75
Fig 4.18	Variations of the temperature at various locations in the CPL (a) and thermal resistance of the CPL (b) with the input power to the evaporator for various relative condenser-evaporator height for the cooling water temperature in the condenser $T_{\text{cold}} = 25$ and liquid inventory of 70% -----	76
Fig 4.19	Variations of the mean evaporator temperature (a) and thermal resistance of the CPL (b) with the input power to the evaporator for various relative condenser-evaporator heights for cooling water temperature in the condenser $T_{\text{cold}} = 25$ and liquid inventory of 70% -----	77
Fig 4.20	Variations of the temperature at various locations in the CPL (a) and thermal resistance of the CPL (b) with the input power to the evaporator for various relative condenser-evaporator height for the cooling water temperature in the condenser $T_{\text{cold}} = 25$ and liquid inventory of 75% -----	78
Fig 4.21	Variations of the mean evaporator temperature (a) and thermal resistance of the CPL (b) with the input power to the evaporator for various relative condenser-evaporator heights for cooling water temperature in the condenser $T_{\text{cold}} = 25$ and liquid inventory of 75% -----	79
Fig 4.22	Variations of the mean evaporator temperature (a) and thermal resistance of the CPL (b) with the input power to the evaporator for various liquid inventories and relative condenser-evaporator heights for cooling water temperature in the condenser $T_{\text{cold}} = 25$ -----	80
Fig 4.23	Variations of the temperature at various locations in the CPL (a) and thermal resistance of the CPL (b) with the input power to the evaporator for various relative condenser-evaporator heights for the cooling water temperature in the condenser $T_{\text{cold}} = 20$ and liquid inventory of 62% -----	81
Fig 4.24	Variations of the mean evaporator temperature (a) and thermal resistance of the CPL (b) with the input power to the evaporator for various relative condenser-evaporator heights for cooling water temperature in the condenser $T_{\text{cold}} = 20$ and liquid inventory of 62% -----	82
Fig 4.25	Variations of the temperature at various locations in the CPL (a) and thermal resistance of the CPL (b) with the input power to the evaporator for	

various relative condenser-evaporator heights for the cooling water temperature in the condenser  $T_{\text{cold}} = 25$  and liquid inventory of 62% ----- 83

Fig 4.26 Variations of the mean evaporator temperature (a) and thermal resistance of the CPL (b) with the input power to the evaporator for various relative condenser-evaporator heights for cooling water temperature in the condenser  $T_{\text{cold}} = 25$  and liquid inventory of 62% ----- 84

Fig 4.27 Variations of the temperature at various locations in the CPL (a) and thermal resistance of the CPL (b) with the input power to the evaporator for various relative condenser-evaporator heights for the cooling water temperature in the condenser  $T_{\text{cold}} = 30$  and liquid inventory of 62% ----- 85

Fig 4.28 Variations of the mean evaporator temperature (a) and thermal resistance of the CPL (b) with the input power to the evaporator for various relative condenser-evaporator heights for cooling water temperature in the condenser  $T_{\text{cold}} = 30$  and liquid inventory of 62% ----- 86

Fig 4.29 Variations of the temperature at various locations in the CPL (a) and thermal resistance of the CPL (b) with the input power to the evaporator for various relative condenser-evaporator heights for the cooling water temperature in the condenser  $T_{\text{cold}} = 40$  and liquid inventory of 62% ----- 87

Fig 4.30 Variations of the mean evaporator temperature (a) and thermal resistance of the CPL (b) with the input power to the evaporator for various relative condenser-evaporator heights for cooling water temperature in the condenser  $T_{\text{cold}} = 40$  and liquid inventory of 62% ----- 88

Fig 4.31 Variations of the mean evaporator temperature (a) and thermal resistance of the CPL (b) with the input power to the evaporator for various cooling water temperatures in the condenser and various relative condenser-evaporator heights for the liquid inventory of 62% ----- 89

Fig 4.32 Variations of the mean evaporator temperature (a) and thermal resistance of the CPL (b) with the input power to the evaporator for the CPL with and without cotton gauze covering for various relative condenser-evaporator heights for cooling water temperature in the condenser  $T_{\text{cold}} = 25$  and liquid inventory of 50% ----- 90

- Fig 4.33 Variations of the mean evaporator temperature (a) and thermal resistance of the CPL (b) with the input power to the evaporator for the CPL with and without cotton gauze covering for various relative condenser-evaporator heights for cooling water temperature in the condenser  $T_{\text{cold}} = 25$  and liquid inventory of 57%----- 91
- Fig 4.34 Variations of the mean evaporator temperature (a) and thermal resistance of the CPL (b) with the input power to the evaporator for the CPL with and without cotton gauze covering for various relative condenser-evaporator heights for cooling water temperature in the condenser  $T_{\text{cold}} = 25$  and liquid inventory of 62%----- 92
- Fig 4.35 Variations of the mean evaporator temperature (a) and thermal resistance of the CPL (b) with the input power to the evaporator for the CPL with and without cotton gauze covering for various relative condenser-evaporator heights for cooling water temperature in the condenser  $T_{\text{cold}} = 25$  and liquid inventory of 70%----- 93
- Fig 4.36 Variations of the mean evaporator temperature (a) and thermal resistance of the CPL (b) with the input power to the evaporator for the CPL with and without cotton gauze covering for various relative condenser-evaporator heights for cooling water temperature in the condenser  $T_{\text{cold}} = 25$  and liquid inventory of 75%----- 94
- Fig 4.37 Variations of the temperature at various locations in the CPL (a) and thermal resistance of the CPL (b) with the input power to the evaporator for the CPL with and without cotton gauze covering for cooling water temperature in the condenser  $T_{\text{cold}} = 25$  , liquid inventory of 62% and relative condenser-evaporator height of 0 cm----- 95
- Fig 4.38 Variations of the mean evaporator temperature (a) and thermal resistance of the CPL (b) with the input power to the evaporator for the CPL with and without cotton gauze covering for various relative condenser-evaporator heights for cooling water temperature in the condenser  $T_{\text{cold}} = 20$  and liquid inventory of 62%----- 96
- Fig 4.39 Variations of the mean evaporator temperature (a) and thermal resistance of



the CPL (b) with the input power to the evaporator for the CPL with and without cotton gauze covering for various relative condenser-evaporator heights for cooling water temperature in the condenser  $T_{\text{cold}} = 25$  and liquid inventory of 62%----- 97

Fig 4.40 Variations of the mean evaporator temperature (a) and thermal resistance of the CPL (b) with the input power to the evaporator for the CPL with and without cotton gauze covering for various relative condenser-evaporator heights for cooling water temperature in the condenser  $T_{\text{cold}} = 30$  and liquid inventory of 62%----- 98

Fig 4.41 Variations of the mean evaporator temperature (a) and thermal resistance of the CPL (b) with the input power to the evaporator for the CPL with and without cotton gauze covering for various relative condenser-evaporator heights for cooling water temperature in the condenser  $T_{\text{cold}} = 40$  and liquid inventory of 62%----- 99

Fig 4.42 Variations of the maximum obtainable power input to the evaporator(a) and thermal resistance of the CPL (b) with the liquid inventory for the CPL with and without cotton gauze covering for various relative condenser-evaporator heights for cooling water temperature in the condenser  $T_{\text{cold}} = 25$  ----- 100

Fig 4.43 Comparison of the measured data for maximum power input to the evaporator without the cotton gauze covering with the proposed correlation- ----- 101

Fig 4.44 Comparison of the measured data for maximum power input to the evaporator with the cotton gauze covering with the proposed correlation - ----- 102

Fig 4.45 Comparison of the measured data for minimal thermal resistance of the CPL without the cotton gauze covering with the proposed correlation - ----- 103

Fig 4.46 Comparison of the measured data for minimal thermal resistance of the CPL with the cotton gauze covering with the proposed correlation - ----- 104

## LIST OF TABLE

Table 1.1	Summary of some features in previous CPL studies -----	-9
Table 2.1	Geometric and material characteristics of present CPL system-----	19
Table 2.2	Experimental parameters-----	20
Table 3.1	Summary of the results from the pressure drop analysis for $h = 0$ cm at $T_{\text{cold}} = 25$ -----	39
Table 3.2	Summary of the results from the pressure drop analysis for $h = 5$ cm at $T_{\text{cold}} = 25$ -----	40
Table 3.3	Summary of the results from the pressure drop analysis for $h = 10$ cm at $T_{\text{cold}} = 25$ -----	41
Table 3.4	Summary of the uncertainty analysis-----	42
Table 4.1	Volume of each component in the CPL system -----	54
Table 4.2	Maximum obtainable power input to the evaporator for various liquid inventories and relation condenser-evaporator heights at $T_{\text{cold}}=25$ for the CPL without cotton gauze covering. -----	55
Table 4.3	Maximum obtainable power input to the evaporator for various liquid inventories and relation condenser-evaporator heights at $T_{\text{cold}}=25$ for the CPL with cotton gauze covering. -----	56
Table 4.4	Maximum obtainable power input to the evaporator for cooling water temperature in the condenser and relative condenser-evaporator heights for the liquid inventory of 62% for the CPL without cotton gauze covering. -----	57
Table 4.5	Maximum obtainable power input to the evaporator for cooling water temperature in the condenser and relative condenser-evaporator heights for the liquid inventory of 62% for the CPL with cotton gauze covering -----	58

## NOMENCLATURE

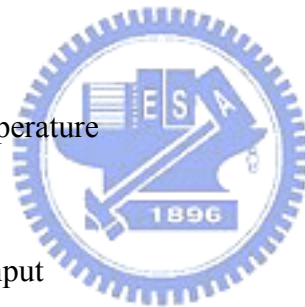
A	cross sectional area, $m^2$
$c_p$	specific heat, J/kg
D	diameter of tube, m
f	friction factor
F	dimensionless factor
g	gravitational acceleration, $m/s^2$
$H_g$	difference in heights of evaporator and condenser, m
h	relative height, m, or heat transfer coefficient, $W/m^2$
$h_{n,t}$	heat transfer coefficient from the top of evaporator section to ambient, $W/m^2$
$h_{n,r}$	heat transfer coefficient from the radial surface of evaporator section to ambient, $W/m^2$
$h_{n,b}$	heat transfer coefficient from the bottom of evaporator section to ambient, $W/m^2$
K	permeability, $m^2$
k	thermal conductivity, $W/m K$
I	measured current from DC power supply, A
L	length, m, or liquid inventory
$\dot{m}$	mass flow rate, kg/s
N	number of grooved channel
P	pressure, kPa
Q	heat load, W
R	thermal resistance, $^{\circ}C/W$
Re	Reynolds number
T	temperature,
V	measured voltage from DC power supply; velocity, m/s
z	thickness of wick, m

## Greek Symbols

$\Delta P$	pressure drop, kPa
$\Delta T$	temperature difference,
$\rho$	density, kg/m <sup>3</sup>
$\sigma$	surface tension, N/m
$\delta$	cotton gauze layer thickness, m
$\mu$	viscosity, N-S/m <sup>2</sup>
$\varepsilon$	porosity, %
$\ell$	thickness of wick
	contact angle

## Subscripts

cap	capillary term
cold	cooling water temperature
cond	condenser
e	effective power input
evap	evaporator
env	environment
g	gravitational or grooved channel
i	inner wall
l	liquid phase
loss	loss term
n	natural convection
o	outer wall
s	surface area
T	teflon
t	total power input



th	thermal resistance
v	vapor phase
vg	vapor in grooved channel
w	wick structure
z	z direction



# CHAPTER 1

## INTRODUCTION

### 1.1 Motive

With the recent quick increase in the computational frequencies of micro-processors, heat dissipation is becoming a serious problem for the CPUs of portable computers to function normally. It is well known that the surface temperature of the CPU chips should not exceed 85 °C to avoid the system shutdown. In the past, the heat dissipation of CPUs was about 10W for the 80486 series. The heat dissipated in the CPU chips in the series was successfully removed by combining fans and fins. In the current Pentium 4 series the heat dissipation is much higher and is over 80W. The methods based on air-cooling are not enough to dissipate the heat generated in the chips. In addition, spacing is relatively limited for thermal modules especially when applied to portable electronic devices, like notebook PC or PDA. The conventional gas cooling methods could not remove the high heat fluxes generated from the today's fast speed micro-processors sufficiently. Recently, some commercial products employed the methods based on the liquid cooling to take the high heat dissipation away. The liquid cooling can be used with or without boiling. Moreover, the two-phase heat transfer associated with boiling or condensation has high latent heat involved in the process and hence it is known to be the most effective and popular.

Aside from the above methods, several exotic cooling approaches such as jet impingement, spray, heat pipe and capillary pumped loop have been developed. Among these approaches, the jet impingement or spray cooling needs extra power to drive the flow. Thus they are not practical in a self-regulated loop system preferred in electronic cooling. The heat removal capability of heat pipes is often not sufficient to

cool high heat flux surfaces. Besides, there are some physical limits for heat pipes, such as the sonic limit, capillary limit, viscous limit, boiling limit, and entrainment limit. In the thermal management of electronic devices, the application of capillary pumped loops have received increasing attention in recent years.

Capillary pumped loop (CPL) is a capillary driven two-phase heat transport system that consists of an evaporator with wicking structure, a condenser, a liquid reservoir, and distinct liquid and vapor lines. A typical CPL is schematically shown in Fig. 1.1. Heat enters the loop through the evaporator, causing the liquid in it to vaporize. The vapor then moves to a lower pressure region and then flows to the condenser in which the working fluid condenses and releases heat to the ambient. The capillary force generated by the wick structure pumps the condensed liquid to the evaporator. And the loop is completed. Note that in the CPL the liquid and vapor phases are transported in separated lines to avoid the flow interaction between the phases. Thus the liquid-vapor counter-current flow and entrainment limits do not occur. The heat transfer capability of the capillary pumped loop is expected to be better than heat pipes and the device has high potential in high power density electronic cooling systems.

## 1.2 Literature Review

As is well known in the early development for space applications, a capillary pumped loop utilizes the capillary forces developed in a fine-pore wick to circulate the working fluid, which can transfer a large amount of heat in a small temperature difference without a need of external pumping power. Stenger [1] at NASA/Lewis U.S.A. first proposed the initial CPL concept in the mid-1960s. But not until the late-1970s serious CPL development for spacecraft applications began. Then in the 1980s the concept of CPL was extensively tested and applied in flight and

Commercial experiments. Subsequently in 1993, Ku [2] conducted an overview of capillary pumped loop technology. Characterization of CPL and verification of CPL performance were addressed. He also presented some performance anomalies. These include 1) sudden deprime of evaporators: non-condensable gas accumulation inside the wick or vapor penetration into the wick during startup; 2) evaporator deprime during rapid power step down: very complex interaction among the reservoir, evaporator and condensers; 3) pressure oscillations during steady operation: when accompanied by changes in other conditions it was suspected to cause evaporator deprimes. An example of a deprime is that when the evaporator is starved of liquid due to vapor existing in the liquid side of the wick. The phenomenon of deprimes should be avoided in the CPL operation. If deprimes happen, the system will stop working and will be broken. Maldanik et al. [3] experimentally and analytically investigated physical mechanisms during a CPL startup. They found that the startup process could be characterized by three main stages of different durations. The first stage is a steady growth of temperature and pressure in the loop in the absence of vapor phase. The second stage occurs when boiling in the liquid is initiated, resulting in quick lowering of evaporator temperature and pressure. In the last stage both the temperature and pressure become constant. They also predicted the minimum heat load for a reliable startup. Ku [2] and Meyer et al. [4] also agreed with these findings. Later Mo et al. [5, 6] experimentally examined how the CPL startup process was affected by applying an electric field to the evaporator wick. They noted that the induced Maxwell stress at the liquid-vapor interface tended to reduce the startup time and improve the system performance. Besides, the depriming phenomenon can also be prevented.

The pressure and temperature oscillations in steady operation of CPLs can significantly affect their performance. In an experimental study Kolos and Herold [7]



found that the oscillations of temperature and pressure were resulted from the presence of the bubbles in the evaporator core. Specifically, the bubble growth and collapse cause the oscillations. O'Connell and Ku [8] suggested the factors leading to the unsteadiness of CPL pressure, including wick permeability, size of transport lines, reservoir volume, power input, sink temperature, and reservoir set point. Besides, their experimental results showed that when the transport line diameter was reduced, the pressure oscillation became more severe. O'Connell and Hoang [9] examined effects of wick properties on pressure oscillation. They noted that a more severe pressure oscillation was caused by the reducing permeability of the wick with a smaller pore size.

The evaporator deprime has received some attention. Ku [2] indicated that a sudden change in the input power would lead to an evaporator deprime. A step wise input power was applied to an evaporator by Pouzet et al. [10] to study its fundamental response mechanisms. The oscillations of temperature and pressure following the power change were noted. Using acetone and ammonia as working fluids, Bazzo and Rienl [11] examined the CPL startup and its operating ability when the different heat loads were applied to the capillary evaporator. The experimental results show that heat transfer capacity is better for ammonia. The acetone in the evaporator was heated more quickly for most cases, which in turn resulted in the evaporator dry out. Regarding the CPL operating principles, Ku [12] used thermodynamic diagrams to identify the state of the working fluid in various components of the system for different operating conditions. He also discussed some CPL operating limits, such as the capillary limit, subcooling limit and vapor pressure limit. The capillary limit was considered as the key to the whole system. When the capillary limit was lower than the vapor pressure limit, the system would stop working. Thus the vapor pressure of the system needs to be controlled under the

capillary limit in order to prevent the system failure.

More attention has been paid to investigating the heat transfer characteristics for CPL systems. Dickey and Peterson [13] examined the effects of the input power and adverse gravitation with the evaporator located higher than the condenser on the CPL heat transfer characteristics. At the same time, they also developed a computer model for the loop and the results for the steady-state variations of the temperature were presented. Later Liao and Zhao [14-16] moved further to examine the CPL heat transfer capability affected by the capillary structure height and particle size and the entrance temperature. They found that at increasing imposed heat flux the heat transfer coefficient increased to a maximum value and then decreased afterwards. Strong effects of the height between the liquid tube and vapor tube were experimentally investigated by Meyer et al. [4]. Similarly, Chen and Lin [17] studied the influences of the relative height between the evaporator and condenser, fluid inventory and power input. At increasing height the heat transfer capability of the CPL using FC-72 as working fluid is noted to increase. But, when it increases to certain height, thermal resistance does not reduce further. Instead the thermal resistance remains at a constant. This is attributed to the fact that for an increase in the height the potential energy increases. So, the mass flux in the CPL increases, which in turn results in a higher pressure drop in the liquid and vapor tubes. The experimental results also show that the fluid inventory has an optimal value. Similar conclusion was reached earlier by Miyasaka et al. [18].

Methods to improve CPL heat transfer capability were also examined by some research groups. Pohner and Antoniuk [19] showed that machining the vaporization enhancement grooves (VEGs) into the lands of the evaporator extrusion could raise the heat transfer coefficient. A fibrous slab wick running through the entire condenser tube to serve as a non-condensable gas trap was noted to increase the CPL reliability

and operational lifetime too. A similar measure was taken by Muraoka et al. [20] by using a porous structure inside the condenser to stabilize the interface between the liquid and vapor phases. Schweickart et al. [21] showed that adding a mechanical pump could effectively prevent the evaporator deprime.

Using the techniques of MEMS, Kirshberg and Yerkes [22], Pettigrew and Kirshberg [23] and Meyer et al. [24] fabricated a miniature CPL system on a silicon chip. For traditional CPL an evaporator capillary structure is normally employed to produce capillary forces. However, for the tiny CPL system very small channels are etched on the chip to yield the required capillary forces. More uniform temperature distribution can be obtained and the resulting heat transfer capability increases. When a liquid is in contact with a solid surface in the tiny channel, the extended meniscus can be divided into three parts, the intrinsic meniscus region, the thin film region and the adsorbed region [25]. Park et al. [26, 27] utilized a mathematical model to investigate the transport phenomena and heat transfer characteristics in the thin film region in a micro-channel. They found the length and the thickness of the thin film region decrease exponentially at increasing heat flux, leading to higher capillary force and heat transfer coefficient.

Over the past numerical simulation was also conducted to elucidate the flow and heat transfer within the porous structure in the evaporator. Cao and Faghri [28, 29] used a numerical analysis to simulate flat-plate type evaporator. The results show that some limitations exist between the wick and heater interface. Specifically, as the babble grows to a size to cover the heater surface, the capillary forces resulting from the porous structure disappear. The liquid-vapor interface is destroyed and this is similar to the boiling limit for traditional heat pipes. Zhao and Liao [30] moved further to consider the effects of the groove size and the thermal conductivity of the capillary structure. They noted that the low thermal conductivity of the capillary

structure could result in a very steep temperature gradient at the fin/porous structure interface. Zhao et al. [31] also investigated the flow in a vertical porous channel heated symmetrically along its vertical walls. Very different flow phenomena in the single-phase and two-phase flow motions in the porous structure were noted. In single-phase flow the mass flux increases with the heat flux, but in the two-phase flow the mass flux drops sharply for an increase in the heat flux. Hanlon and Ma [32] developed a mathematical model to study the heat transfer capability for a sintered wick structure. The results show that the evaporation heat transfer coefficient can be enhanced by reducing the average particle size. They also proposed that thin film evaporation played an important role in the enhancement of evaporating heat transfer. Some feature and major results obtained in the previous study of CPLs reported in the open literature are given in Table 1.1.



### 1.3 Objective

The above literature review clearly indicates that the basic flow and heat transfer mechanisms associated with the traditional CPLs have been extensively investigated. Besides, the CPL systems have been used successfully in large heat dissipation systems for spacecraft applications. But a flat shape evaporator has been proposed for CPU heat dissipation [33]. In this experimental study, we intend to develop and test an improved CPL system aiming at the high power density CPU cooling. A typical evaporator design is schematically shown in Fig. 1.2. More specifically, the evaporator consists of a grooved copper plate attached on the wick surface, acting as the heating zone, and the vapor can move in the grooves. Thus, the resistance to the vapor flow is reduced. In addition, it is inefficient to use only the upper surfaces of the fins for heating. The vertical and bottom surfaces of the grooved channels will also be covered by the thin wick. This will increase the heated surface

area for liquid vaporization, which is expected to enhance heat transfer in the evaporator. Effects of the input power, liquid inventory, cooling water temperature in the condenser, and relative height between the evaporator and condenser on the heat transfer performance of the CPL will be investigated.



Table 1.1 Summary of some features in previous CPL studies.

References	Working fluid Liquid inventories	$H_g^*$ (cm)	$T_{evap,max}^*$ ( )	$q_{e,max}^*$ ( $\frac{W}{cm^2}$ ) $Q_{e,max}$ (W)	Wick properties	Applications
Maldanik et al. (1993)	Ammonia	0	32	3.5 775	pore radius = 1.3 $\mu$ m, polyethylene	spacecraft
Meyer et al. (1993)	Ammonia	0	58	7.9 1129	pore radius = 1.5 $\mu$ m, sintered nickel powder	spacecraft
Mo et al. (1999)	R-134a	0	26.5	0.247 50	pore radius = 1.5 $\mu$ m, polyethylene	spacecraft
Mo et al. (2000)	R-134a	0	26	3.21 650	pore radius = 1.5 $\mu$ m, polyethylene	spacecraft
Ku (1996)	Ammonia	0	30	1.27 500	pore radius = 13, 16 $\mu$ m	spacecraft
O'Connell and Hoang (1996)	Ammonia	0	30	1.27 500	pore radius = 8.3, 13.02, 16.12, 19.08 $\mu$ m	spacecraft
Pouzet et al. (2004)	R-134a	0	33	5 600	pore radius = 20 $\mu$ m	spacecraft
Bazzo and Riehl (2003)	Acetone, Ammonia	0	30	2.8 100	pore radius = 20 $\mu$ m	electronics cooling
Dickey and Peterson (1994)	Ammonia	0	58	2.87 130	pore radius = 1~1.5 $\mu$ m, sintered nickel powder	electronics cooling

Table 1.1 Continued (1)

References	Working fluid Liquid inventories	$H_g^*$ (cm)	$\bar{T}_{evap,max}^*$ ( )	$q_{e,max}''$ ( $W/cm^2$ ) $Q_{e,max}$ (W)	Wick properties	Applications
Liao and Zhao (1999)	Water	-0.5	168	32 887	particle diameters = 0.55, 1.09, 1.99, 2.56 mm	electronics cooling
Liao and Zhao (2000)	Water	1	144.6	32 256	particle diameters = 2.0 mm	electronics cooling
Zhao and Liao (2000)	Water	-3.5	135	25.9 740	particle diameters =1.09 mm	electronics cooling
Chen and Lin (2001)	FC-72 50%	12	83	2.5 40	pore radius =10 $\mu$ m	electronics cooling
Miyasaka et al. (1995)	HCFCs-142b 40%	0	38	7 43.7	Capillary pipe diameters =2mm	electronics cooling
Pohner and Antoniuk (1991)	Ammonia	0	32	3.16 500	pore radius = 20 $\mu$ m	spacecraft
Muraoka et al. (1998)	Ethanol	0	60	3.81 120	Sintered bronze	electronics cooling
Kirshberg and Yerkes (2000)	Water	0	100	375 7.5	MEMS Groove height/width =50/50 $\mu$ m	electronics cooling
Pettigrew and Kirshberg (2001)	Water	0	100	375 7.5	MEMS Groove height/width =50/50 $\mu$ m	electronics cooling

Table 1.1 Continued (2)

References	Working fluid Liquid inventories	$H_g^*$ (cm)	$\bar{T}_{evap,max}^*$ ( )	$q_{e,max}^*$ ( $W/cm^2$ ) $Q_{e,max}$ (W)	Wick properties	Applications
Meyer and Dasgupta (2003)	Water	0	100	224 4.8	MEMS Groove height/width =30/22 $\mu$ m	electronics cooling
Zhao and Liao (1994)	Water	0	100	4.12 123.6	particle diameters = 0.55 mm	humidistat
Tsai et al. (2005)	Methanol	0	98	25.62 50.00	Copper screen	electronics cooling
Maydanik et al. (2005)	Water	0	100	35 140	pore radius = 1~10 $\mu$ m, sintered copper powder	electronics cooling

\*  $\bar{T}_{evap,max}$  denotes maximum mean evaporator temperature allowed in the experiment.

\*  $H_g$  denotes condenser-evaporator relative height.



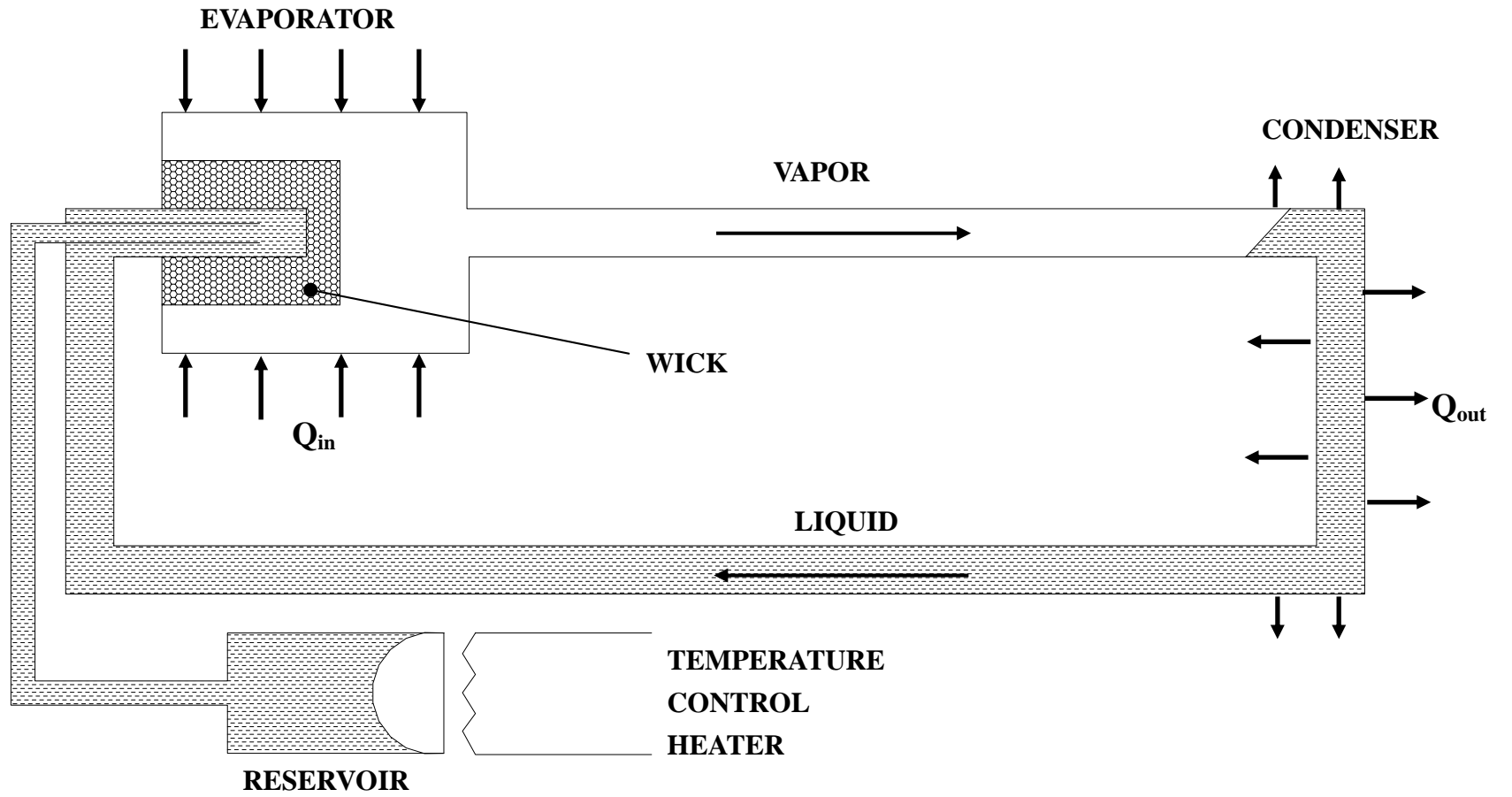


Fig.1.1 Schematic of a Capillary Pumped Loop [37].

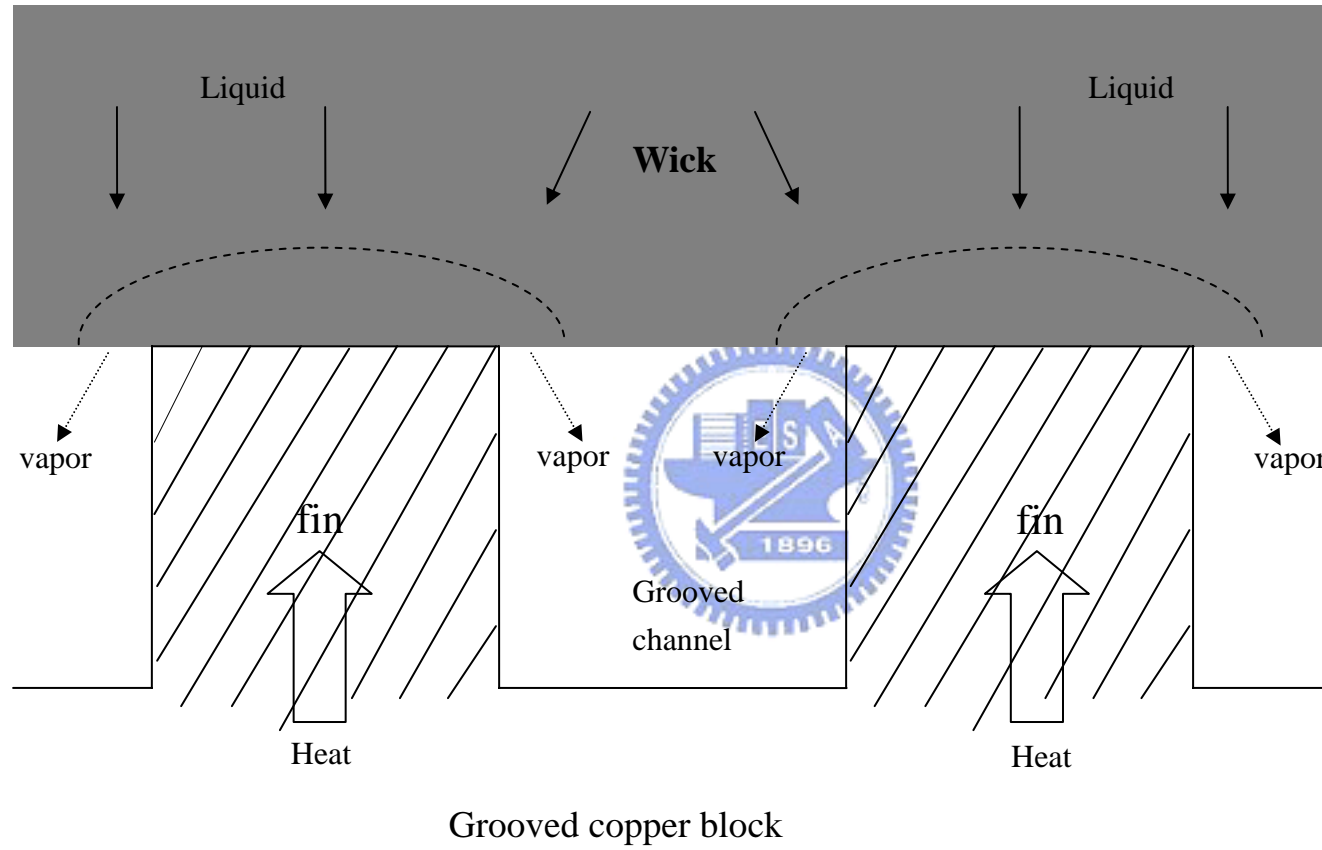


Fig.1.2 Schematic of a typical evaporator design.

## CHAPTER 2

### EXPERIMENTAL APPARATUS AND PROCEDURES

The experimental system established in the present study to test an improved design of a CPL is schematically depicted in Fig. 2.1. The experimental system consists of four major parts, namely, a test CPL loop, a fluid inventory unit, a cold-water loop and a measurement unit. These parts are described in the following.

#### 2.1 CPL Loop

The test CPL loop includes an evaporator, a condenser, and vapor and liquid transport lines, as shown in Fig. 2.2 by a three-dimensional plot. The detailed dimensions and materials employed in the loop are given in Table 2.1. Note that here the evaporator and condenser are plotted at the same height and the gravity effects do not exist.

Plots showing the detailed structure of the evaporator are given in Figs. 2.3 and 2.4. The evaporator is mainly made of a rectangular grooved copper block with a heated rectangular copper block glued onto its lower surface and with a layer of wick glued onto its upper surface. As shown in Fig. 2.5, two resistance heaters are inserted into the heated copper block and the heaters are covered with heat conducting grease to reduce the thermal contact resistance. The outside surfaces of the heated copper block, grooved copper block and wick are all thermally insulated by teflon wraps. They are then installed in a cylindrical teflon base. In order to further reduce heat loss, the outside surface of the whole evaporator is covered with adiabatic cotton. The wick used in present study is made from open-cell blowing foam of polyvinyl alcohol (PVA), and the structure of this PVA is illustrated by the photos given in Fig. 2.6 (its

mean pore radius is  $21 \mu\text{m}$ , porosity 5%, and permeability  $3.0 \times 10^{-11} \text{m}^2$ ) and the wick layer is  $30\text{mm} \times 30\text{mm} \times 3\text{mm}$  in size. An observational window is also opened in the teflon cover to facilitate the visualization of the flow in it. Besides, to prevent the flooding of the grooved channels, a cotton gauze layer of  $150 \mu\text{m}$  is placed on the wick (Fig. 2.7). Moreover, the vertical and bottom surfaces of the grooved channel are also covered by the cotton gauze layer to allow the liquid to flow into the gauze, as show in Fig. 2.8. The evaporator is connected with the condenser through the liquid and vapor transport lines.

In designing the condenser, the heat transfer area and the cooling mechanisms to cool down the working fluid need to be considered. Specifically, the condenser must have the following characteristics:

- 1) Small temperature difference between the condenser and heat sink.
- 2) Small flow resistance inside the condenser.
- 3) Small gravity force effect under 1G environment.
- 4) High reliability and light weight.
- 5) Easy fabrication and low cost.

Herein, we chose a double-tube heat exchanger as the condenser. Cold water is used to condense the vapor and to control the temperature of the condenser.

The transport lines include the vapor line and the liquid line. In normal operation the vapor from the evaporator flows through the vapor line and enters the condenser and the liquid from the condenser flows to the evaporator through the liquid line. In order to reduce the friction loss, smooth teflon tubes with inside diameter of  $4.5 \text{mm}$  are chosen for the transport lines.

## 2.2 Fluid Inventory Unit

Before the working fluid is input to the CPL, it is important to insure that the

system is in a vacuum condition and no noncondensable gas exists in the CPL. The working fluid inventory unit includes a working fluid tank, a dispensing burette, and a vacuum pump, which connects with the CPL loop through tubes and valves.

To maximize the capillary limit and heat transport of the CPL, the working fluid should have the following properties:

- 1) large surface tension
- 2) high density
- 3) large latent heat
- 4) low viscosity

In this study deionized water is chosen as the working fluid.

### **2.3 Cold-Water Loop**

The cold-water loop is designed for condensing the water vapor from the evaporator. Using a cold-water thermostat and a spherical valve, we can adjust the temperature and flow rate of cold water in the cold-water loop. This arrangement allows us to control the temperature of the condenser.

### **2.4 Measurement Unit**

T-type (copper-constantan) thermocouples are used to measure the temperatures at selected locations in the test CPL loop. Specifically, six calibrated thermocouples are employed to measure the temperature of the grooved copper block. They are placed at locations near the bottom of the grooved channel and near the top of the channel, as schematically shown in Fig. 2.9. To estimate the heat loss from the evaporator, the temperature of the outer wall of the adiabatic cotton is also measured, as schematically shown in Fig. 2.10. Besides, the temperature of the working fluid at the inlets and exits of the evaporator and condenser shown in Fig. 2.2, are measured.

## 2.5 Equipments

### 1) DC Power Supply:

A DC power supply of 60V and 3A is selected to supply the required electric current to the heaters in the evaporator section (Fig. 2.5). The DC current through the heaters is measured by a Yokogawa DC meter with an accuracy of  $\pm 0.2\%$ . Then the voltage drop across the heater is measured by a Yokogawa multimeter. Thus the power input to the heater can be calculated.

### 2) Data Acquisition:

The data acquisition unit employed to record the signals from various transducers is a 30-channel data logger (YOKOGAWA MW-100), which is connected to a personal computer. The voltage signals from the thermocouples and pressure transducers are converted to the temperature and pressure by the internal calibration equations in the computer and are displayed on the screen simultaneously.

### 3) Thermostat:

The maximum cooling capacity of the thermostat is 1200 W with a maximum water volume flow rate of 5 L/min

### 4) Vacuum Pump:

An oil rotary vacuum pump (VLVAC G-100D) with an ultimate pressure of  $5 \times 10^{-4}$  torr and a pumping speed of 120 L/min is used here

## 2.6 Experimental Procedures

Before each experiment, the vacuum pump is connected with the CPL to get rid of the non-condensable gas possibly existing in the CPL loop. Then the working fluid is injected into the CPL from the fluid inventory unit. Besides, the thermostat of the

cold-water loop is set at a predetermined level and the DC power supply is turned on to input the preset amount of heat to the evaporator. After the system reaches a statistically stable state, the temperature and pressure data from various transducers are recorded and processed by the data acquisition unit.

## **2.7 Experimental Parameters**

The present study intends to test the performance of an improved CPL system design. In the study the experimental parameters include the input power to the evaporator, the liquid inventory in the loop, the cooling water temperature in the condenser, and the elevation difference between the condenser and evaporator. The ranges of the experimental parameters to be investigated are listed in Table 2.2.



Table 2.1 Geometric and material characteristics of the present CPL system.

<b>Evaporator</b>		
Wick structure	Size (mm <sup>3</sup> )	30×30×3
	Mean pore radius ( $\mu m$ )	21
	Porosity (%)	65
	Permeability (m <sup>2</sup> )	$3.0 \times 10^{-11} m^2$
	Material	polyvinyl alcohol
Grooves block	Size (mm <sup>3</sup> )	30×30×7
	Grooves length/height/width (mm)	30/3/2.4
	Number of grooves	5
	Fin length/height/width (mm)	30/3/3
	Number of fin	6
	Material	copper
<b>Condenser</b>		
Outer tube	Inner diameter (mm)	20
	Length(mm)	350
	Material	copper
Inner tube	Outer diameter (mm)	6.35
	Inner diameter (mm)	4.5
	Length(mm)	350
	Material	copper
<b>Transport Line</b>		
Liquid line	Outer diameter (mm)	6.35
	Inner diameter (mm)	4.5
	Length(mm)	790
	Material	teflon
Vapor line	Outer diameter (mm)	6.35
	Inner diameter (mm)	4.5
	Length(mm)	790
	Material	teflon



Table 2.2 Experimental parameters

<b>Parameter</b>	<b>Range</b>	<b>Unit</b>
Input power	5 ~ 260	W
Liquid inventory	50 ~ 75	%
Cooling water temperature in condenser	20 ~ 40	°C
Relative height between the evaporator and condenser	0 ~ 10	cm



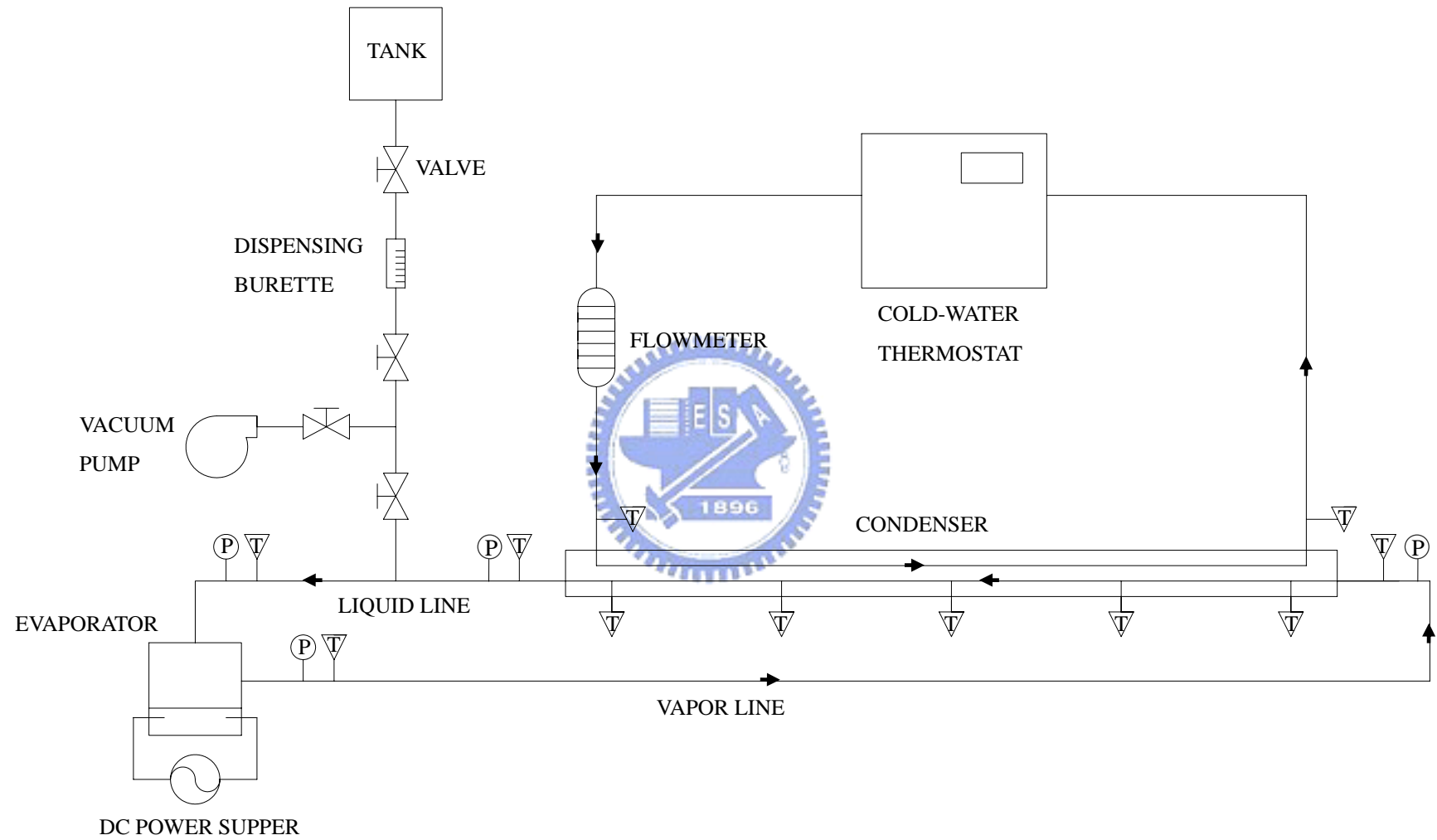


Fig. 2.1 Schematic diagram of experimental apparatus.

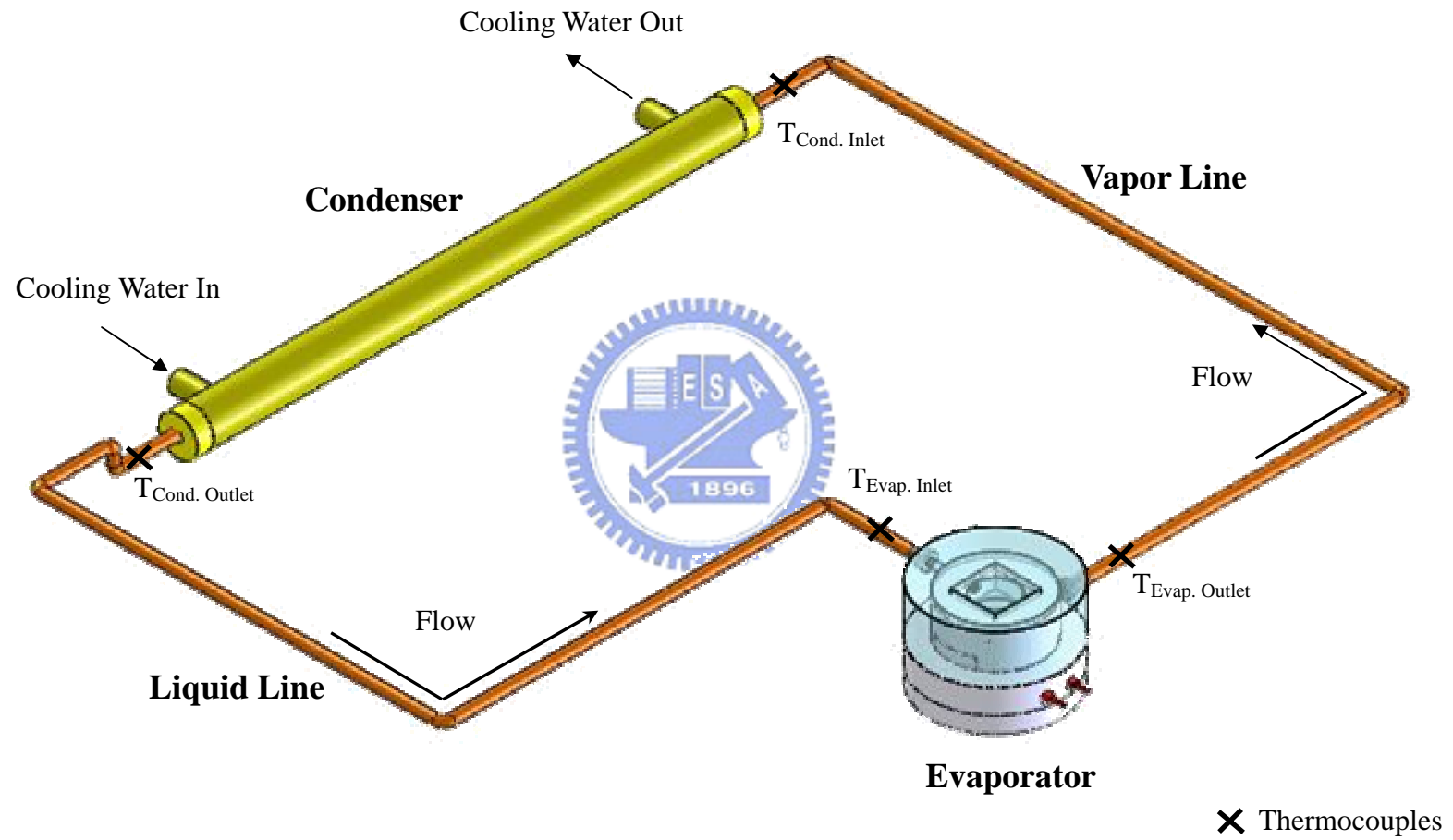


Fig. 2.2 Three-dimensional plots illustrating the CPL test loop.

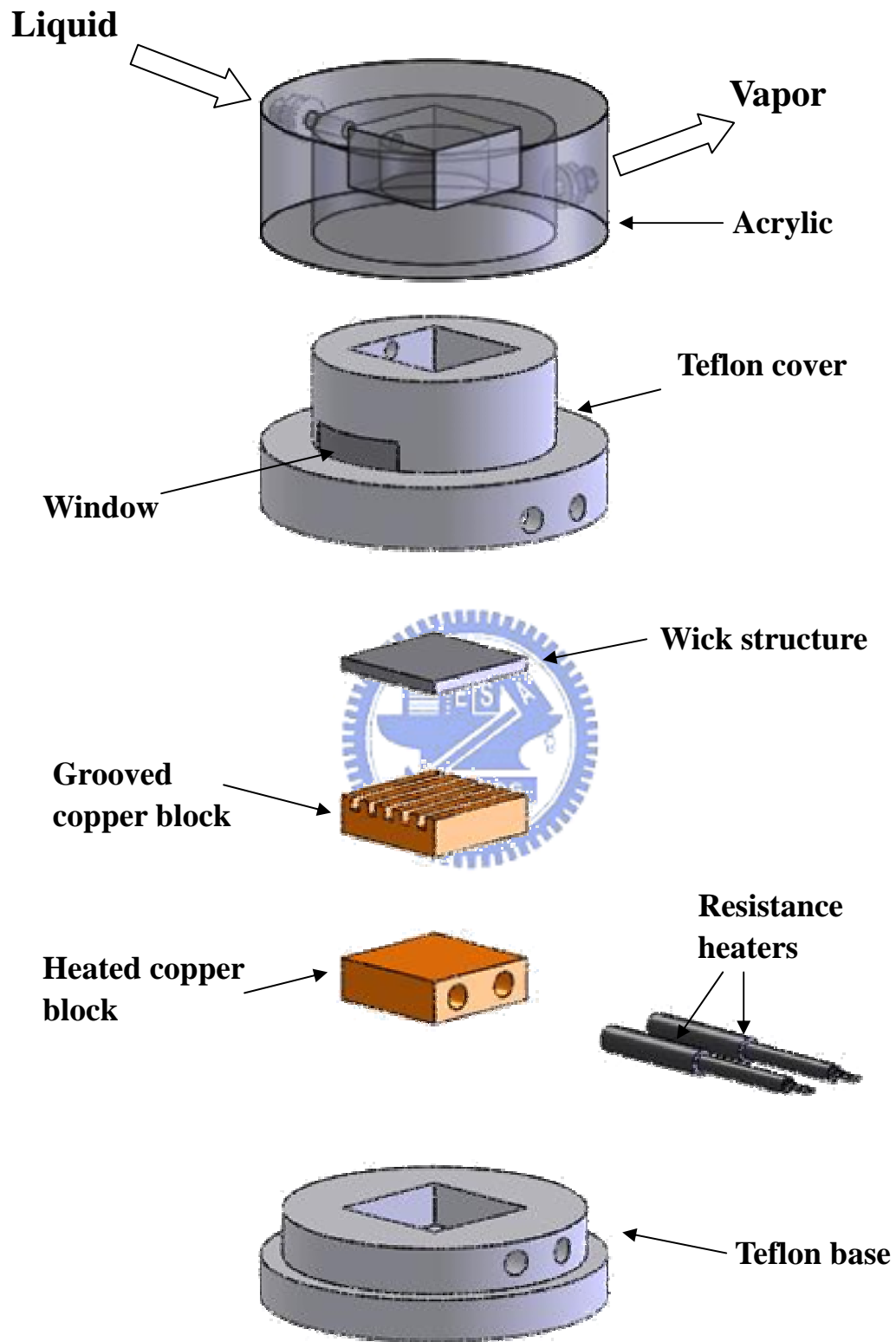


Fig. 2.3 The detailed structure of evaporator.

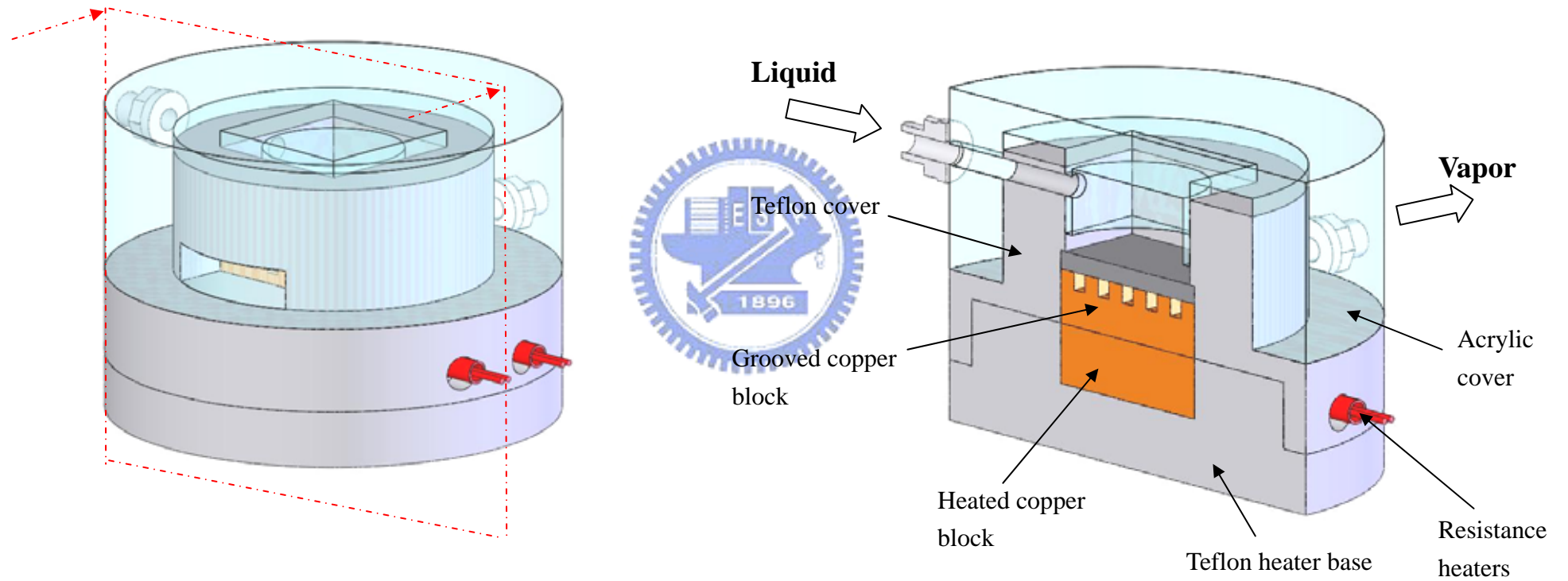
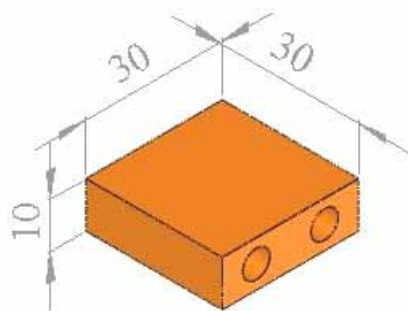
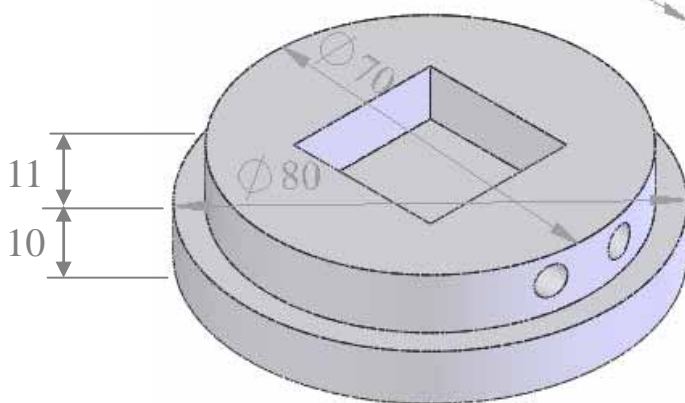
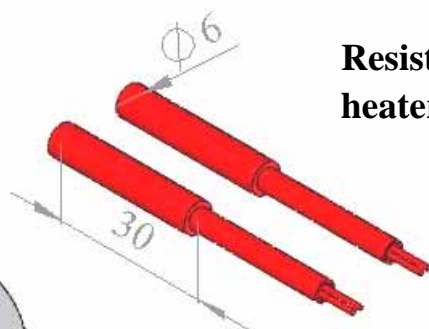


Fig. 2.4 A cutaway view of evaporator.

**Heated copper  
block**



**Resistance  
heaters**



**Teflon base**

Unit: mm

Fig. 2.5 Dimension of heater base.

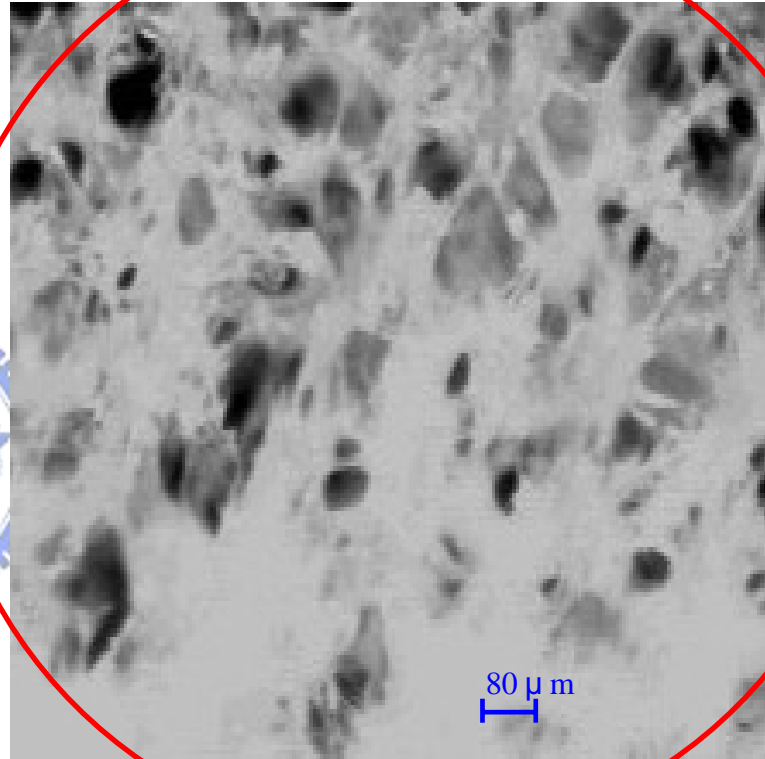
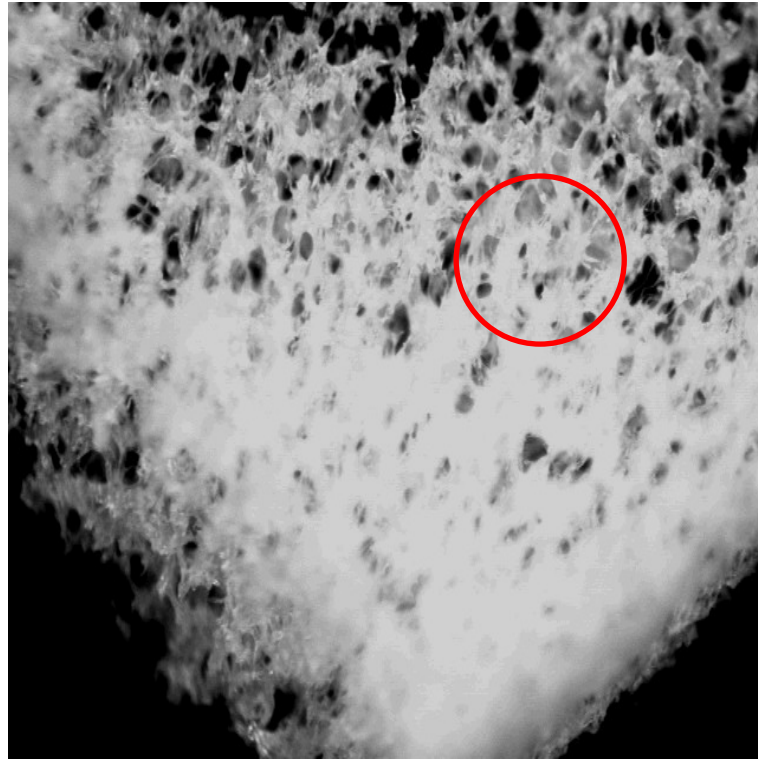


Fig. 2.6 Photographs of the polyvinyl alcohol.

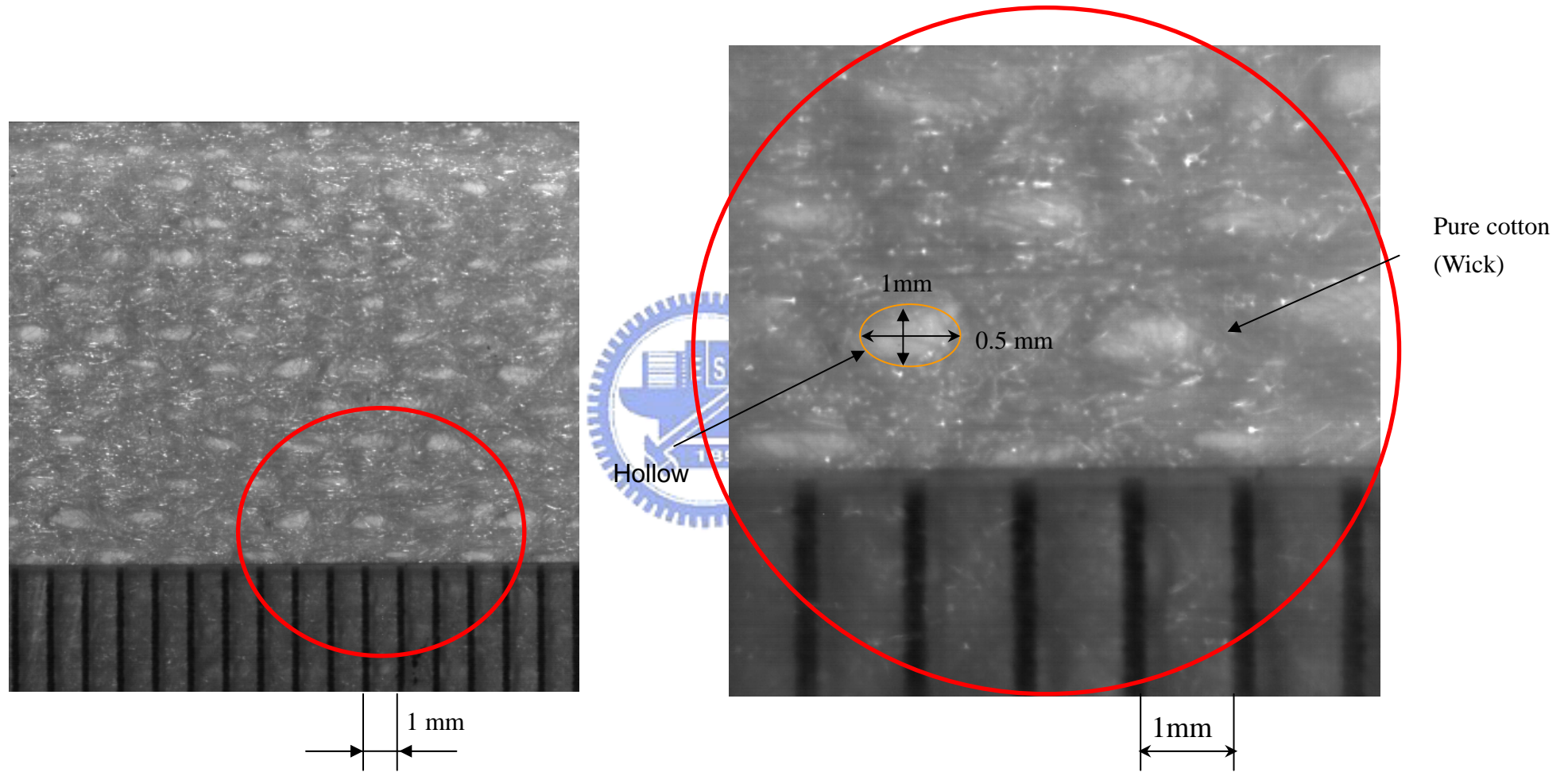


Fig. 2.7 Photographs of the cotton gauze.



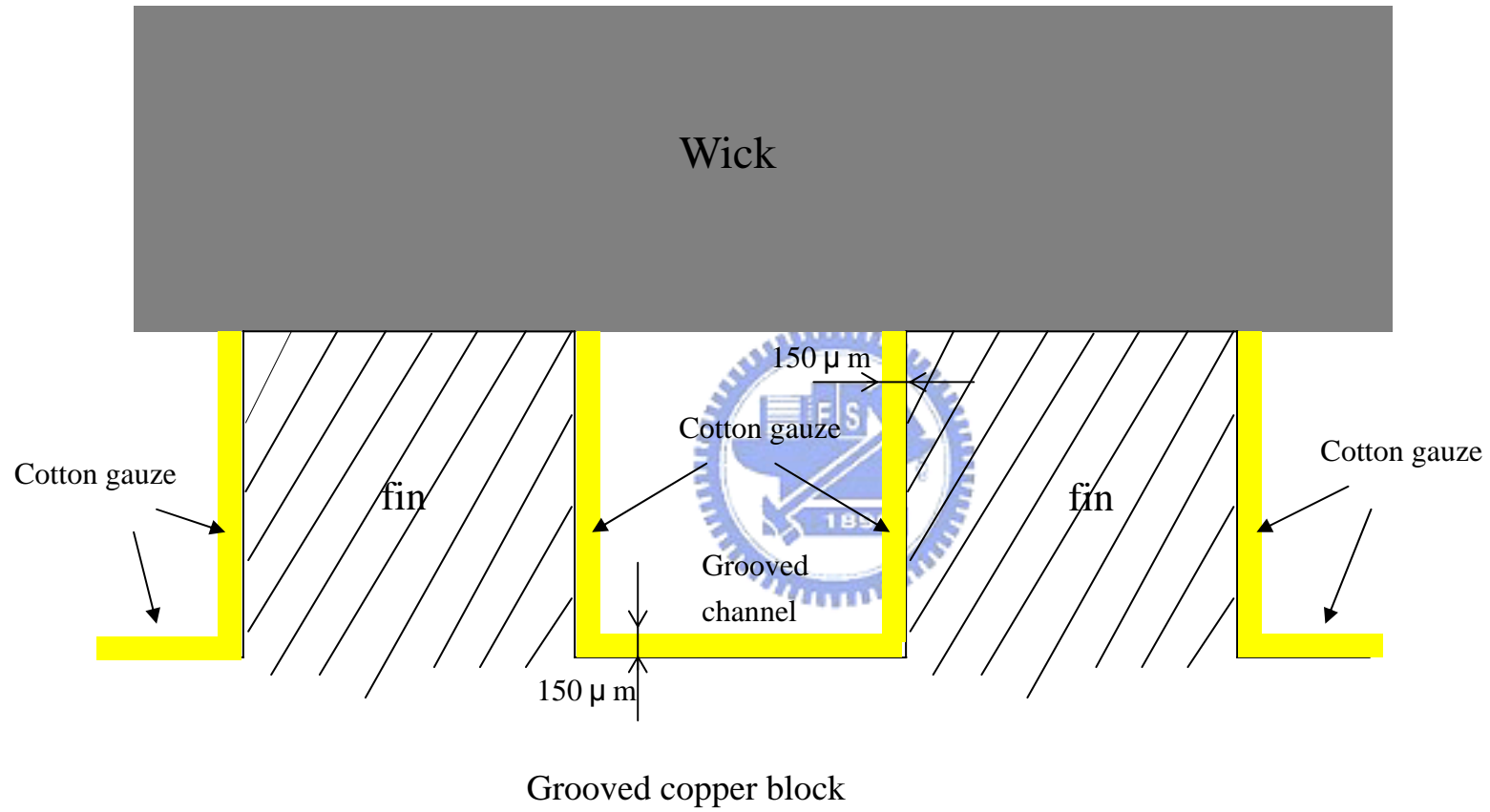
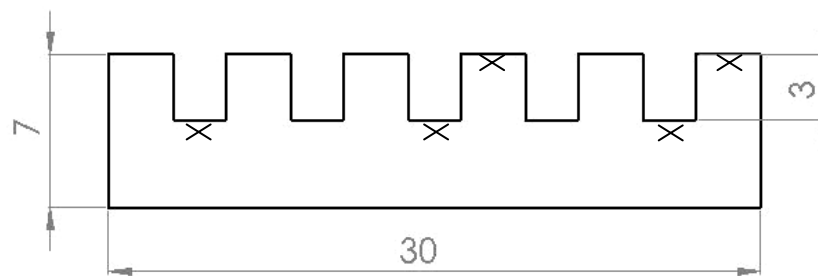
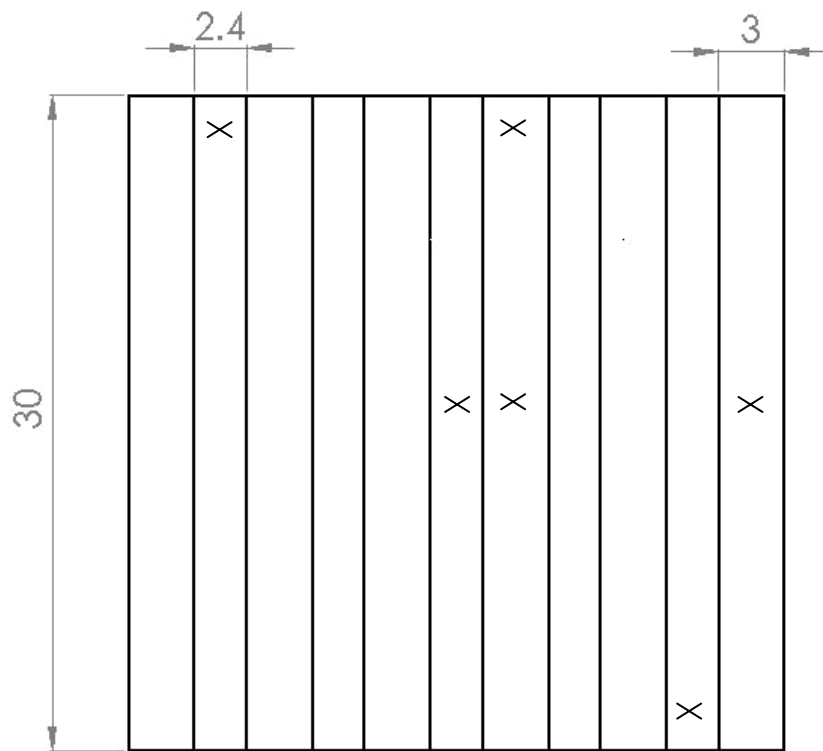


Fig. 2.8 Schematic of enhance grooved of the evaporator design.



× Thermocouples

Unit: mm

Fig. 2.9 Locations of the thermocouples and dimension of grooved copper block.

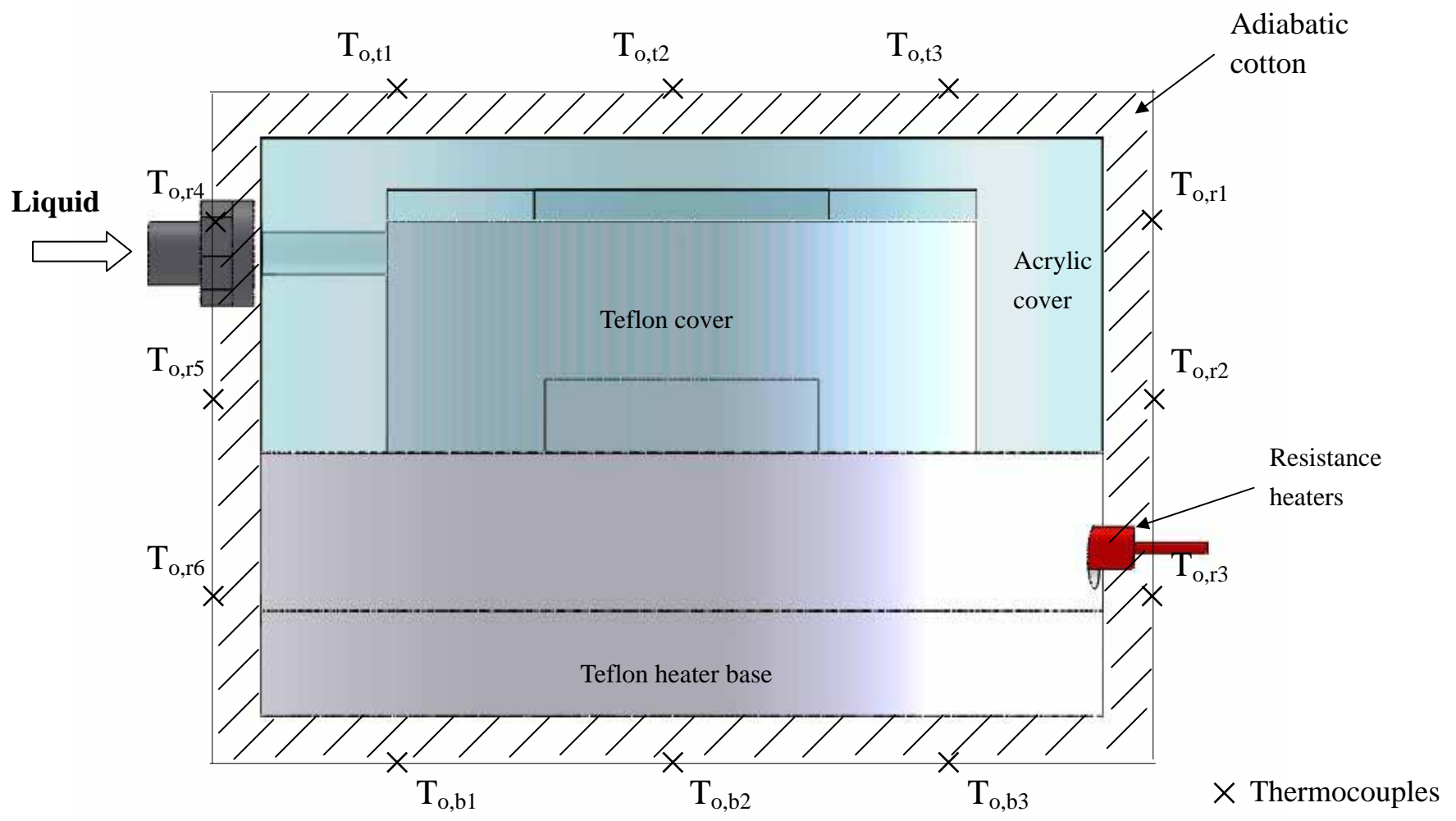


Fig. 2.10 Locations of the thermocouples of the outer wall of the adiabatic cotton.

## CHAPTER 3

### DATA REDUCTION AND SIMPLE ANALYSIS

In the present test of an improved CPL system design, a data reduction analysis is needed to calculate the system thermal resistance from the measured raw data. On the other hand, the thermodynamic states, heat transfer limitation and pressure drop of the CPL loop are discussed in the following.

#### 3.1 Data Reduction

Conventionally, the concept of the thermal resistance is adopted to represent the CPL performance. It shows the heat removal capacity of a CPL. The thermal resistance is usually defined as

$$R_{th} = \frac{T_{evap} - T_{cond}}{Q_e} \quad (3.1)$$

where  $T_{evap}$  is the mean temperature of the evaporator,  $T_{cond}$  is the mean temperature of the condenser, and  $Q_e$  is the effective power input to the CPL. The total power input  $Q_t$  and the effective power input  $Q_e$  are respectively evaluated from the equations

$$Q_t = V \cdot I \quad (3.2)$$

where V and I are individually the voltage drop across and current through the resistance heaters, and

$$Q_e = Q_t - Q_{loss} \quad (3.3)$$

Here the heat loss from the evaporator  $Q_{loss}$  is approximately estimated from the relation

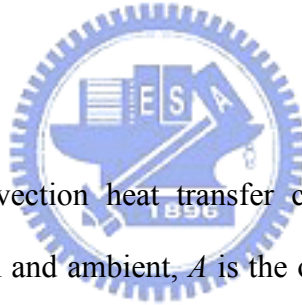
$$Q_{loss} = h_{n,t} A_t (\overline{T_{o,t}} - T_{amb}) + h_{n,r} A_r (\overline{T_{o,r}} - T_{amb}) + h_{n,b} A_b (\overline{T_{o,b}} - T_{amb}) \quad (3.4)$$

indicating that the natural convection heat transfer from the outside surfaces of the evaporator to the ambient includes three major parts, namely, from the top, circumferential and bottom surfaces of the evaporator to the ambient. The associated natural convection heat transfer coefficients can be approximately evaluated from the empirical correlations [34] as

$$h_{n,t} = 1.32 \left[ \frac{(\overline{T}_{o,t} - T_{amb})}{d} \right]^{0.25} \quad (3.5)$$

$$h_{n,r} = 1.42 \left[ \frac{(\overline{T}_{o,r} - T_{amb})}{d} \right]^{0.25} \quad (3.6)$$

$$h_{n,b} = 0.59 \left[ \frac{(\overline{T}_{o,b} - T_{amb})}{d} \right]^{0.25} \quad (3.7)$$



where  $h_n$  is the natural convection heat transfer coefficient between the outside surface of the adiabatic cotton and ambient,  $A$  is the outside surface area of adiabatic cotton,  $\overline{T}_o$  is the average temperature of the outer wall of the adiabatic cotton,  $T_{amb}$  is the temperature of the ambient, and  $d$  is the diameter of the evaporator, as schematically shown in Fig. 2.10. The relative heat loss from the evaporator is defined as

$$\varepsilon = \frac{(Q_t - Q_e)}{Q_t} \times 100 \% \quad (3.6)$$

From the thermocouple data measured at the outside surfaces of the adiabatic cotton covering the evaporator, the heat loss from the evaporator to the ambient is estimated. The results from this estimation show that the heat losses for all cases investigated here are all less than 3.0 %.

### 3.2 Thermodynamic States and Heat Transfer Limitation

As discussed in chapter 1, CPL is a two-phase liquid-vapor heat transport device composing an evaporator with wick structure, condenser, reservoir, and distinct liquid and vapor lines. There is no reservoir element in the present study. Figure 3.1(a) schematically shows a typical CPL system without reservoir. The corresponding thermodynamic states of the working fluid at various locations of the CPL are indicated in Fig. 3.1(b). At location 1 (the wick-copper block contacted heating zone), liquid vaporizes at the saturation state and the vapor moves through the grooves, resulting in some pressure loss and the vapor becomes superheated at location 2. The vapor finally flows into the vapor line. Some pressure loss also results in the vapor line as the vapor moves through it and the vapor is still superheated at location 3. Upon entering the condenser, the vapor condensation occurs. Thus we have two-phase liquid-vapor mixture at locations 4 and 5. Beyond location 5, all vapor is condensed and the working fluid is in liquid state. The working fluid continues to cool down in the condenser and reaches a subcooled temperature at the condenser exit at location 7. The liquid flows back to the evaporator through the liquid line, accompanying with some pressure loss. At the inlet of the evaporator (location 8) the liquid is subcooled. As the liquid moves into the wick, it gets heated. Boiling and evaporation take place near the wick- copper block contacted region at location 9. This complete the thermodynamic cycle for the CPL.

The heat transfer limits of a CPL are similar to that of heat pipe. The major heat transport limits for a CPL are:

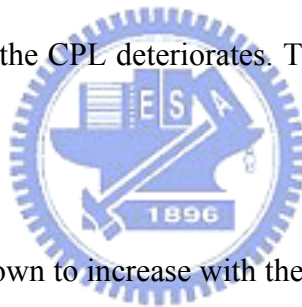
1) Capillary limit:

In a normal CPL operation, the wick structure should produce sufficient capillary force to drive the vapor and liquid flows. For a raise in the heat input to the evaporator, the liquid and vapor flows speed up, leading to an increase in the flow

resistance as the menisci form at the liquid/vapor interface. This means that the capillary force should be high enough to circulate the flow of the working fluid along the loop. When the radii of curvature for the menisci get larger at a higher heat input so that they are equal to the capillary radius, the capillary pressure reaches a maximum level, resulting the so called “capillary limit”.

2) Boiling limit:

As the heat input to the evaporator exceeds certain value, boiling of liquid begins and vapor bubbles start to appear inside the wick structure. At a relatively high heat input bubbles are generated at a large size and at a vary high rate. The bubbles would block the wick structure and form a layer of vapor film in the contact zone. Therefore, the resulting thermal resistance becomes very large and heat transfer capability of the CPL deteriorates. This is designated as the “boiling limit”.



3) Sonic limit:

The vapor mass flux is known to increase with the magnitude of heat input. As the vapor speed arrives at the sonic point, the flow in the CPL will be choked, resulting the “sonic limit”.

4) Entrainment limit:

When the heat input increases and the vapor speed arrives at certain level, a vapor shear force exerts on the liquid at the vapor-liquid interface. If the shear force is large enough, surface tension of liquid will be overcome and certain amount of the liquid can be blown away to become fine droplets, resulting the so called “entrainment limit”. Because a CPL has distinct liquid and vapor lines, the entrainment phenomenon will not occur in this system.

### 3.3 System Pressure Drop Analysis

In view of the presence of the capillary limit, the maximum capillary pressure generated in the wick should be greater than or equal to the overall loop pressure drop for a CPL to function well. Hence,

$$\Delta P_{cap,max} \geq \Delta P_v + \Delta P_l + \Delta P_{vg} + \Delta P_w + \Delta P_g \quad (3.7)$$

here  $\Delta P_{cap,max}$  is the maximum capillary pressure,  $\Delta P_v$  the total pressure drop in the vapor line,  $\Delta P_l$  the total pressure drop in the liquid line,  $\Delta P_{vg}$  the total pressure drop in the grooved channel,  $\Delta P_w$  the total pressure drop of fluid passing through the wick structure, and  $\Delta P_g$  the pressure drop due to the gravity. These terms are described in the following.

#### 3.3.1 Maximum capillary pressure

In steady CPL operation, the capillary pressure can be calculated from the contact angle of vapor-liquid interface  $\theta$ , working fluid surface tension  $\sigma$  and effective capillary radius  $r_c$ . When the contact angle is equal to zero, we obtain a maximum capillary pressure. In that case, the curvature radius of the vapor-liquid interface is equal to the effective capillary radius. Specifically,

$$\Delta P_{cap} = \frac{2\sigma \cos \theta}{r_c} \quad (3.8)$$

When  $\theta = 0$ ,

$$\Delta P_{cap,max} = \frac{2\sigma}{r_c} \quad (3.9)$$

#### 3.3.2 Pressure drop in transport lines

The transport lines include the vapor line and liquid line. Note that in the transport lines the fluid flow in the tubes is assumed to be fully-developed. The total pressure drop in the tube due to the friction, the so called “major losses”, can be evaluated from the relation



$$\Delta P_{major} = f \frac{L}{D} \frac{\rho V^2}{2} \quad (3.10)$$

where  $f$  is the friction factor,  $L$  is the flow length,  $D$  is the tube diameter,  $\rho$  is the density of working fluid,  $V$  is the average speed of the working fluid.

If the flow is laminar and fully-developed for the Reynolds number  $\leq 2300$ , the friction factor can be expressed in a simple relation as

$$f = \frac{64}{Re} \quad (3.11)$$

For  $2300 < Re < 10,000$  the friction factor can be approximately evaluated from the Gnielinski correlation [35] as

$$f = (1.82 \log_{10} Re - 1.64)^{-2} \quad (3.12)$$

For  $Re > 10,000$  the flow can be considered as turbulent. When the tube is smooth and the flow is turbulent, the friction factor can be approximately evaluated from the Blasius correlation [36] as

$$f = \frac{0.316}{Re^{1/4}} \quad (3.13)$$



### 3.3.3 Pressure drop in grooved channels

The pressure drop of vapor which passes through grooves channel of evaporator

$$\Delta P_{vg} = f \frac{L}{D_h} \frac{\rho V^2}{2} \quad (3.14)$$

where  $L$  is the grooved channel length,  $D_h$  is the hydraulic diameter of grooved channel

### 3.3.4 Pressure drop in wick structure

According to the Darcy's law for a low speed single-phase liquid flow moving in a porous medium and assuming the flow being one-dimensional in  $z$ -direction and laminar, the flow speed can be approximated as

$$V_z = -\frac{K_w}{\mu_l} \left( \frac{\partial p}{\partial z} \right) \quad (3.15)$$

From the Conservation of Mass, we also have

$$V_z = \frac{\dot{m}}{\rho_l A_c} \quad (3.16)$$

Combining the above two equations gives

$$\Delta P_w = \frac{\mu_l \dot{m} \ell}{\rho_l A_c K_w} \quad (3.17)$$

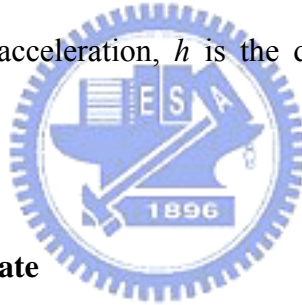
here  $K_w$  is the permeability of wick structure,  $\mu_l$  is the viscosity of the working fluid,  $\ell$  is the thickness of the wick structure,  $A_c$  is the cross-sectional area of the wick structure,  $\dot{m}$  is the mass flow rate, and  $V_z$  is the vertical flow velocity.

### 3.3.5 Pressure drop due to gravity

When a relative height between the evaporator and condenser exists, there is an effect of gravitational head. It can be calculated from the relation

$$\Delta P_g = \rho_l g h \quad (3.18)$$

where  $g$  is the gravitational acceleration,  $h$  is the difference in the heights of the evaporator and condenser.



### 3.4 Estimate of Mass Flow Rate

In a steady CPL operation, the energy balance for the evaporator can be expressed as

$$Q_e = Q_{h_{fg}} + Q_{C_p \Delta T} \quad (3.19)$$

Assume the sensible energy transfer is small compared with the latent energy transfer, the above equation can be written as

$$Q_e \approx Q_{h_{fg}} = \dot{m} h_{fg} \quad (3.20)$$

Thus the mass flow rate of the working flow in the CPL can be calculated from the relation

$$\dot{m} = \frac{Q_e}{h_{fg}} \quad (3.21)$$

here  $Q_e$  is the effective power input to the CPL,  $\dot{m}$  is the mass flow rate, and  $h_{fg}$  is

the latent heat of evaporation

Using this estimated mass flow rate in the above equations for the pressure drop analysis we can evaluate the pressure drops in each section of the CPL. The detailed results from this pressure drop analysis for selected cases are summarized in Tables 3.1-3.3. In these tables  $\Delta P_{tot}$  denotes the total pressure drop in the loop. Thus

$$\Delta P_{tot} = \Delta P_v + \Delta P_l + \Delta P_{vg} + \Delta P_w + \Delta P_g \quad (3.22)$$

Here  $\Delta P_{vg}$  is the vapor pressure drop in the grooved channels.

### 3.5 Uncertainty Analysis

Uncertainties of the thermal resistance are estimated according to the procedures proposed by Kline et al. [37]. The detailed results from this uncertainty analysis are summarized in Table 3.4.

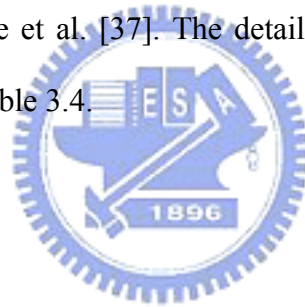


Table 3.1 Summary of the results from the pressure drop analysis for  $H_g=0$  cm at  $T_{\text{cold}}=25$  .

$Q_c$ (W)	$Re_l$	$Re_v$	$Re_{vg}$	$\Delta P_L$ (Pa)	$\Delta P_v$ (Pa)	$\Delta P_{vg}$ (Pa)	$\Delta P_{\text{wick}}$ (Pa)	$\Delta P_g$ (Pa)	$\Delta P_{\text{tot}}$ (Pa)	$\Delta P_{\text{cap,max}}$ (Pa)
8.38	1.11	97.26	32.78	0.32	88.42	24.89	0.34	0.00	113.97	6761.45
17.99	2.40	207.70	70.01	0.70	169.52	47.71	0.73	0.00	218.66	6719.97
27.79	3.74	319.08	107.55	1.07	236.02	66.43	1.12	0.00	304.64	6675.39
37.93	5.16	432.79	145.88	1.46	293.05	82.48	1.52	0.00	378.51	6626.95
47.88	6.55	543.89	183.33	1.84	348.05	97.96	1.92	0.00	449.77	6590.14
57.76	7.94	651.99	219.77	2.22	389.08	109.51	2.32	0.00	503.14	6536.94
67.78	9.35	760.19	256.24	2.61	426.81	120.13	2.73	0.00	552.29	6483.97
77.38	10.72	863.89	291.20	2.98	465.34	130.98	3.12	0.00	602.42	6445.77
87.04	12.07	968.06	326.31	3.37	503.88	141.83	3.52	0.00	652.59	6413.61
97.37	13.49	1079.43	363.85	3.78	545.65	153.58	3.95	0.00	706.97	6385.94
107.26	14.85	1182.12	398.47	4.20	567.77	159.81	4.39	0.00	736.16	6336.64
116.98	16.16	1285.94	433.46	4.60	604.45	170.13	4.81	0.00	783.98	6314.84
126.13	17.46	1382.19	465.91	4.97	633.44	178.29	5.19	0.00	821.88	6287.43
136.63	18.93	1493.56	503.45	5.39	672.82	189.38	5.63	0.00	873.22	6266.59
145.47	20.51	1582.75	533.51	5.67	695.10	195.65	5.92	0.00	902.34	6225.98
155.34	21.82	1686.00	568.31	6.09	735.01	206.88	6.36	0.00	954.34	6204.51
166.00	23.21	1797.16	605.78	6.55	782.07	220.13	6.85	0.00	1015.60	6182.77

Table 3.2 Summary of the results from the pressure drop analysis for  $H_g=5$  cm at  $T_{\text{cold}}=25$  .

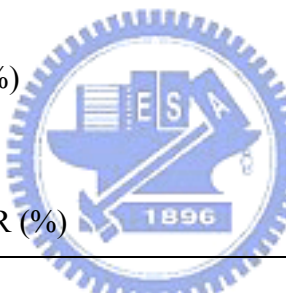
$Q_c$ (W)	$Re_l$	$Re_v$	$Re_{vg}$	$\Delta P_l$ (Pa)	$\Delta P_v$ (Pa)	$\Delta P_{vg}$ (Pa)	$\Delta P_{\text{wick}}$ (Pa)	$\Delta P_g$ (Pa)	$\Delta P_{\text{tot}}$ (Pa)	$\Delta P_{\text{cap,max}}$ (Pa)
8.40	1.12	97.26	32.78	0.32	84.44	23.77	0.34	-489.55	-380.68	6744.47
18.00	2.44	207.67	70.00	0.69	167.83	47.24	0.72	-489.54	-273.07	6715.83
27.69	3.79	318.01	107.19	1.05	236.97	66.70	1.10	-489.53	-183.72	6679.02
37.88	5.18	432.84	145.90	1.44	298.01	83.88	1.51	-489.53	-104.69	6636.84
47.94	6.57	545.37	183.83	1.83	354.56	99.80	1.92	-489.53	-31.43	6600.98
57.67	7.87	651.84	219.72	2.23	394.32	110.99	2.33	-489.54	20.33	6547.99
67.67	9.21	761.11	256.55	2.63	438.79	123.50	2.75	-489.54	78.13	6507.57
77.32	10.56	865.47	291.73	3.02	477.01	134.26	3.15	-489.54	127.90	6467.05
87.04	11.91	969.76	326.88	3.41	512.77	144.33	3.56	-489.54	174.52	6428.42
97.42	13.38	1080.92	364.36	3.82	550.70	155.00	3.99	-489.54	223.96	6393.36
107.48	14.81	1188.26	400.54	4.21	586.64	165.12	4.40	-489.54	270.83	6363.40
117.20	16.26	1290.84	435.11	4.58	616.55	173.54	4.78	-489.54	309.91	6331.10
126.28	17.62	1385.67	467.08	4.93	641.50	180.56	5.15	-489.53	342.60	6298.73
136.78	19.14	1495.79	504.20	5.34	675.58	190.15	5.58	-489.53	387.11	6269.93
145.36	20.29	1584.46	534.09	5.71	701.76	197.52	5.96	-489.54	421.42	6241.97
155.30	21.64	1687.07	568.68	6.13	736.99	207.44	6.41	-489.54	467.42	6212.18
166.07	23.17	1798.61	606.27	6.57	782.60	220.28	6.86	-489.54	526.77	6185.64
175.54	24.55	1896.58	639.30	6.94	828.42	233.17	7.26	-489.54	586.26	6164.60
184.96	25.98	1991.13	671.17	7.31	887.21	249.72	7.64	-489.54	662.35	6132.92
194.56	27.27	2090.46	704.65	7.72	949.06	267.13	8.07	-489.54	742.44	6115.85
206.06	28.94	2207.06	743.95	8.19	1046.41	294.53	8.56	-489.54	868.15	6088.13

Table 3.3 Summary of the results from the pressure drop analysis for  $H_g=10$  cm at  $T_{\text{cold}}=25$  .

$Q_c$ (W)	$Re_l$	$Re_v$	$Re_{vg}$	$\Delta P_l$ (Pa)	$\Delta P_v$ (Pa)	$\Delta P_{vg}$ (Pa)	$\Delta P_{\text{wick}}$ (Pa)	$\Delta P_g$ (Pa)	$\Delta P_{\text{tot}}$ (Pa)	$\Delta P_{\text{cap,max}}$ (Pa)
8.40	1.38	123.27	32.83	0.42	110.40	24.55	0.35	-979.15	-843.42	6756.04
18.00	3.03	263.69	70.23	0.88	227.40	50.57	0.73	-979.10	-699.52	6741.93
27.80	4.72	406.01	108.13	1.35	329.28	73.23	1.12	-979.09	-574.11	6717.32
38.00	6.53	553.20	147.34	1.83	423.08	94.09	1.51	-979.07	-458.55	6691.42
48.00	8.31	696.76	185.57	2.31	508.64	113.12	1.90	-979.06	-353.09	6668.75
57.88	10.11	837.79	223.13	2.77	584.71	130.04	2.28	-979.05	-259.25	6644.65
67.97	11.94	981.37	261.37	3.24	661.96	147.22	2.67	-979.04	-163.96	6624.60
77.65	13.67	1117.01	297.50	3.70	719.51	160.02	3.06	-979.04	-92.75	6594.69
87.38	15.34	1253.39	333.82	4.19	780.54	173.59	3.46	-979.05	-17.26	6570.45
97.82	17.03	1397.72	372.26	4.75	835.67	185.85	3.92	-979.07	51.13	6538.49
107.76	18.77	1535.56	408.97	5.25	894.34	198.90	4.33	-979.07	123.75	6516.44
117.47	20.28	1666.01	443.72	5.80	928.37	206.46	4.79	-979.09	166.33	6477.12
126.57	21.77	1789.58	476.62	6.29	969.51	215.61	5.20	-979.10	217.51	6451.12
137.15	23.59	1935.67	515.54	6.83	1031.91	229.49	5.64	-979.10	294.78	6436.08
145.92	25.12	2052.33	546.61	7.29	1060.31	235.81	6.02	-979.10	330.32	6406.57
155.92	26.87	2187.78	582.68	7.80	1107.17	246.23	6.44	-979.10	388.54	6387.02
166.62	28.77	2331.66	621.00	8.34	2082.18	256.14	6.89	-979.10	1374.46	6363.92
175.90	30.44	2454.42	653.70	8.82	2209.30	262.87	7.28	-979.10	1509.17	6339.28
185.59	32.21	2582.01	687.68	9.30	2342.96	269.71	7.68	-979.10	1650.55	6314.08
195.11	33.85	2708.50	721.36	9.81	2491.92	278.00	8.10	-979.10	1808.73	6295.35
206.63	35.88	2862.99	762.51	10.40	2693.60	289.72	8.59	-979.10	2023.21	6279.10
215.62	37.46	2980.22	793.73	10.87	2832.56	296.69	8.98	-979.10	2170.00	6258.11
227.30	39.53	3135.38	835.06	11.47	3047.37	308.62	9.47	-979.10	2397.83	6240.78
232.34	40.46	3200.02	852.27	11.73	3130.63	312.77	9.69	-979.10	2485.72	6227.54
241.93	42.22	3325.56	885.71	12.22	3316.13	322.90	10.09	-979.10	2682.23	6210.30

Table 3.4 Summary of the uncertainty analysis

<b>Parameter</b>	<b>Uncertainty</b>
Length of grooved copper block (m)	$\pm 0.0005$
Width of grooved copper block (m)	$\pm 0.0005$
Thickness of grooved copper block (m)	$\pm 0.0005$
Dimensions of grooved channel (m)	$\pm 0.00005$
Temperature, T ( )	$\pm 0.2$
Temperature difference, $\Delta T$ ( )	$\pm 0.28$
Current, I (%)	$\pm 0.206$
Voltage, V (%)	$\pm 0.05$
Total heat load, $Q_t$ (%)	$\pm 0.212$
Heat loss, $Q_{loss}$ (%)	$\pm 10.2$
Thermal resistance, R (%)	$\pm 11.1$







## CHAPTER 4

### RESULTS AND DISCUSSION

This chapter presents selected data obtained in the present investigation of an improved capillary pumped loop system aiming at the high power density CPU cooling through covering a thin cotton gauze layer on the side and bottom walls of the grooved channels. The effects of the liquid inventory, cooling water temperature in the condenser, and relative height between the evaporator and condenser on the heat transfer performance of the CPL are to be examined. Besides, the mean evaporator temperature ( $\bar{T}_{evap}$ ) and condenser temperature ( $\bar{T}_{cond}$ ), which are the average temperatures measured at selected locations in the grooved copper block and the condenser (double-tube heat exchanger) and the temperature of the working fluid measured at the inlets and exits of the evaporator and condenser shown in Figs. 2.2 and 2.9 will be inspected. It should be mentioned that an experimental test of the CPL system will be terminated as the mean evaporator temperature exceeds 80 °C.

Before examining the present data, it should be pointed out that the temperature oscillation in the evaporator is relatively small in the CPL system tested here, unlike that observed in the large CPL systems employed in the space applications. Thus the data for the time variations of  $T_{evap}$  are not presented here.

#### 4.1 Effects of Liquid Inventory

The effects of the liquid inventory, which is defined as the ratio of the total liquid volume of the working fluid input to CPL to the total loop volume available for the working fluid are examined first. Table 4.1 shows the volume of each component in the CPL system available for the working fluid to pass through. Here in the tests of

the liquid inventory effects, the cooling water temperature in the condenser is set at 25 °C and the relative height between the evaporator and condenser is fixed at 0 cm. The liquid inventory is varied from 50% to 75%. Besides, in the tests the side and bottom walls of the grooved channels are not covered with the thin cotton gauze layer except in section 4.4 where the effects of the gauze layer covering are investigated. The measured data for the variations of the mean evaporator and condenser temperatures and the temperatures at the evaporator and condenser inlets and exits along with the thermal resistances of the CPL with the power input to the evaporator are shown in Figs. 4.1- 4.5 for various liquid inventories. It is first noted from Figs. 4.1(a)-4.5(a) that in the sections where the vapor flow dominates at the evaporator outlet and condenser inlet the measured temperatures increase significantly with  $Q_e$ , so does the evaporator temperature. While at the condenser outlet and evaporator inlet the liquid flow prevails, the measured temperatures are close to the saturated value. We also note from Figs. 4.1(b)-4.5(b) that the thermal resistance of the loop decreases substantially with the power input to the evaporator except at the lower liquid inventory of 50%. A close examination of the data given in Fig. 4.6 reveals that for  $Q_e > 30\text{W}$  the thermal resistance of the loop is only slightly affected by the liquid inventory when the liquid inventory is below 62%. But at the higher liquid inventories of 70% and 75% the thermal resistance is higher. It is important to further note that at the liquid inventory of 62% the power input to the evaporator can be increased to 166W before  $T_{\text{evap}}$  exceeds 80 °C. This power input is designated as the maximum allowable power input to the CPL for the given liquid inventory and  $T_{\text{cold}}$ . The maximum allowable power input to the evaporator  $Q_{e,\text{max}}$ , however, reduces to a significant amount when the liquid inventory is lowered to 57% and 50% or is raised to 70% and 75%. More specifically, at the low inventory of 50% the maximum power input  $Q_{e,\text{max}}$  is only 100W. This large reduction in  $Q_{e,\text{max}}$  is attributed to the dryout of

the liquid in the wick due to the insufficient liquid supply from the liquid line at this small liquid inventory. The evaporator thus rises sharply to exceed 80 at this low  $Q_{e,max}$ . For the high inventories of 70% and 75% the maximum power input to the evaporator are respectively reduced to 107W and 68W. This is the direct consequence of the flooding of the grooved channels at these high liquid inventories. Besides, the liquid appears in the vapor transport line and the CPL operation is somewhat abnormal. Hence at these high liquid inventories the vaporization of the working fluid near the contact surface between the wick and grooved copper block is retarded to a significant degree, causing the deterioration of phase change heat transfer in the evaporator. The above results clearly manifest that an optimal liquid inventory exists for the heat transfer performance of the CPL.

#### 4.2 Effects of the Cooling Water Temperature in the Condenser

Next, results are presented to illustrate the effects of the cooling water temperature in the condenser on the performance of the CPL. The measured data are shown in Figs. 4.7-4.11 for various cooling water temperatures in the condenser for the liquid inventory set at 62% and the relative height between the evaporator and condenser fixed at 0 cm. The results in Fig. 4.7 for  $T_{cold}=20$  indicate that the thermal resistance of the loop decrease significantly with the power input to the evaporator. Similar trends are noted in Figs. 4.8 and 4.9 for the cooling water temperature in the condenser of 25 and 30 . But for the high  $T_{cold}$  of 40 the thermal resistance of the loop only changes slightly with  $Q_e$ . A close inspection of the data given in Fig.4.11 reveals that the maximum allowable power input to the evaporator  $Q_{e,max}$  is lowered to a certain degree for an increase in the cooling water temperature in the condenser. This is conjectured to result from the higher pressure in the condenser for a higher  $T_{cold}$ . Consequently, the pressure difference between the

evaporator and condenser is smaller. This, in turn, results in a lower vapor flow rate in the vapor line and heat transfer in the evaporator is retarded to some extent. Besides, at a higher  $T_{\text{cold}}$  the mean evaporator temperature is slightly higher. It is further noted that for  $T_{\text{cold}} = 30$  the thermal resistance of the loop is only slightly affected by the cooling water temperature in the condenser except at low  $Q_e$  ( $< 60\text{W}$ ).

### 4.3 Effects of the Relative Height between the Evaporator and Condenser

Then, how the relative height between the condenser and evaporator affects the performance of the CPL is examined. The results are presented in Figs. 4.12-4.22 for the cooling water in the condenser set at  $25$  for various relative heights and liquid inventories. Note that for all liquid inventories tested here the thermal resistance of the loop reduces to a noticeable degree for an increase in the height between the condenser and evaporator except at the low liquid inventory of 50%. Most importantly, the maximum allowable power input to the evaporator is substantially augmented when the relative height is increased, as evident from the data given in Figs. 4.13, 4.15, 4.17, 4.19 and 4.21. Moreover, for given  $Q_e$  and liquid inventory the mean evaporator temperature is considerably lower for a larger relative height.

It is of interest to investigate the effects of the liquid inventory on the performance of the CPL for different relative heights between the condenser and evaporator. This is illustrated in Fig. 4.22. The results indicate that the liquid inventory exhibits slighter effects on the CPL performance for a larger relative height. But for all condenser-evaporator relative heights tested here highest  $Q_{e,\text{max}}$  all appears for the liquid inventory of 62%. Note that at this optimal liquid inventory  $Q_{e,\text{max}}$  can reach 242W for the condenser-evaporator relative height of 10 cm.

A close inspection of the data given in Figs. 4.12-4.21 reveals that at the liquid inventory of 62% and at  $Q_{e,\text{max}}$  the thermal resistance of the loop reduces significantly

from 0.30 W to 0.20 W when the relative height is increased from 0 cm to 10 cm. While the corresponding maximum allowable power input to the evaporator is increased from 166W to 242W. Similar situation is noted for other liquid inventories.

The profound influences of the relative height between the condenser and evaporator on the CPL performance presented above can be attributed to the large increase in the gravitational force acting on the downward liquid flow in the liquid transport line for an increase in the relative height. Thus the liquid supply to the wick is greatly enhanced by the relative height increase, which can significantly augment the heat transfer capacity of the evaporator and  $Q_{e,max}$ . Besides, the thermal resistance of the loop is reduced substantially.

We move further to illustrate the effects of the condenser-evaporator relative height on the CPL performance for different cooling water temperatures in the condenser in Figs. 4.23-4.30 for the liquid inventory of 62%. Similar trends are noted from these data. But at the high  $T_{cold}$  of 40 the thermal resistance of the loop is less affected by the relative condenser-evaporator height (Fig. 4.30(b)).

Figure 4.31 shows the influence of  $T_{cold}$  on the CPL performance at different relative condenser-evaporator heights. The results indicate that for a larger relative height the thermal resistance of the loop is less affected by  $T_{cold}$ . But the opposite is the case for the mean evaporator temperature.

#### **4.4 Effects of Covering Cotton Gauze Layer on Grooved Channel Surfaces**

Finally, the CPL performance affected by covering thin layers of cotton gauze on the vertical and bottom surfaces of the grooved channels on the copper block shown in Fig. 2.8 are investigated. The data obtained in this investigation are presented in Figs. 4.32-4.37 for the cooling water temperature in the condenser set at 25 . Comparing the data in Figs. 4.32-4.36 for the variations of the mean evaporator

temperature and loop thermal resistance with  $Q_e$  for the same liquid inventory and same relative height between the condenser and evaporator for the cases with and without the covering of the cotton gauze layers on the grooved channel surfaces shows that the cotton gauze layer covering can somewhat lower the mean evaporator temperature and loop thermal resistance and can substantially increase the maximum allowable power input to the evaporator for most cases. Besides, the effects of the relative condenser-evaporator height on the evaporator temperature and loop thermal resistance are less pronounced for the CPL system with the cotton gauze covering.

To further illustrate the effects of the cotton gauze layer covering on the CPL performance, the measured data for different cooling water temperatures in the condenser are shown in Figs. 4.38-4.41 for the liquid inventory of 62%. Comparing the data in Figs. 4.38-4.41 for the variations of the mean evaporator temperature and loop thermal resistance with  $Q_e$  for the same cooling water temperature in the condenser and same relative height between the condenser and evaporator for the cases with and without the covering of the cotton gauze on the grooved channel surfaces exhibits similar trends to that observed in Figs. 4.32-4.37.

To be more clear on the effects of the cotton gauze layer covering, the above data for the maximum allowable power input to the evaporator and the minimum obtainable thermal resistance of the loop are summarized in Fig. 4.42 and Tables 4.2-4.5. The results clearly indicate that with the cotton gauze layer covering the maximum power input to the evaporator is still the highest and the loop thermal resistance is still the lowest at the liquid inventory of 62%, as that without the cotton gauze layer covering. Besides, at the relative condenser-evaporator height of 0 cm we have the largest increase in  $Q_{e,max}$  through the cotton gauze layer covering at the liquid inventory of 62%. But at the relative height of 5 cm the largest increase occurs at the low liquid inventory of 50%. At the large relative height of 10 cm substantial

augmentation in  $Q_{e,max}$  appears at low inventory of 50% and high inventory of 75%.

#### 4.5 Correlation Equations

It is realized that the qualitative trends of the correlations for  $Q_{e,max}$  and  $R_{th,min}$  can be guided by the simple pressure drop analysis given in Chapter 3. As discussed in chapter 3, the maximum capillary pressure generated in the wick should be greater than or equal to the overall loop pressure drop for a CPL to function well, that is

$$\Delta P_{cap,max} \geq \Delta P_v + \Delta P_l + \Delta P_{vg} + \Delta P_w + \Delta P_g \quad (4.1)$$

where

$$\Delta P_{cap,max} = \frac{2\sigma}{r_c} \quad (4.2)$$

$$\Delta P_v = f \frac{L_v}{D_v} \frac{\rho_v V_v^2}{2} \quad (4.3)$$

$$\Delta P_l = f \frac{L_l}{D_l} \frac{\rho_l V_l^2}{2} \quad (4.4)$$

$$\Delta P_{vg} = f \frac{L_{vg}}{D_{\bullet,g}} \frac{\rho_v V_v^2}{2} \quad (4.5)$$

$$\Delta P_w = \frac{\mu_l m \ell}{\rho_l A_c K_w} \quad (4.6)$$

$$\Delta P_g = \rho_l g h \quad (4.7)$$

If the flow is laminar and fully-developed for the Reynolds number  $\leq 2300$ , the friction factor can be expressed in a simple relation as

$$f = \frac{64}{Re} \quad (4.8)$$

For  $2300 < Re < 10,000$  the friction factor can be approximately evaluated from the Gnielinski correlation [35] as

$$f = (1.82 \log_{10} Re - 1.64)^{-2} \quad (4.9)$$



For  $Re > 10,000$  the flow can be considered as turbulent, the friction factor can be approximately evaluated from the Blasius correlation [36] as

$$f = \frac{0.316}{Re^{1/4}} \quad (4.10)$$

In addition, the mass flow rate of the CPL may be written as

$$\dot{m} = \frac{Q_e}{h_{fg}}$$

Combining the above equations and introducing some empirical constants  $C_1$  to  $C_4$  for each term in Equation (4.1) gives

$$\frac{2\sigma}{r_c} \geq C_1 \frac{\mu_v Q_e L_v}{D_v^4 h_{fg} \rho_v} + C_2 \frac{\mu_l Q_e L_l}{D_l^4 h_{fg} \rho_l} + C_3 \frac{\mu_v Q_e L_{vg}}{D_{vg}^4 h_{fg} \rho_v} + C_4 \frac{\mu_l Q_e \ell}{\rho_l h_{fg} A_c K_w} + \rho_l g h \quad (4.11)$$

Rearranging above equation provides an indication for the approximate upper limit of  $Q_e$ ,

$$Q_e \leq \frac{\frac{2\sigma}{r_c} - \rho_l g h}{C_1 \frac{\mu_v L_v}{D_v^4 h_{fg} \rho_v} + C_2 \frac{\mu_l L_l}{D_l^4 h_{fg} \rho_l} + C_3 \frac{\mu_v L_{vg}}{D_{vg}^4 h_{fg} \rho_v} + C_4 \frac{\mu_l \ell}{\rho_l h_{fg} A_c K_w}} \quad (4.12)$$

According to the present experimental data for the CPL system under normal operation, empirical correlations for the maximum allowable power input  $Q_{e,max}$  to the evaporator of the CPL is proposed here. The maximum power input  $Q_{e,max}$  for the CPL with and without cotton layer gauze covering are respectively correlated by selecting the proper values for the empirical constants  $C_1$ ,  $C_2$ ,  $C_3$  and  $C_4$  appearing in Eq. (4.12) as

$$Q_{e,max} = \frac{\frac{2\sigma}{r_c} - \rho_l g h}{0.55 \frac{\mu_v L_v}{D_v^4 h_{fg} \rho_v} + 0.12 \frac{\mu_l L_l}{D_l^4 h_{fg} \rho_l} + 28 \frac{\mu_v L_{vg}}{D_{vg}^4 h_{fg} \rho_v} - 1.25 \frac{\mu_l \ell}{\rho_l h_{fg} A_c K_w}} \cdot L_{mv}^{0.03} \quad (4.13)$$

and



$$Q_{e,\max} = \frac{\frac{2\sigma}{r_c} - \rho_l gh}{0.49 \frac{\mu_v L_v}{D_v^4 h_{fg} \rho_v} + 0.25 \frac{\mu_l L_l}{D_l^4 h_{fg} \rho_l} + 30 \frac{\mu_v L_{vg}}{D_{vg}^4 h_{fg} \rho_v} - 1.24 \frac{\mu_l \ell}{\rho_l h_{fg} A_c K_w}} \cdot L_{inv}^{0.1} \cdot F_{gu} \quad (4.14)$$

where  $L_{inv}$  is the liquid inventory. Besides, a dimensionless factor  $F_{gu}$  is used to account for the effect of covering cotton gauze layers on the side and bottom walls of the grooved channels and it is defined as

$$F_{gu} = \left( \frac{\delta}{h_g} \right)^{-0.18} \cdot \left( \frac{N \cdot A_{fin,top}}{(N-1) \cdot A_g} \right)^{0.5} \quad (4.15)$$

where  $\delta$  is the cotton gauze layer thickness,  $h_g$  is the grooved channels height,  $N$  is the total number of grooved channels on the evaporator,  $A_{fin,top}$  is the top surface area of a single fin, and  $A_g$  is the total surface area of a single grooved channel. The proposed correlations are compared with the present data in Figs. 4.43 and 4.44. The comparison indicates that most of our data are within  $\pm 25\%$  of the values predicted from the above empirical equations. The corresponding standard deviations of the above two correlations are 8.4% and 5.8%, respectively.

Then, empirical correlations for the minimum thermal resistance  $R_{th,min}$  of the CPL are proposed as

$$R_{th,min} = \frac{(\bar{T}_{exp} - \bar{T}_{cond})}{\left[ \frac{\frac{2\sigma}{r_c} - \rho_l gh}{0.55 \frac{\mu_v L_v}{D_v^4 h_{fg} \rho_v} + 0.12 \frac{\mu_l L_l}{D_l^4 h_{fg} \rho_l} + 28 \frac{\mu_v L_{vg}}{D_{vg}^4 h_{fg} \rho_v} - 1.25 \frac{\mu_l \ell}{\rho_l h_{fg} A_c K_w}} \cdot L_{tw}^{0.03} \right]} \quad (4.16)$$

for the CPL without the cotton gauze layer covering and

$$R_{h,\min} = \frac{(\bar{T}_{\text{exp}} - \bar{T}_{\text{cond}})}{\left[ \frac{\frac{2\sigma}{r_c} - \rho_l g h}{0.49 \frac{\mu L_v}{D_v^4 h_{jg} \rho_v} + 0.25 \frac{\mu L_l}{D_l^4 h_{jg} \rho_l} + 30 \frac{\mu L_{vg}}{D_{vg}^4 h_{jg} \rho_v} - 1.24 \frac{\mu \ell}{\rho_l h_{jg} A K_w}} \cdot L_{tw}^{0.1} \cdot F_{gu} \right]} \quad (4.17)$$

for the CPL with the cotton gauze layer covering. In the above two equations  $\bar{T}_{\text{evap}}$  is the mean evaporator temperature and  $\bar{T}_{\text{cond}}$  is the mean condenser temperature. Figures 4.45 and 4.46 shows that the present experimental data fall with  $\pm 25\%$  of the correlations given in Eqs. (4.16) and (4.17). The corresponding standard deviations of the above two correlations are 8.1% and 5.7%, respectively.



Table 4.1 Volume of each component in the CPL system.

Component		Volume (cm <sup>3</sup> )
Evaporator	liquid storage	7.5
	grooved channel	2
Condenser		5.5
Liquid line		12.5
Vapor line		12.5
Total		40



Table 4.2 Maximum obtainable power input to the evaporator for various liquid inventories and relation condenser-evaporator heights at  $T_{\text{cold}}=25$  for the CPL without cotton gauze covering.

Liquid inventory \ Relative height	(50%)	(57%)	(62%)	(70%)	(75%)
	0 cm	97W	145W	166W	107W
5 cm	136W	195W	206W	155W	136W
10 cm	215W	227W	242W	185W	175W

Table 4.3 Maximum obtainable power input to the evaporator for various liquid inventories and relation condenser-evaporator heights at  $T_{\text{cold}}=25$  for the CPL with cotton gauze covering.

Liquid inventory \ Relative height	(50%)	(57%)	(62%)	(70%)	(75%)
	0 cm	107W	195W	207W	136W
5 cm	206W	215W	215W	176W	155W
10 cm	228W	244W	242W	220W	195W

Table 4.4 Maximum obtainable power input to the evaporator for various cooling water temperatures in the condenser and relative condenser-evaporator heights for the liquid inventory of 62% for the CPL without cotton gauze covering.

Cooling water temperature \ Relative height	20	25	30	40
	0 cm	175W	166W	155W
5 cm	206W	206W	184W	184W
10 cm	254W	242W	237W	227W

Table 4.5 Maximum obtainable power input to the evaporator for various cooling water temperatures in the condenser and relative condenser-evaporator heights for the liquid inventory of 62% for the CPL with cotton gauze covering.

Cooling water temperature \ Relative height	20	25 )	30	40
	0 cm	210W	207W	206W
5 cm	221W	215W	215W	215W
10 cm	255W	244W	242W	232W

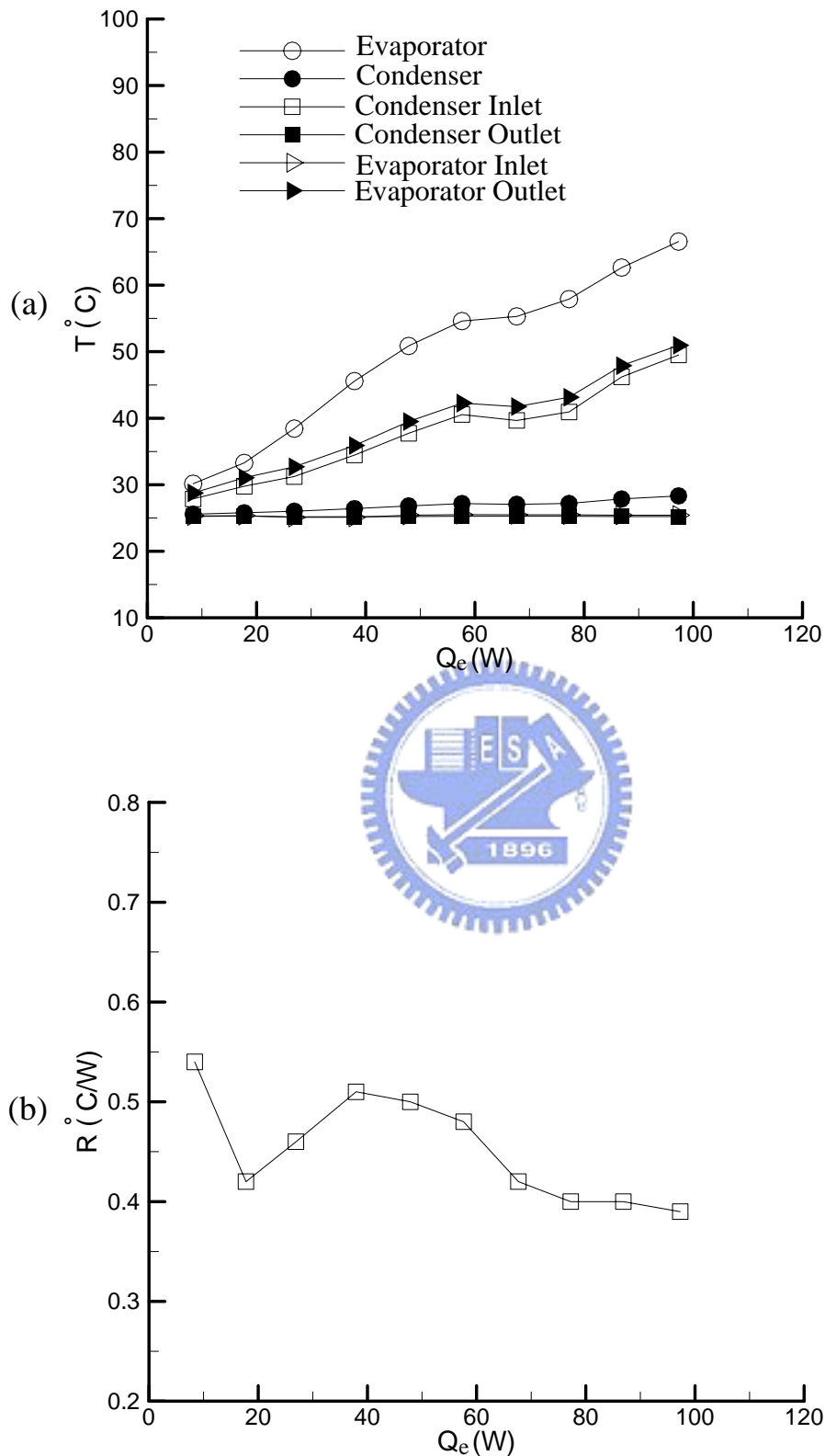


Fig. 4.1 Variations of the temperature at various locations in the CPL (a) and thermal resistance of the CPL (b) with the input power to the evaporator for the cooling water temperature in the condenser  $T_{\text{cold}} = 25$  , liquid inventory of 50% and relative height between condenser and evaporator of 0 cm.



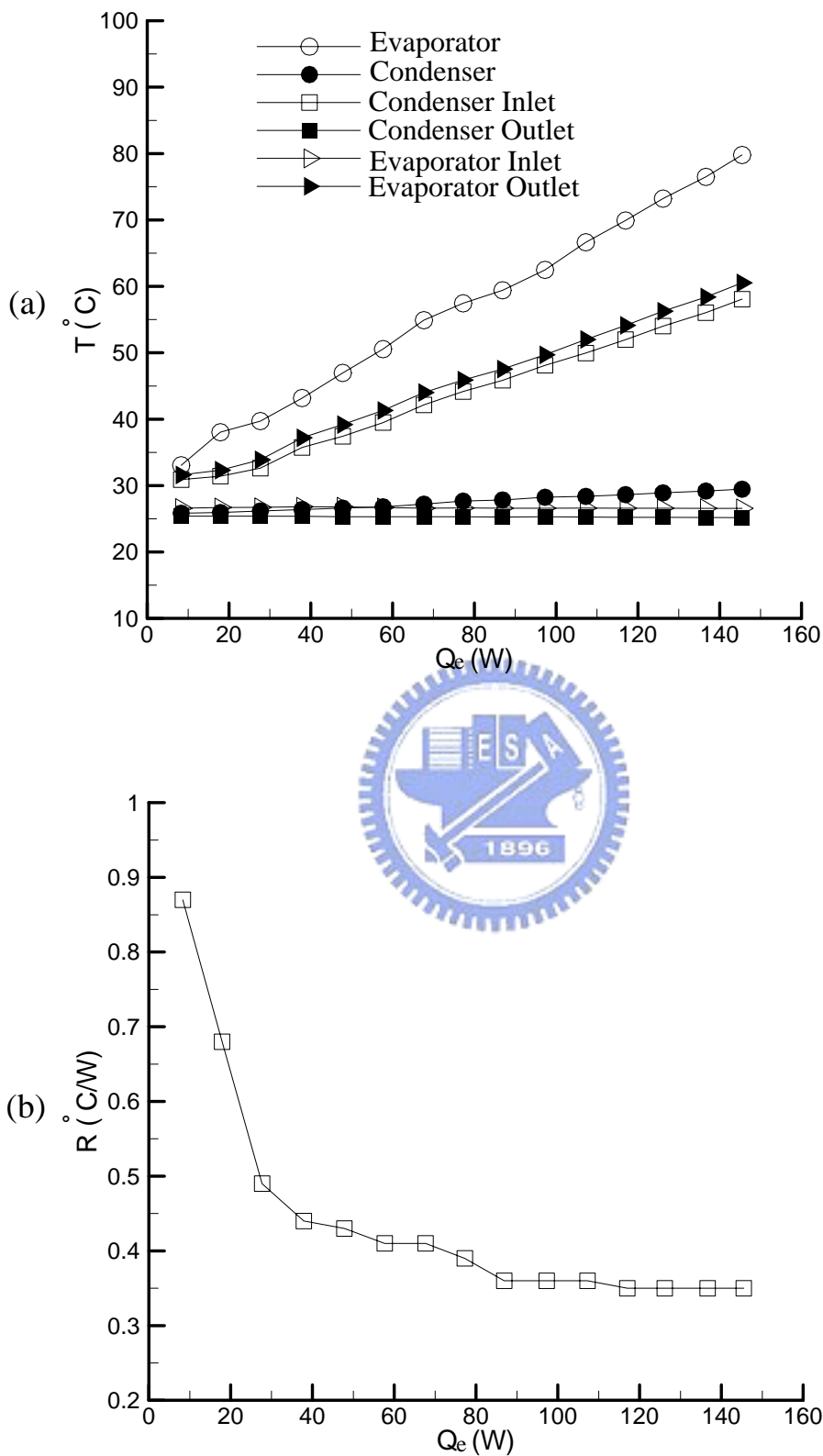


Fig. 4.2 Variations of the temperature at various locations in the CPL (a) and thermal resistance of the CPL (b) with the input power to the evaporator for the cooling water temperature in the condenser  $T_{\text{cold}} = 25$  , liquid inventory of 57% and relative height between condenser and evaporator of 0 cm.

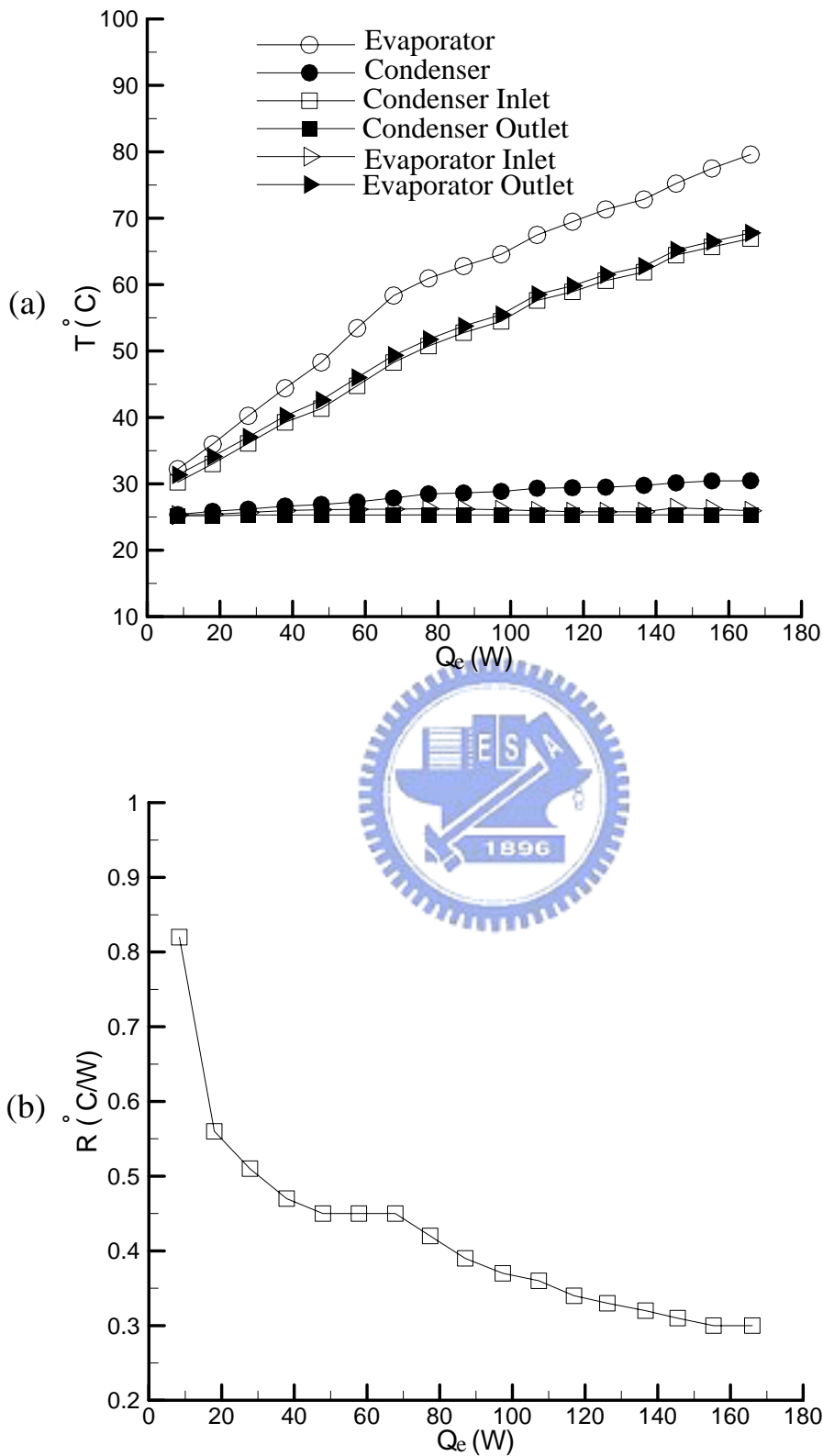


Fig. 4.3 Variations of the temperature at various locations in the CPL (a) and thermal resistance of the CPL (b) with the input power to the evaporator for the cooling water temperature in the condenser  $T_{\text{cold}} = 25$  , liquid inventory of 62% and relative height between condenser and evaporator of 0 cm.

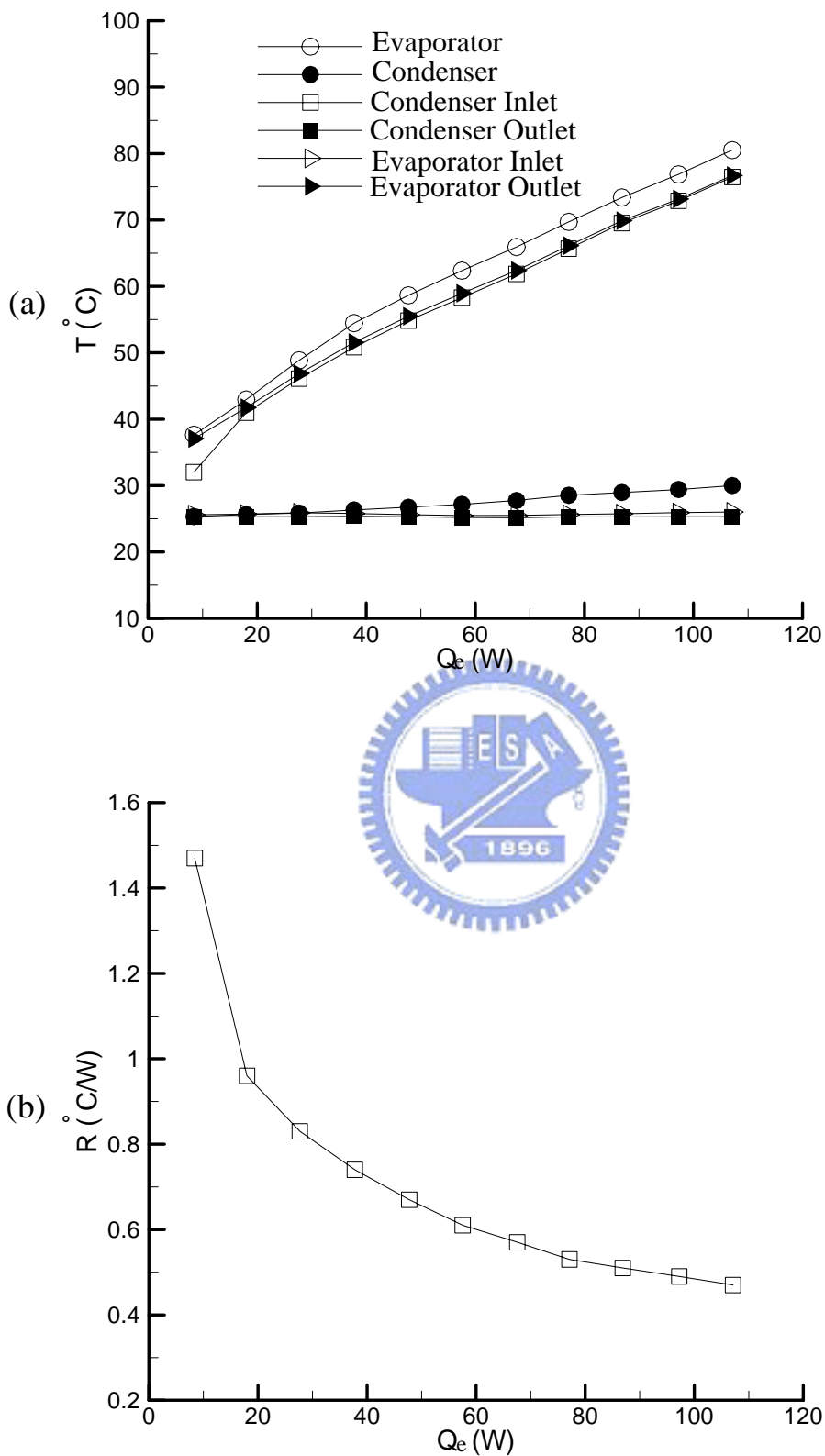


Fig. 4.4 Variations of the temperature at various locations in the CPL (a) and thermal resistance of the CPL (b) with the input power to the evaporator for the cooling water temperature in the condenser  $T_{\text{cold}} = 25$  , liquid inventory of 70% and relative height between condenser and evaporator of 0 cm.

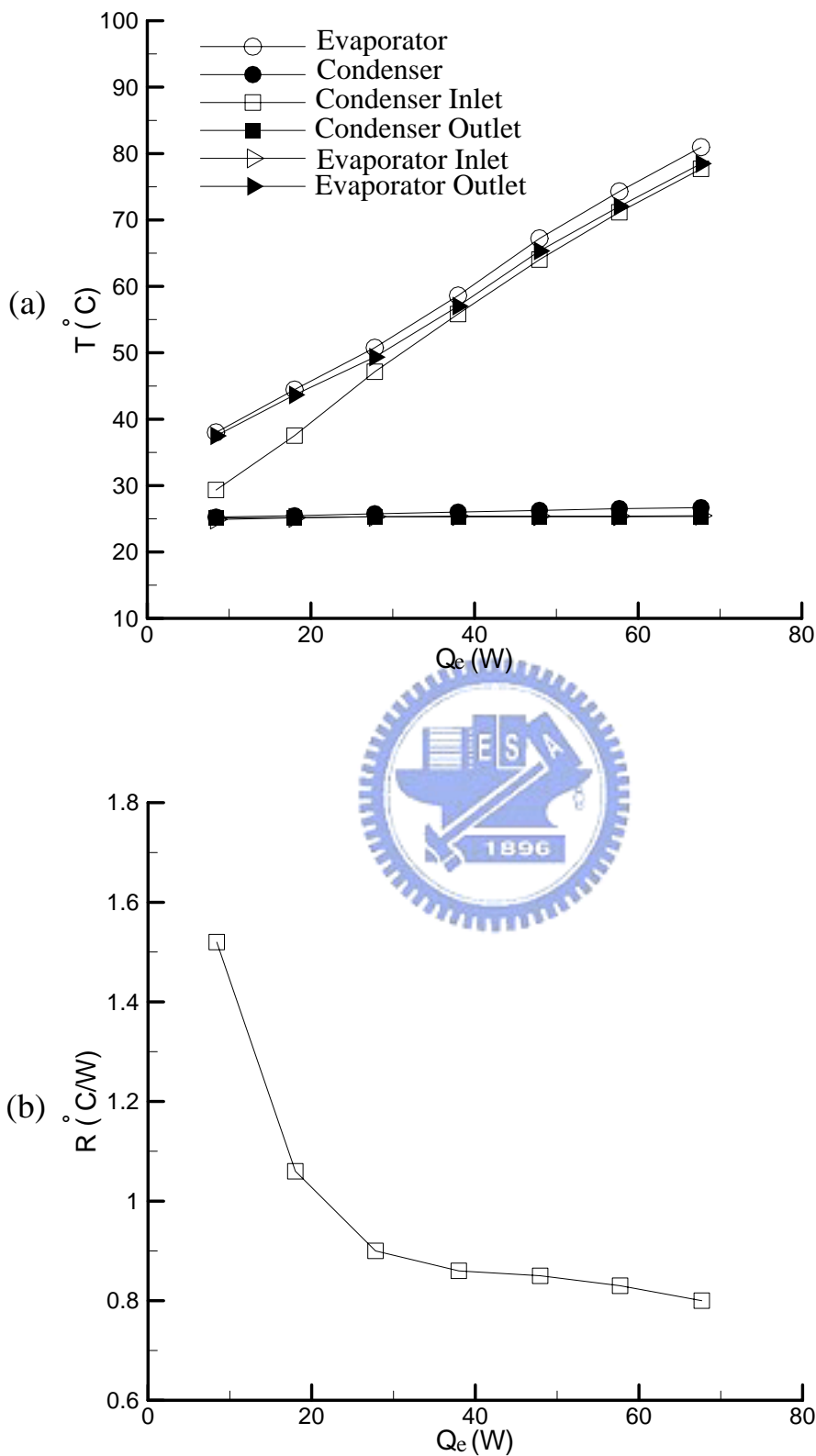


Fig. 4.5 Variations of the temperature at various locations in the CPL (a) and thermal resistance of the CPL (b) with the input power to the evaporator for the cooling water temperature in the condenser  $T_{\text{cold}} = 25$  , liquid inventory of 75% and relative height between condenser and evaporator of 0 cm.

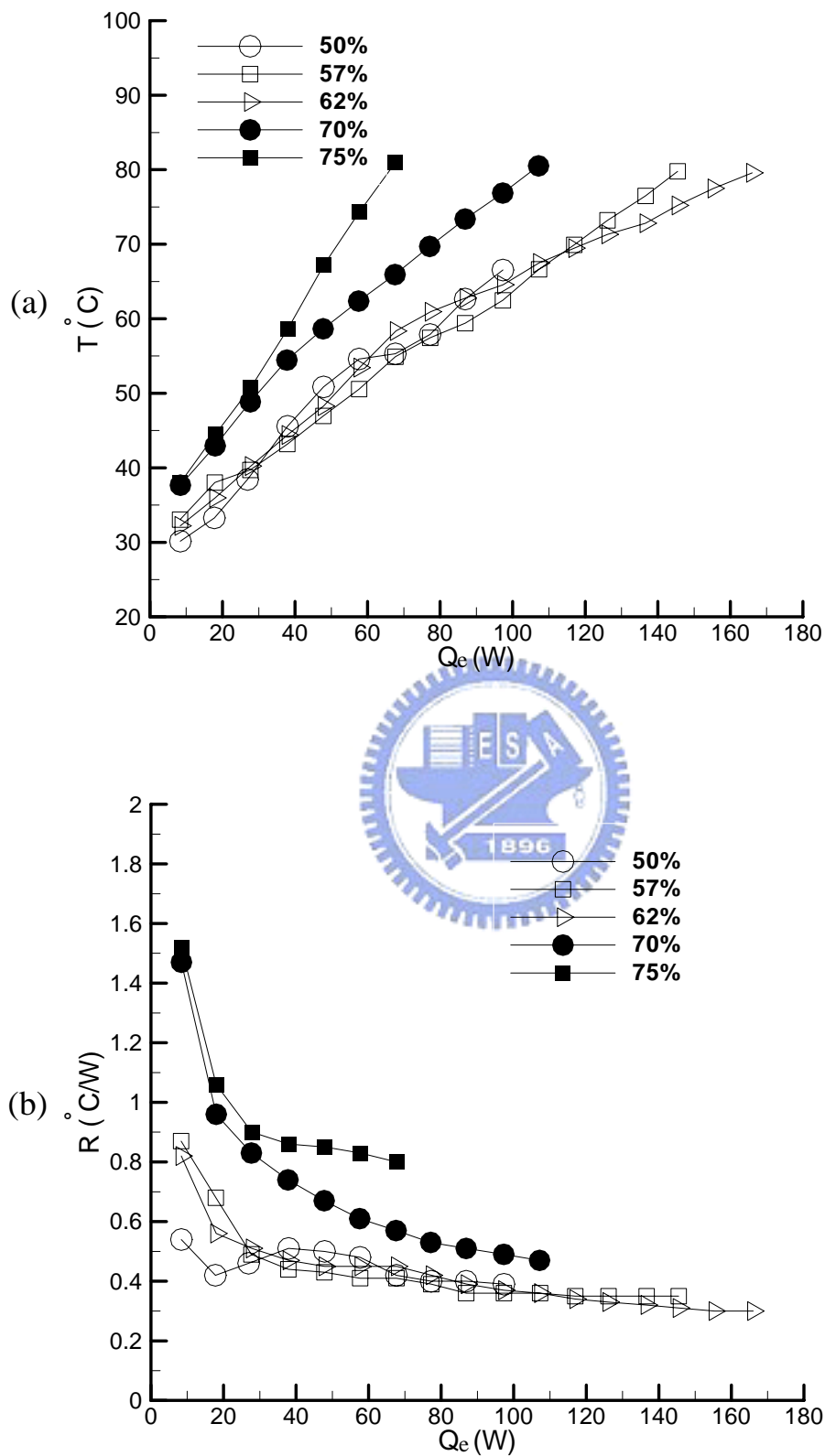


Fig. 4.6 Variations of the mean evaporator temperature (a) and thermal resistance of the CPL (b) with the input power to the evaporator for various liquid inventories for cooling water temperature in the condenser  $T_{\text{cold}} = 25$  and relative condenser-evaporator height of 0 cm.

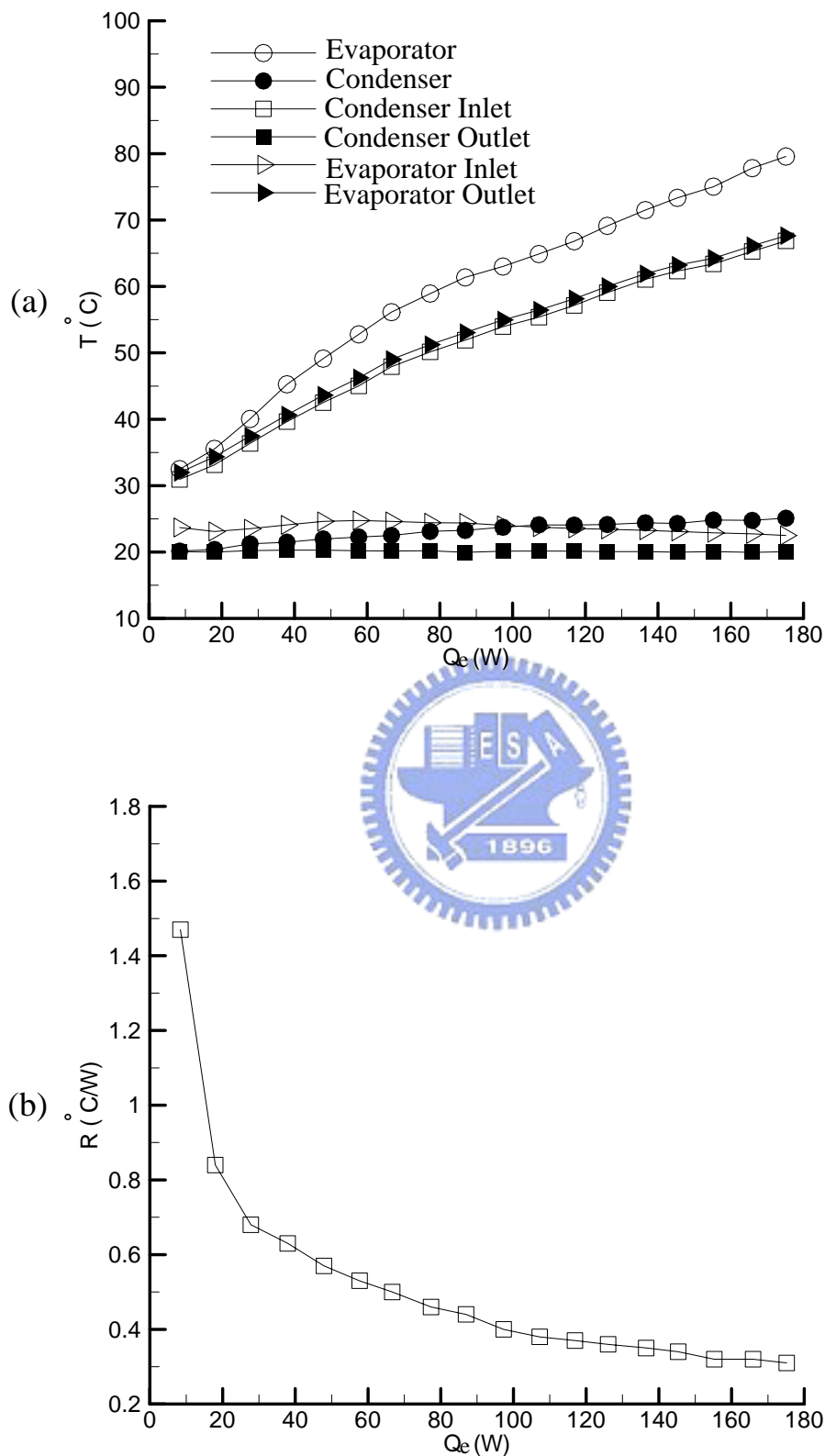


Fig. 4.7 Variations of the temperature at various locations in the CPL (a) and thermal resistance of the CPL (b) with the input power to the evaporator for the cooling water temperature in the condenser  $T_{\text{cold}} = 20$  , liquid inventory of 62% and relative height between condenser and evaporator of 0 cm.

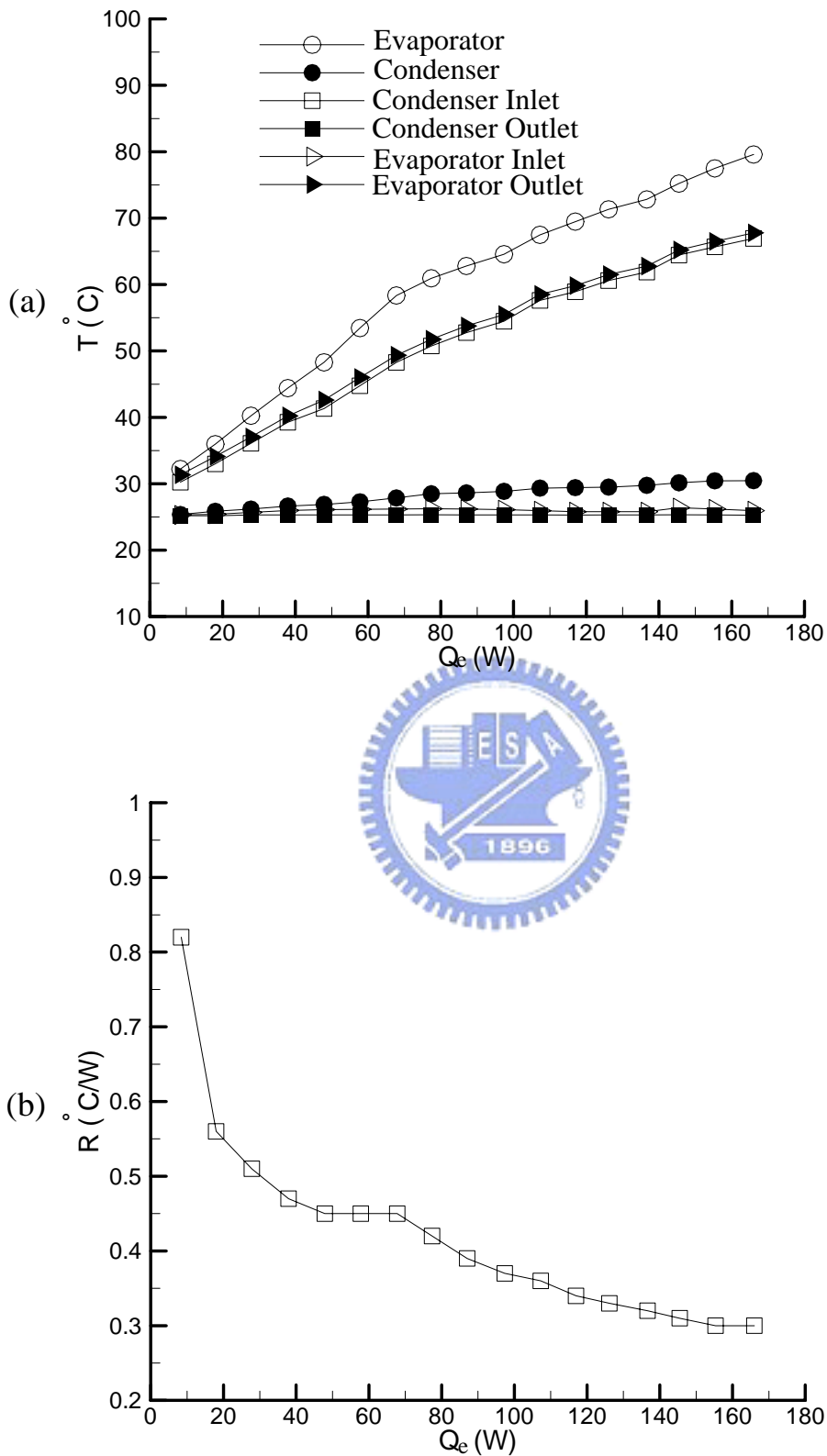


Fig. 4.8 Variations of the temperature at various locations in the CPL (a) and thermal resistance of the CPL (b) with the input power to the evaporator for the cooling water temperature in the condenser  $T_{\text{cold}} = 25$  , liquid inventory of 62% and relative height between condenser and evaporator of 0 cm.

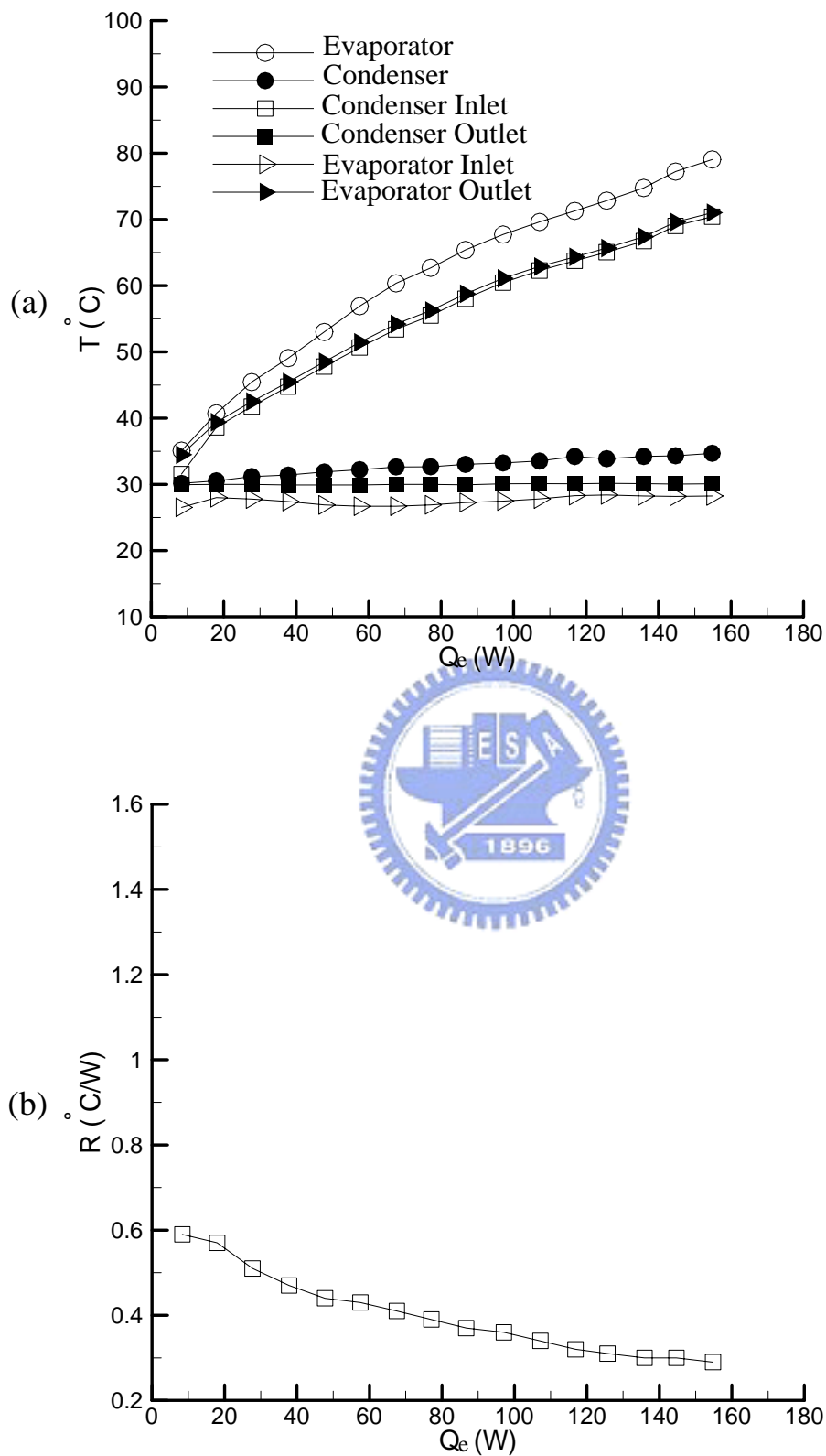


Fig. 4.9 Variations of the temperature at various locations in the CPL (a) and thermal resistance of the CPL (b) with the input power to the evaporator for the cooling water temperature in the condenser  $T_{\text{cold}} = 30$  , liquid inventory of 62% and relative height between condenser and evaporator of 0 cm.



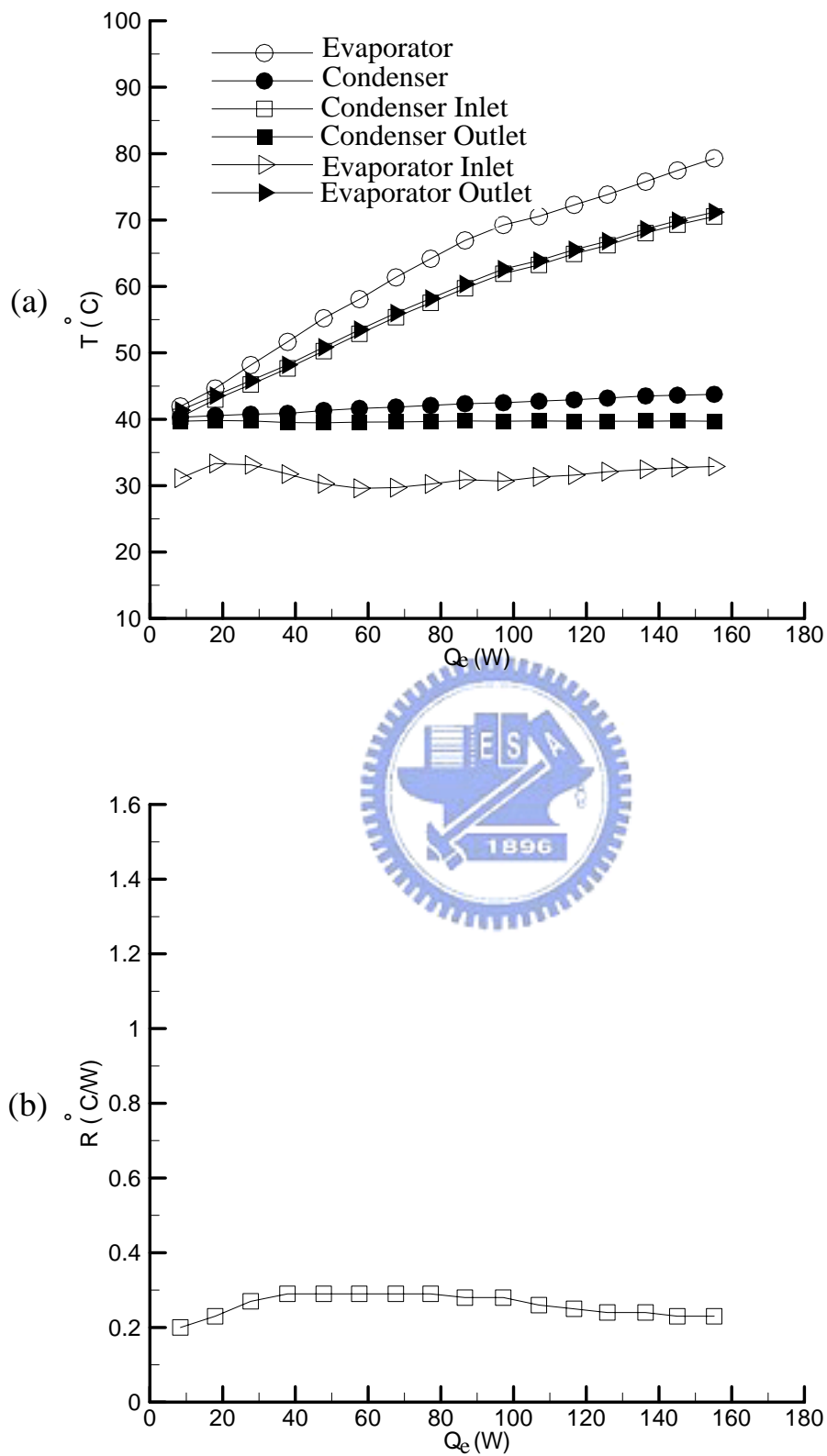


Fig. 4.10 Variations of the temperature at various locations in the CPL (a) and thermal resistance of the CPL (b) with the input power to the evaporator for the cooling water temperature in the condenser  $T_{\text{cold}} = 40$  , liquid inventory of 62% and relative height between condenser and evaporator of 0 cm.

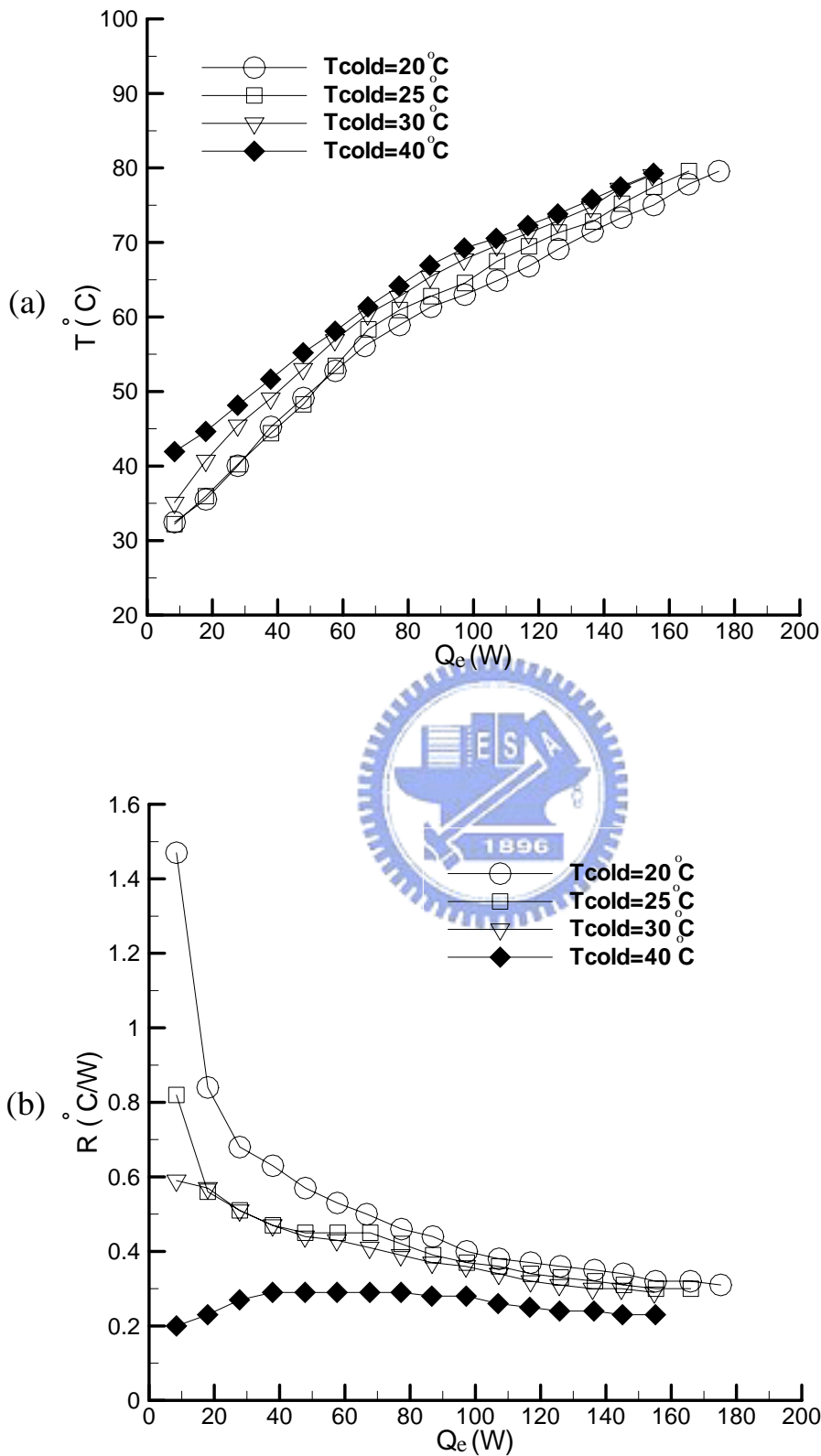


Fig. 4.11 Variations of the evaporator temperature (a) and thermal resistance of the CPL (b) with the power input to the evaporator for various cooling water temperatures in the condenser for the liquid inventory of 62% and relative condenser-evaporator height of 0 cm.

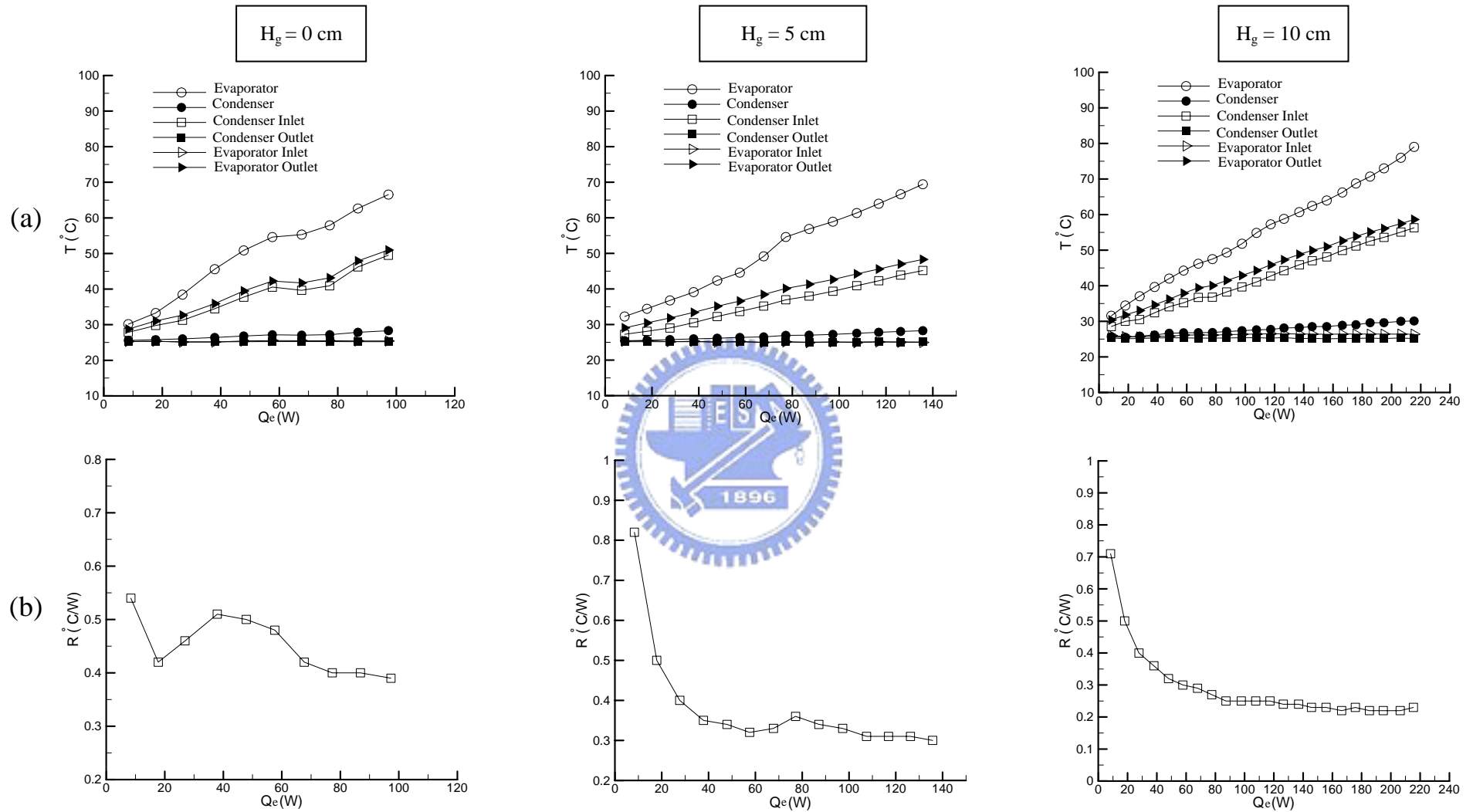


Fig. 4.12 Variations of the temperature at various locations in the CPL (a) and thermal resistance of the CPL (b) with the input power to the evaporator for various relative condenser-evaporator heights for the cooling water temperature in the condenser  $T_{\text{cold}} = 25$  and liquid inventory of 50%.

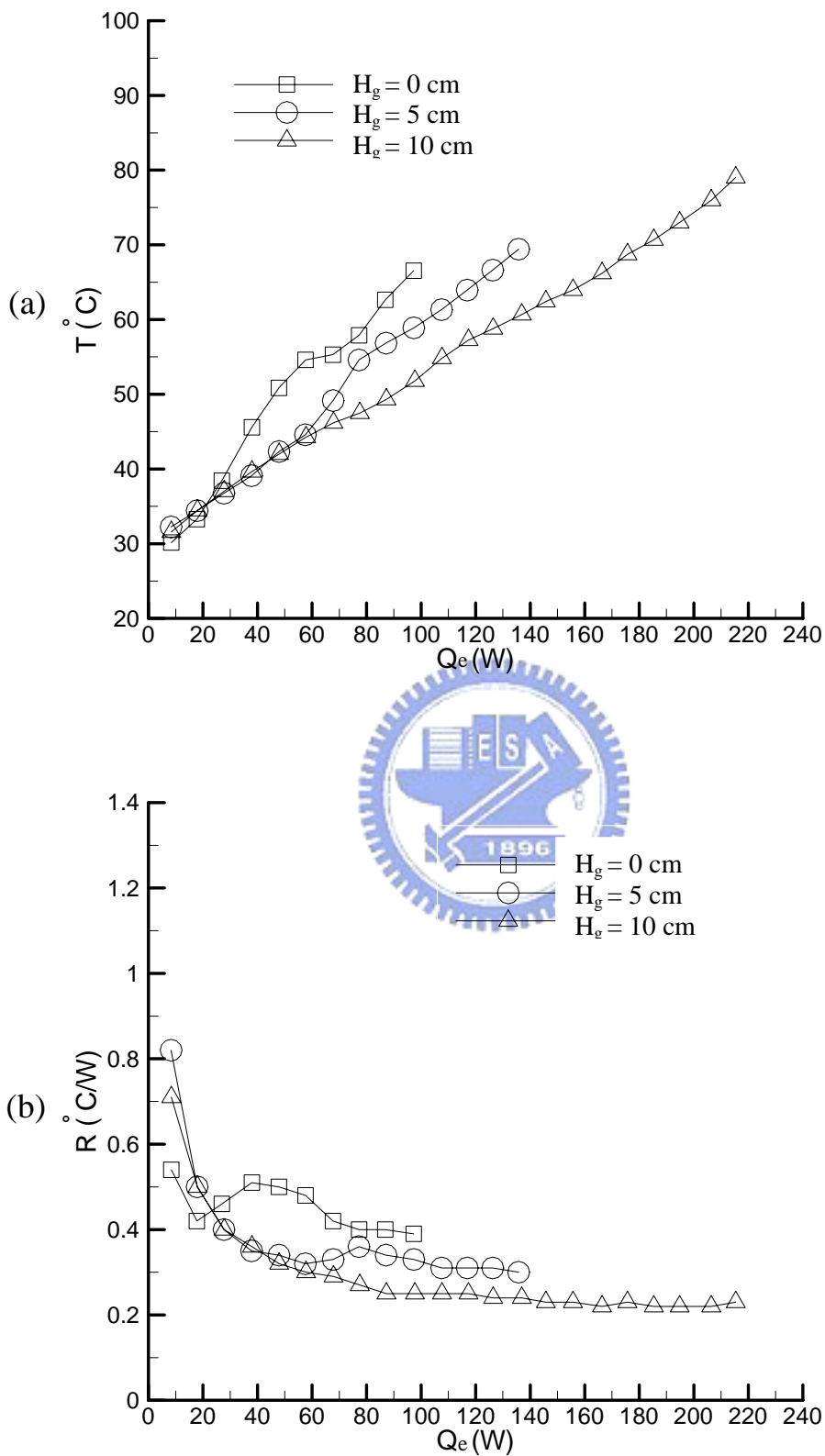


Fig. 4.13 Variations of the mean evaporator temperature (a) and thermal resistance of the CPL (b) with the input power to the evaporator for various relative condenser-evaporator heights for the cooling water temperature in the condenser  $T_{\text{cold}} = 25$  and liquid inventory of 50%.

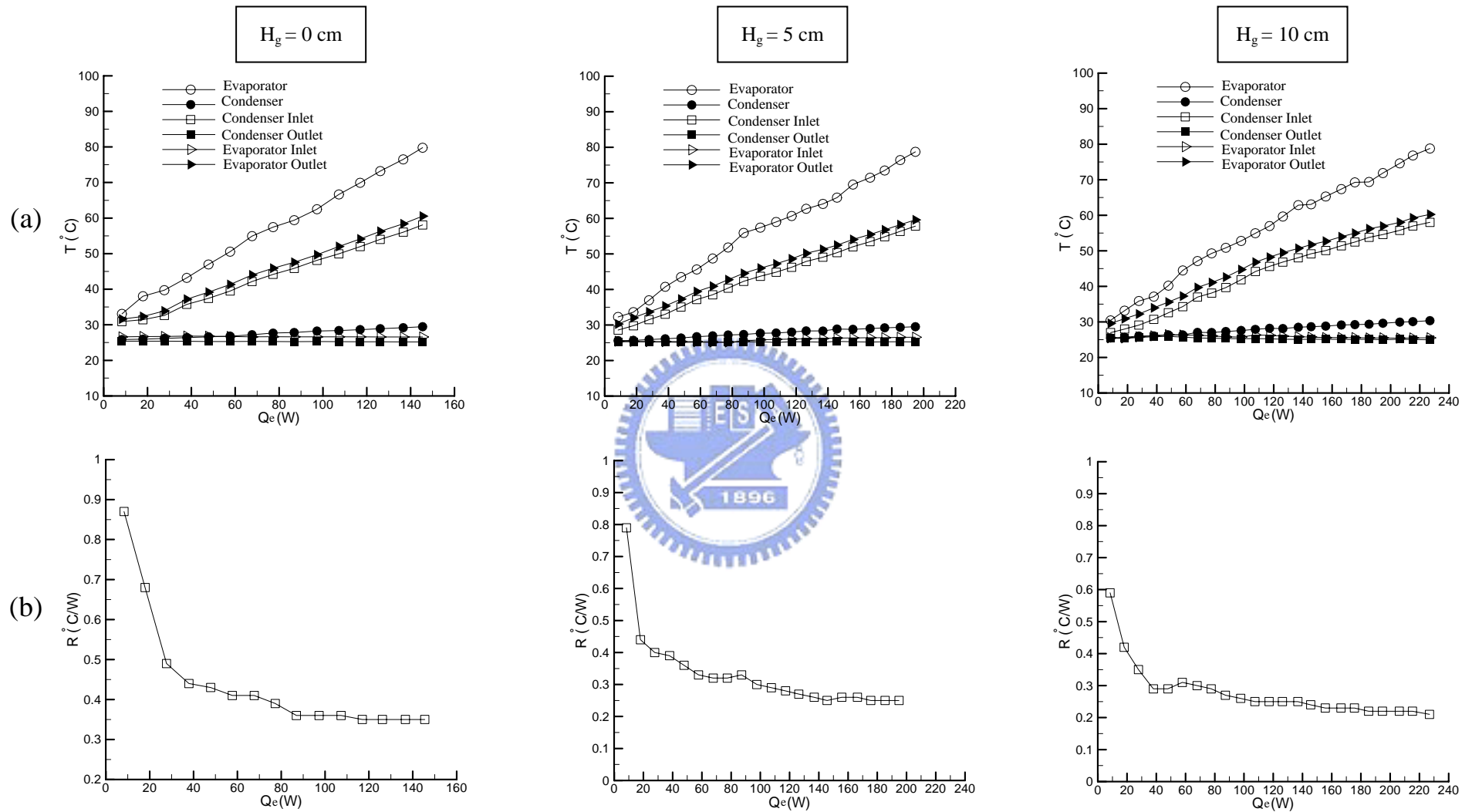


Fig. 4.14 Variations of the temperature at various locations in the CPL (a) and thermal resistance of the CPL (b) with the input power to the evaporator for various relative condenser-evaporator heights for the cooling water temperature in the condenser  $T_{\text{cold}} = 25$  and liquid inventory of 57%.

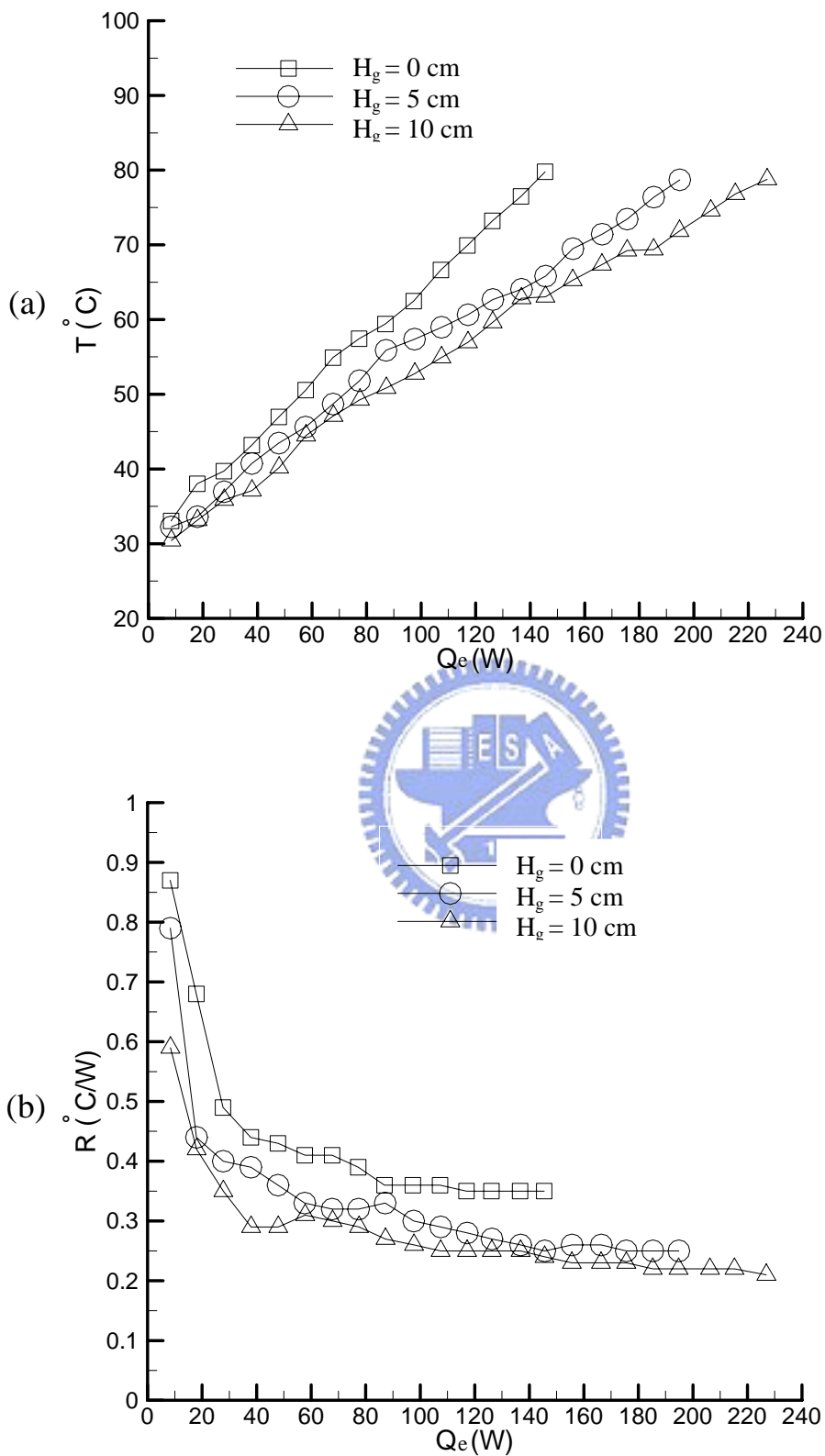


Fig. 4.15 Variations of the mean evaporator temperature (a) and thermal resistance of the CPL (b) with the input power to the evaporator for various relative condenser-evaporator heights for the cooling water temperature in the condenser  $T_{\text{cold}} = 25$  and liquid inventory of 57%.

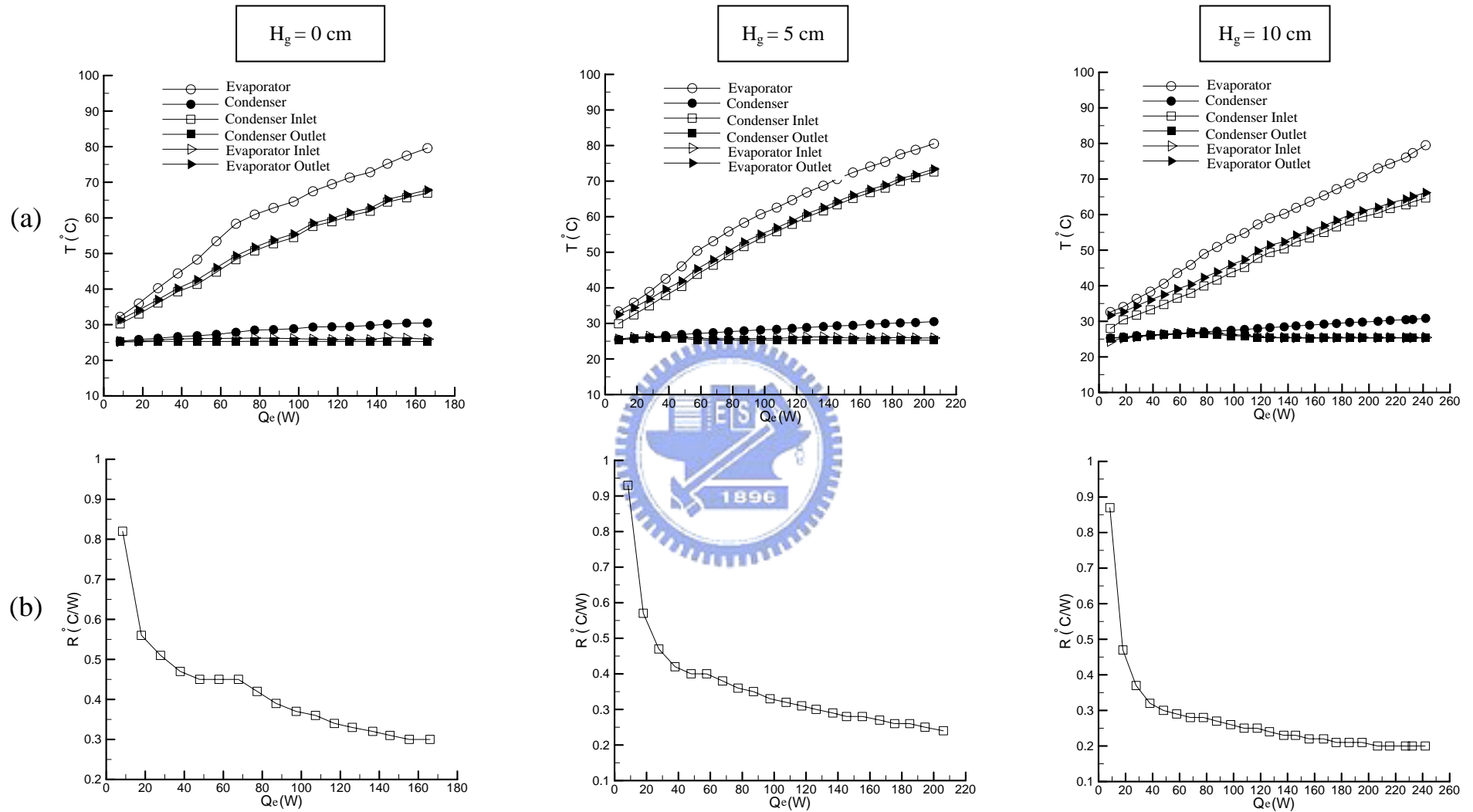


Fig. 4.16 Variations of the temperature at various locations in the CPL (a) and thermal resistance of the CPL (b) with the input power to the evaporator for various relative condenser-evaporator heights for the cooling water temperature in the condenser  $T_{\text{cold}} = 25$  and liquid inventory of 62%.

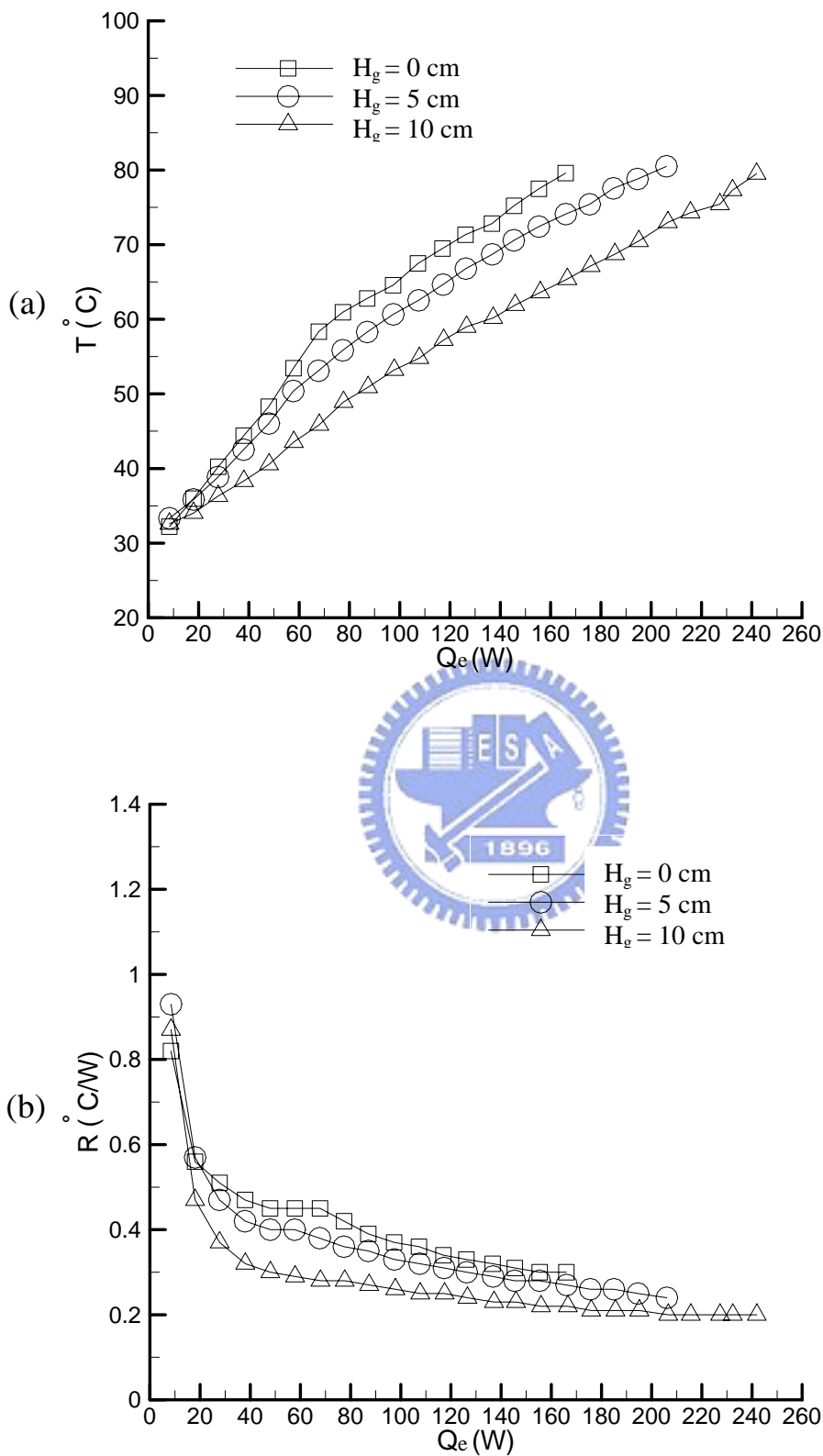


Fig. 4.17 Variations of the mean evaporator temperature (a) and thermal resistance of the CPL (b) with the input power to the evaporator for various relative condenser-evaporator heights for the cooling water temperature in the condenser  $T_{\text{cold}} = 25$  and liquid inventory of 62%.



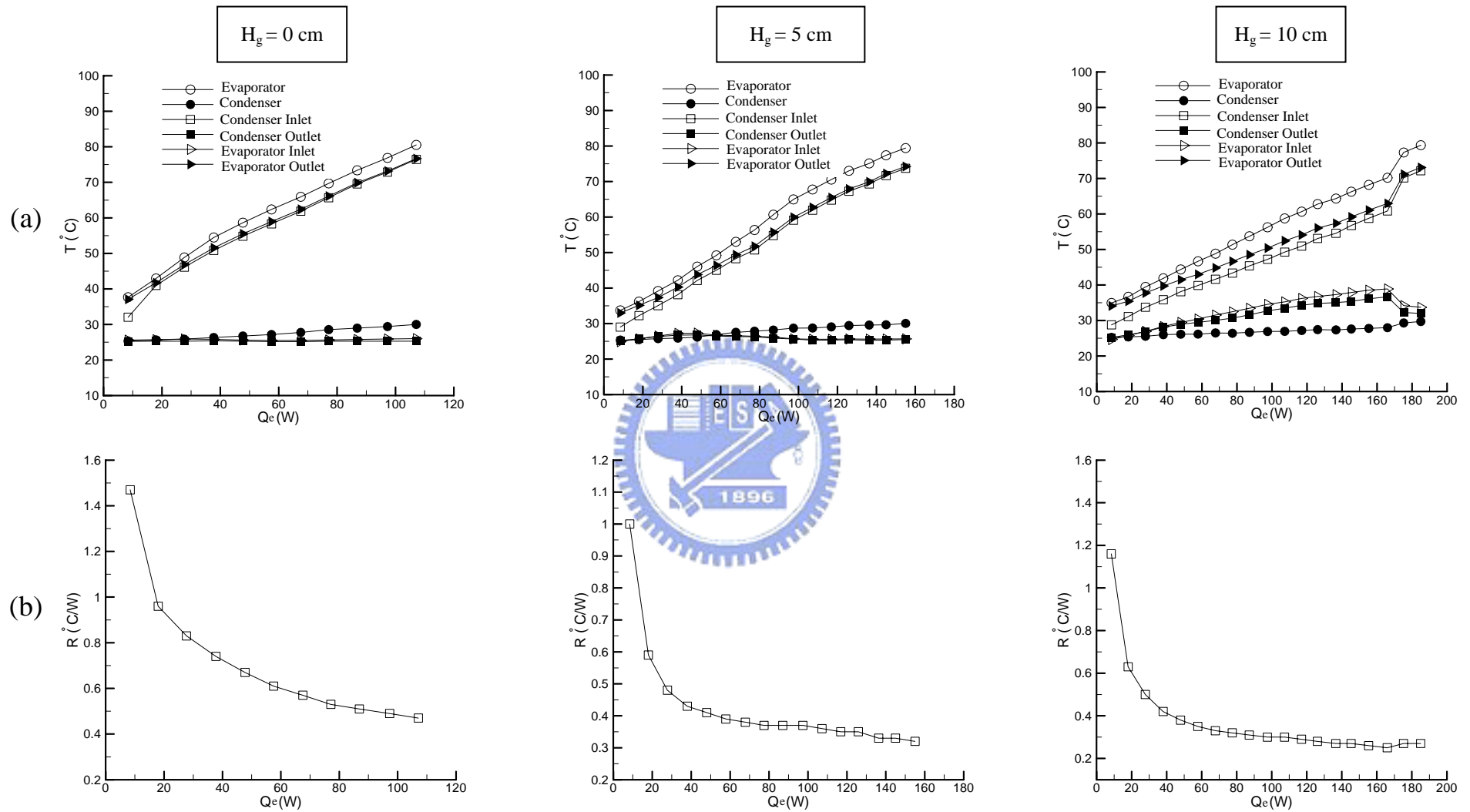


Fig. 4.18 Variations of the temperature at various locations in the CPL (a) and thermal resistance of the CPL (b) with the input power to the evaporator for various relative condenser-evaporator heights for the cooling water temperature in the condenser  $T_{\text{cold}} = 25$  and liquid inventory of 70%.

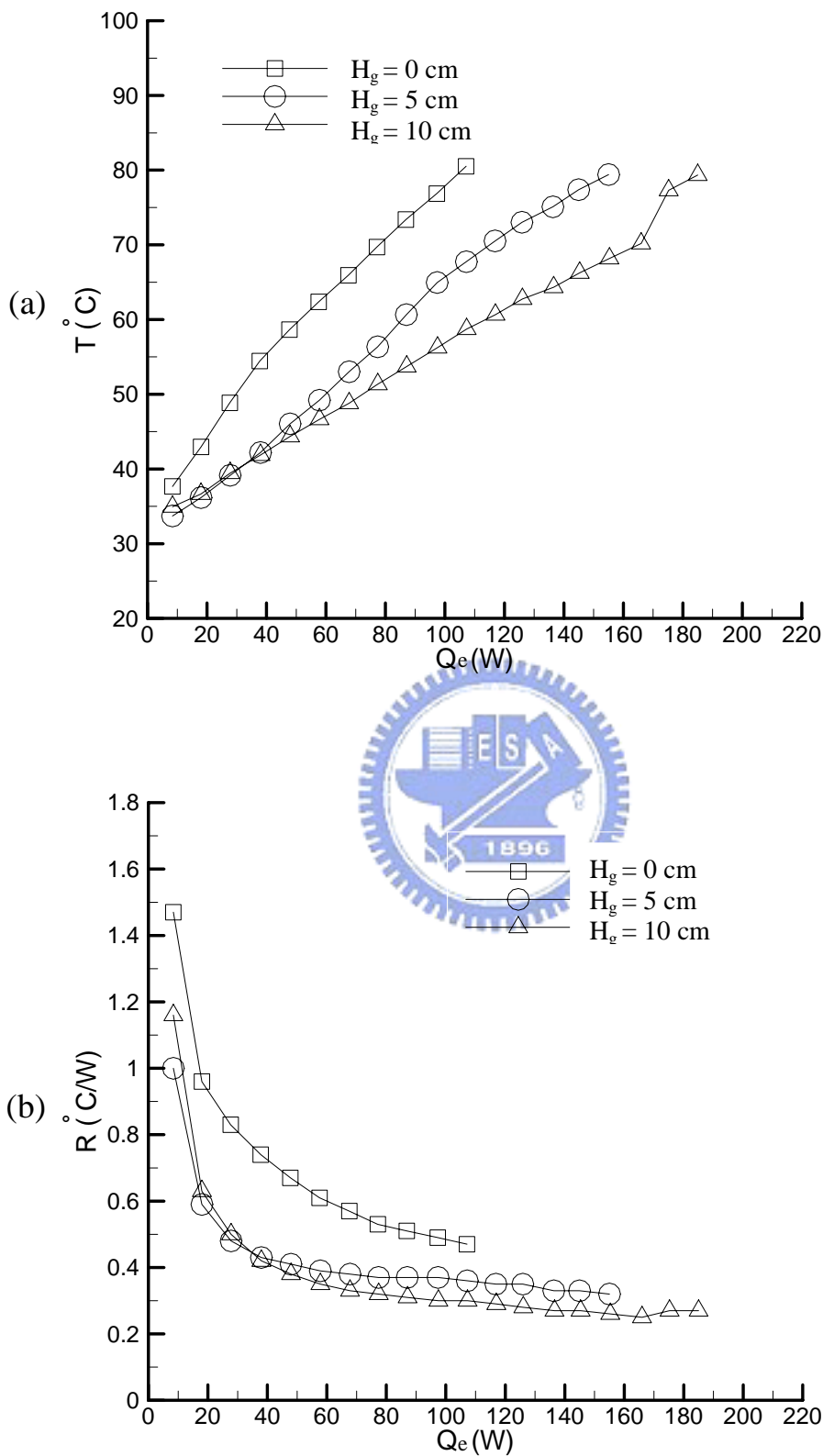


Fig. 4.19 Variations of the mean evaporator temperature (a) and thermal resistance of the CPL (b) with the input power to the evaporator for various relative condenser-evaporator heights for the cooling water temperature in the condenser  $T_{\text{cold}} = 25$  and liquid inventory of 70%.

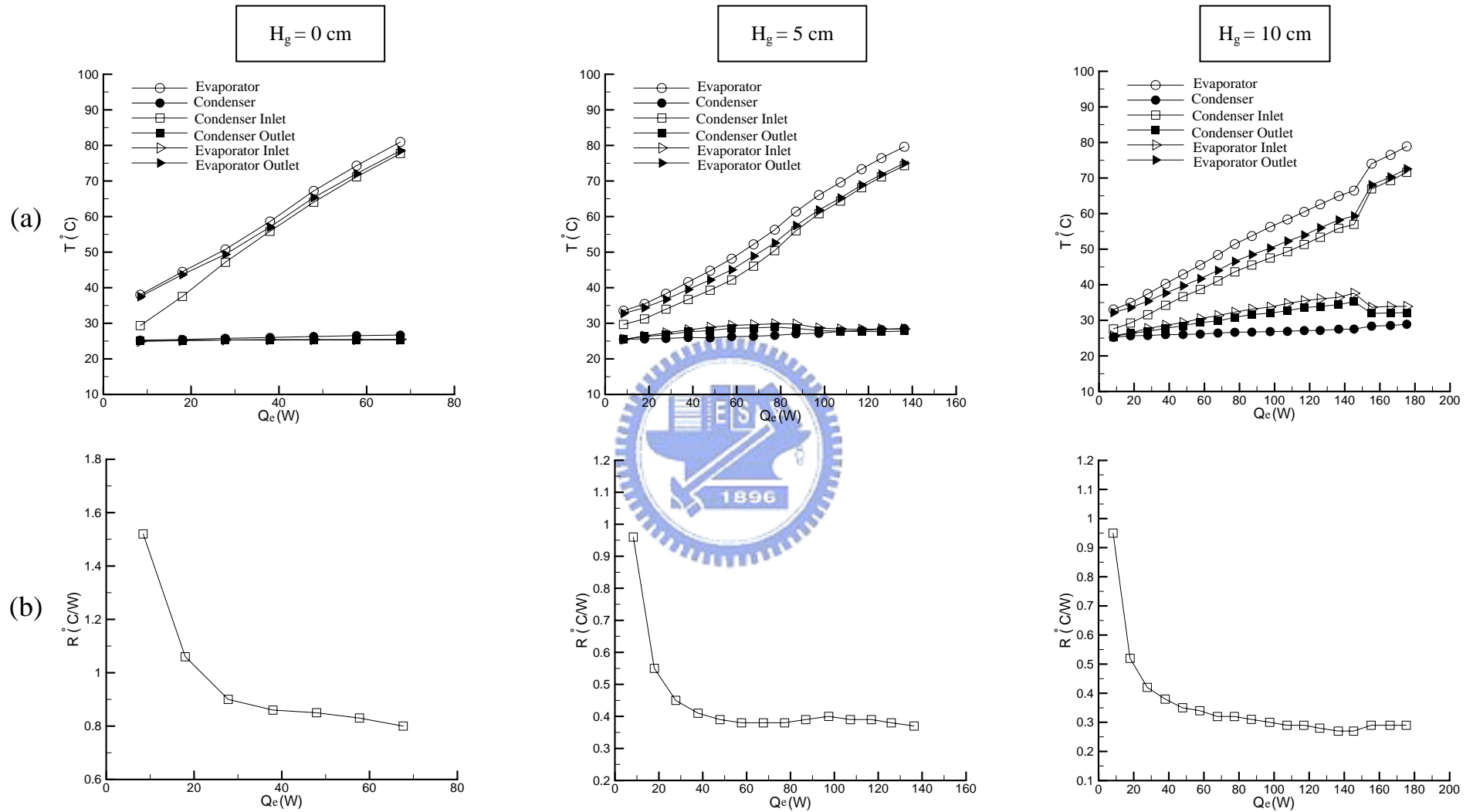


Fig. 4.20 Variations of the temperature at various locations in the CPL (a) and thermal resistance of the CPL (b) with the input power to the evaporator for various relative condenser-evaporator heights for the cooling water temperature in the condenser  $T_{\text{cold}} = 25$  and liquid inventory of 75%.

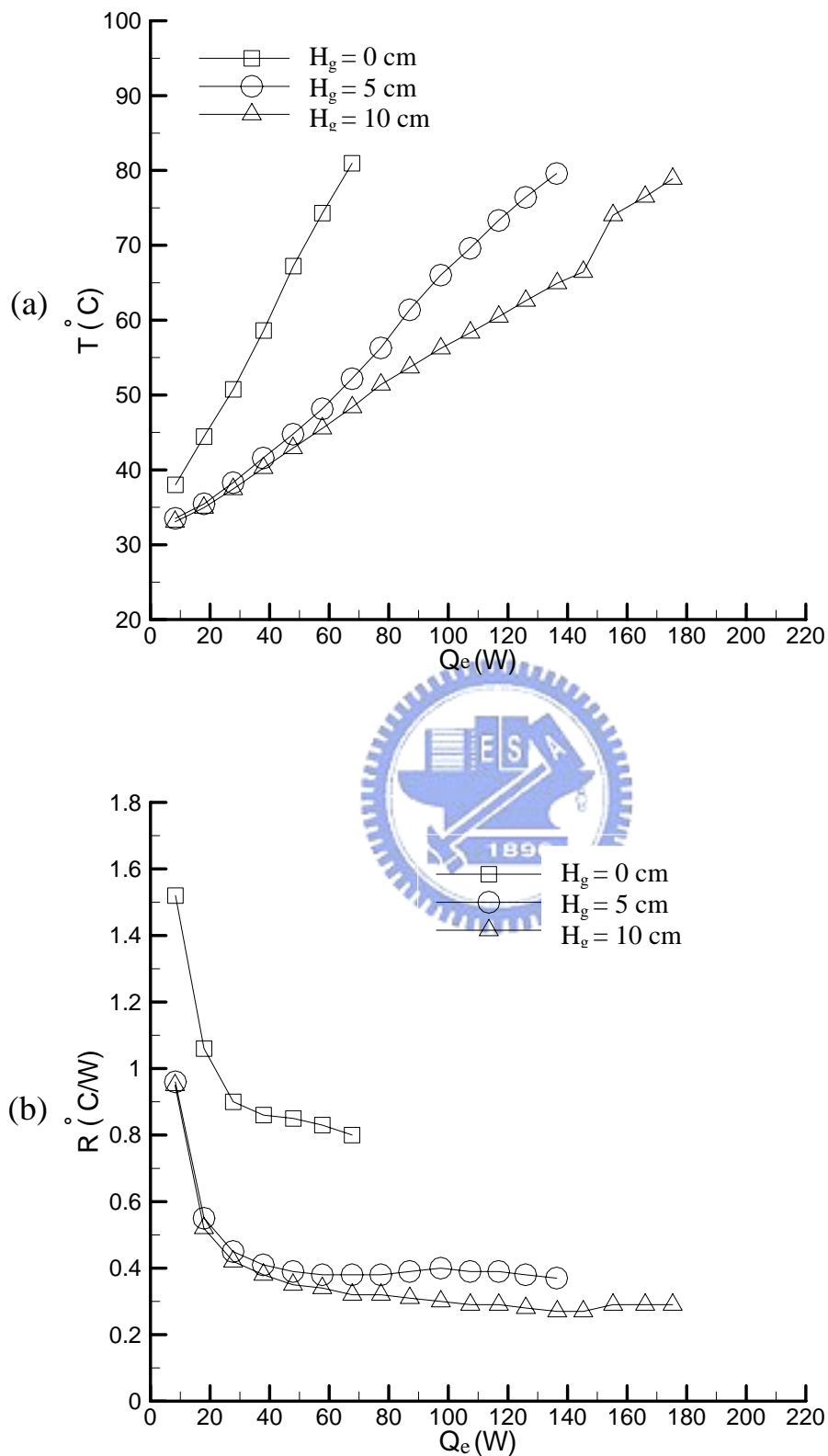


Fig. 4.21 Variations of the mean evaporator temperature (a) and thermal resistance of the CPL (b) with the input power to the evaporator for various relative condenser-evaporator heights for the cooling water temperature in the condenser  $T_{\text{cold}} = 25$  and liquid inventory of 75%.

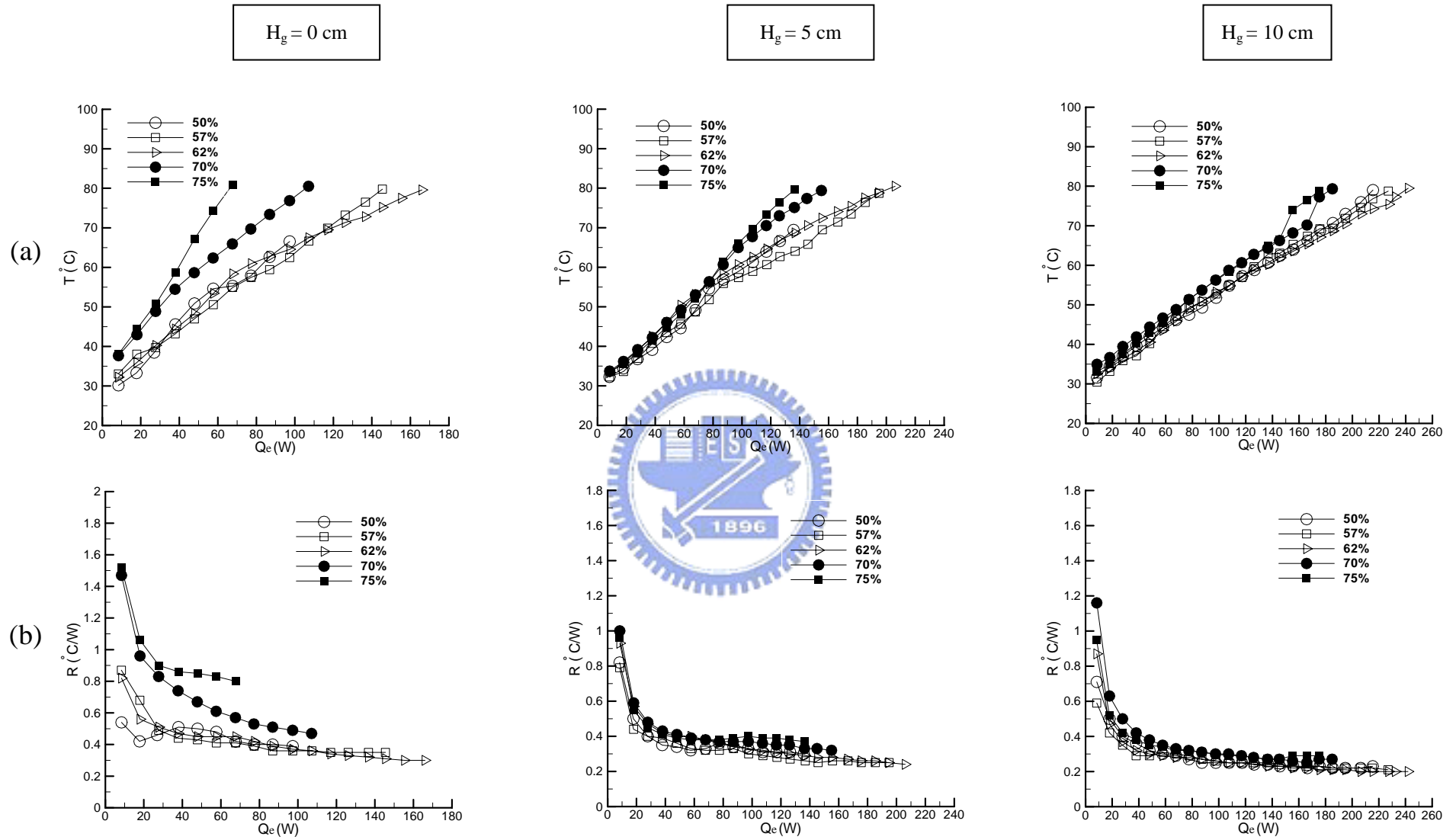


Fig. 4.22 Variations of the mean evaporator temperature (a) and thermal resistance of the CPL (b) with the input power to the evaporator for various liquid inventories and relative condenser-evaporator height for cooling water temperature in the condenser  $T_{\text{cold}} = 25$

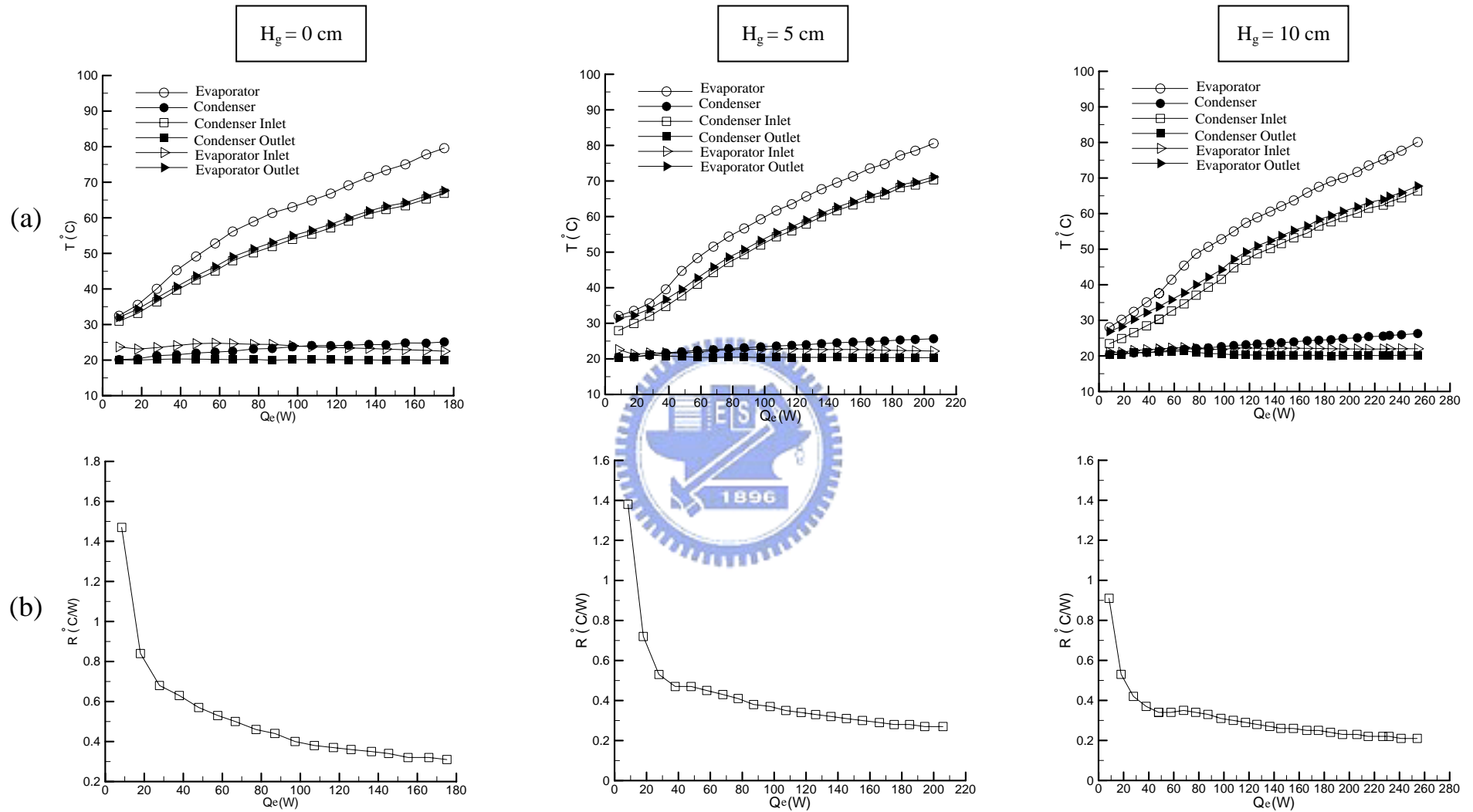


Fig. 4.23 Variations of the temperature at various locations in the CPL (a) and thermal resistance of the CPL (b) with the input power to the evaporator for various relative condenser-evaporator heights for the cooling water temperature in the condenser  $T_{\text{cold}} = 20$  and liquid inventory of 62%.

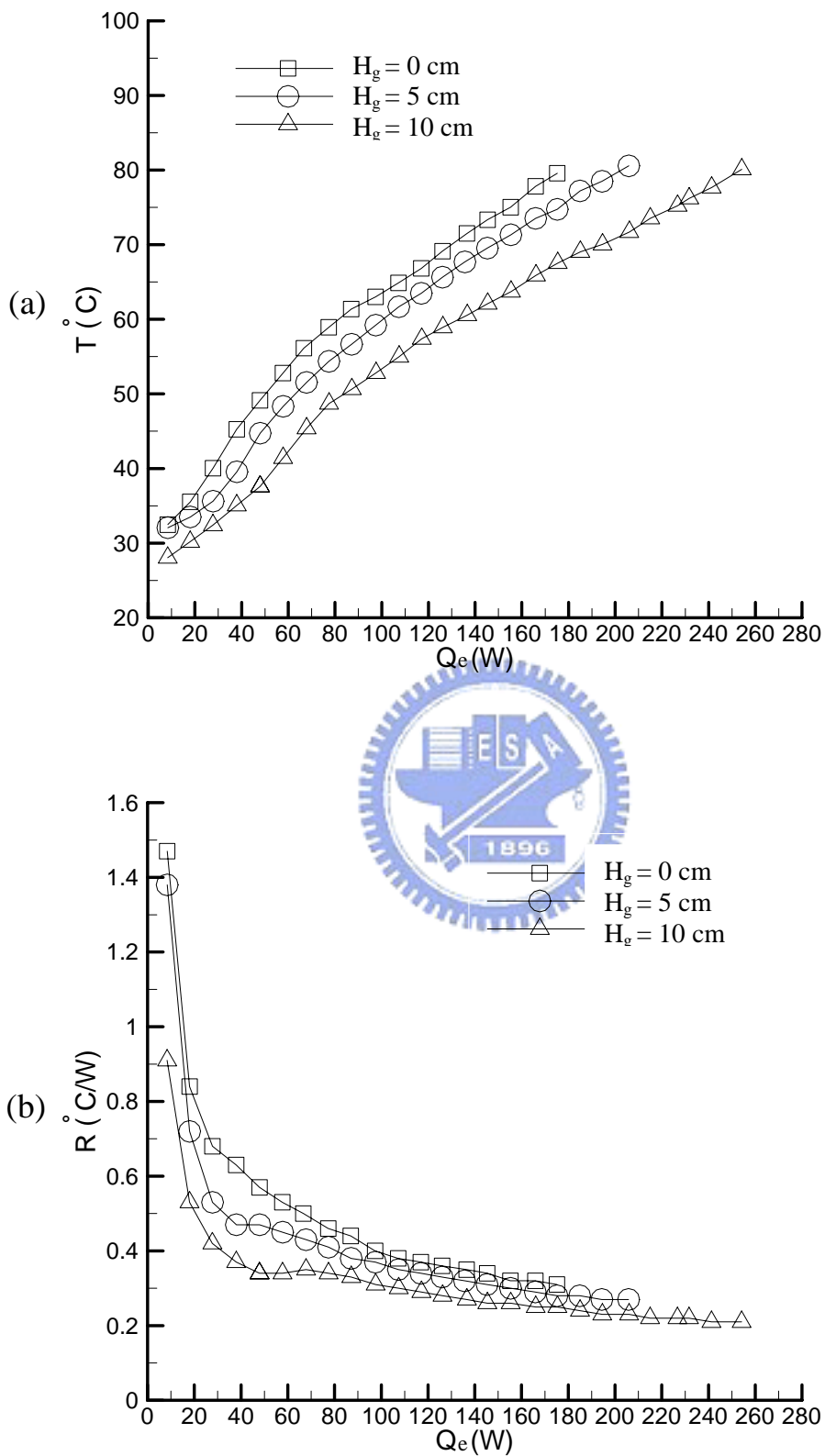


Fig. 4.24 Variations of the mean evaporator temperature (a) and thermal resistance of the CPL (b) with the input power to the evaporator for various relative condenser-evaporator height for cooling water temperature in the condenser  $T_{\text{cold}} = 20$  and liquid inventory of 62%.

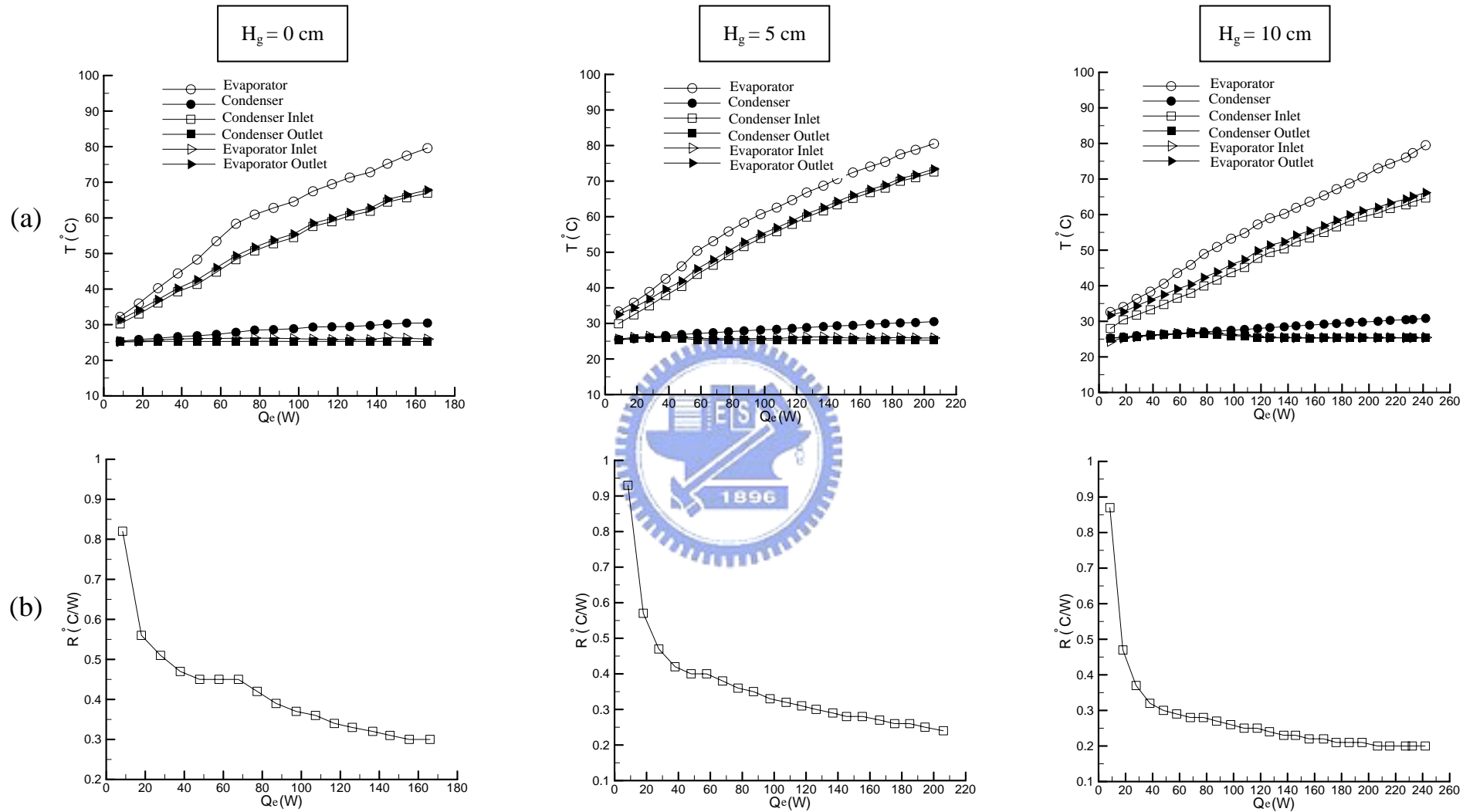


Fig. 4.25 Variations of the temperature at various locations in the CPL (a) and thermal resistance of the CPL (b) with the input power to the evaporator for various relative condenser-evaporator heights for the cooling water temperature in the condenser  $T_{\text{cold}} = 25$  and liquid inventory of 62%.



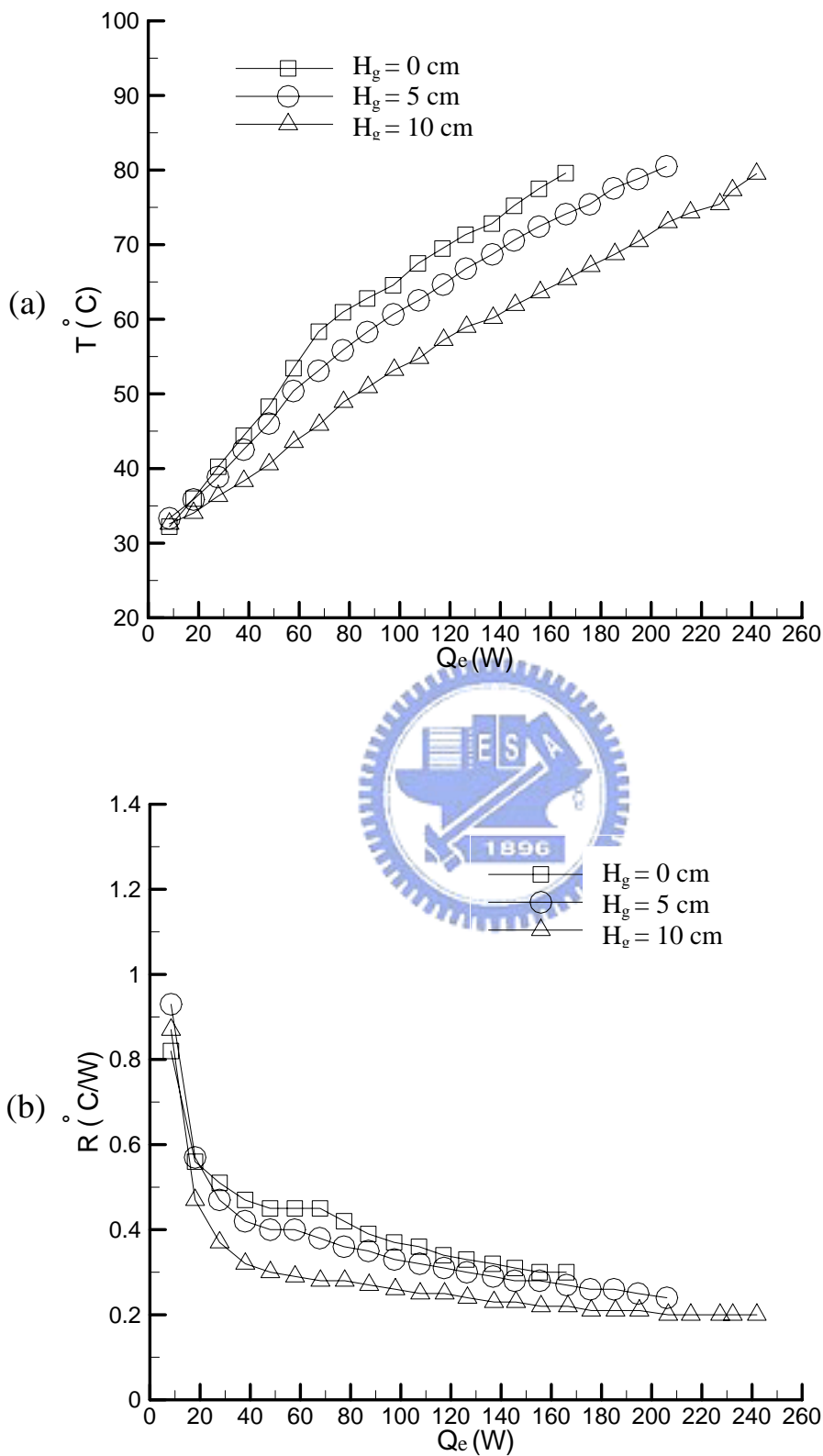


Fig. 4.26 Variations of the mean evaporator temperature (a) and thermal resistance of the CPL (b) with the input power to the evaporator for various relative condenser-evaporator height for cooling water temperature in the condenser  $T_{\text{cold}} = 25$  and liquid inventory of 62%.

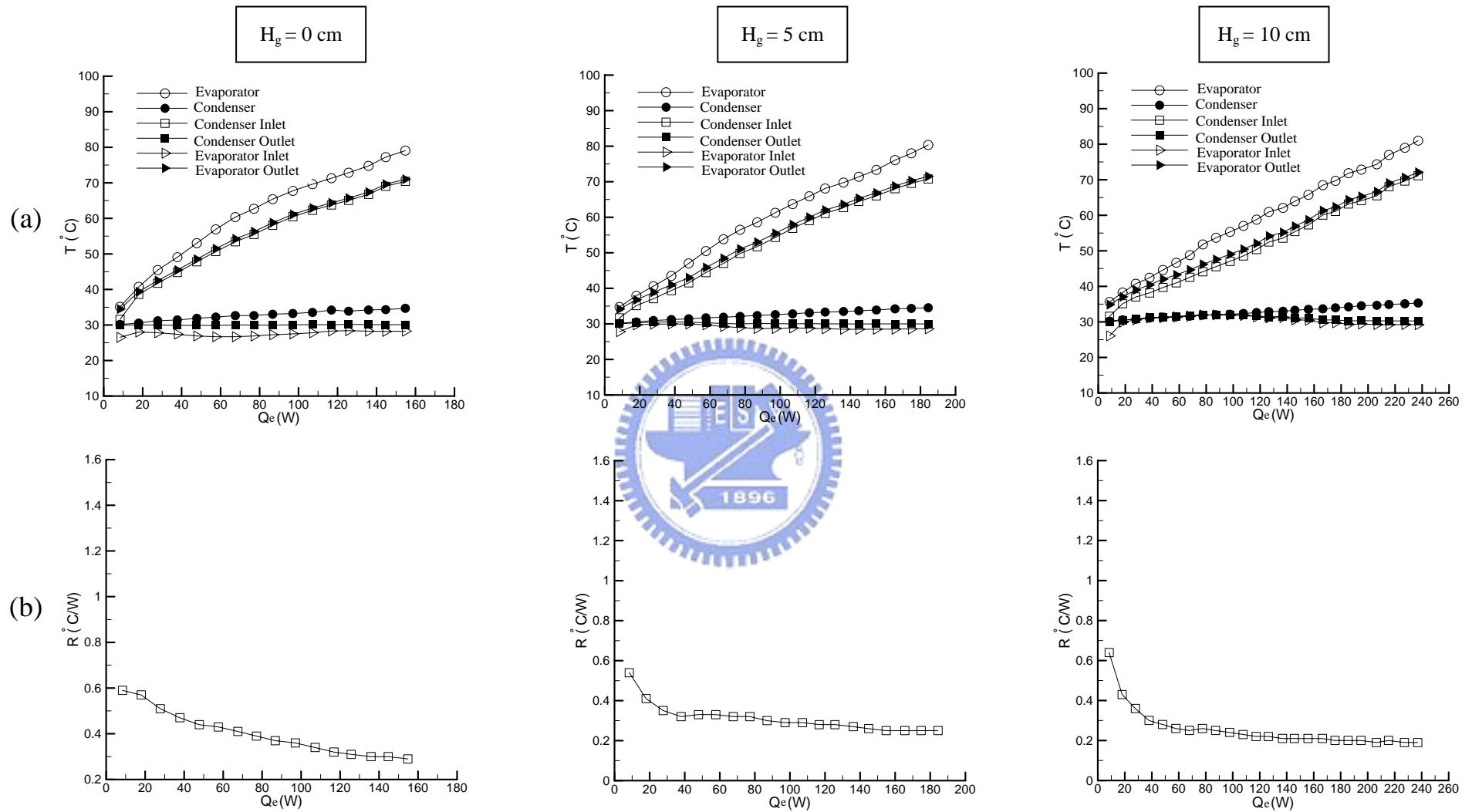


Fig. 4.27 Variations of the temperature at various locations in the CPL (a) and thermal resistance of the CPL (b) with the input power to the evaporator for various relative condenser-evaporator heights for the cooling water temperature in the condenser  $T_{\text{cold}} = 30$  and liquid inventory of 62%.

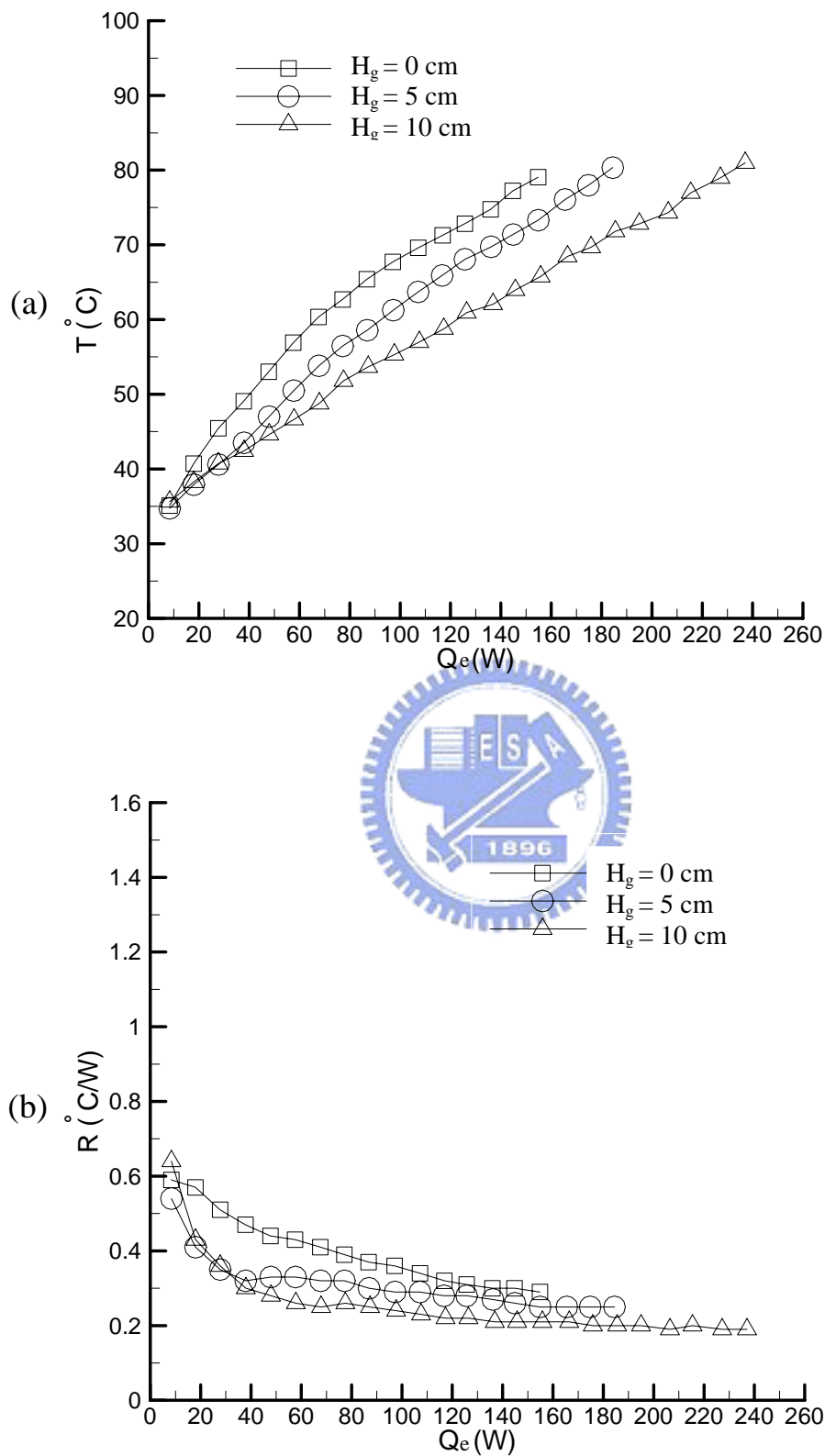


Fig. 4.28 Variations of the mean evaporator temperature (a) and thermal resistance of the CPL (b) with the input power to the evaporator for various relative condenser-evaporator height for cooling water temperature in the condenser  $T_{\text{cold}} = 30$  and liquid inventory of 62%.

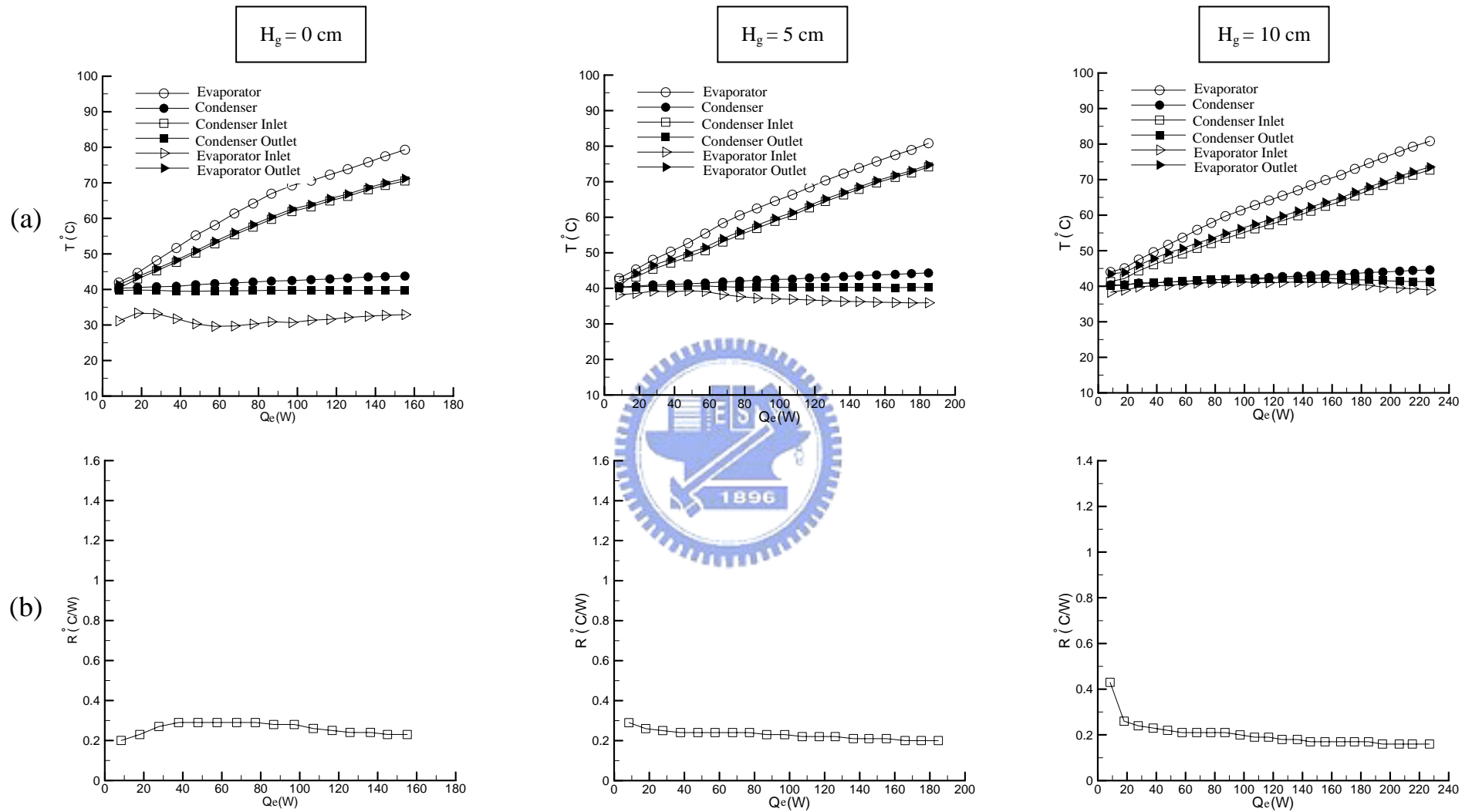


Fig. 4.29 Variations of the temperature at various locations in the CPL (a) and thermal resistance of the CPL (b) with the input power to the evaporator for various relative condenser-evaporator heights for the cooling water temperature in the condenser  $T_{\text{cold}} = 40$  and liquid inventory of 62%.

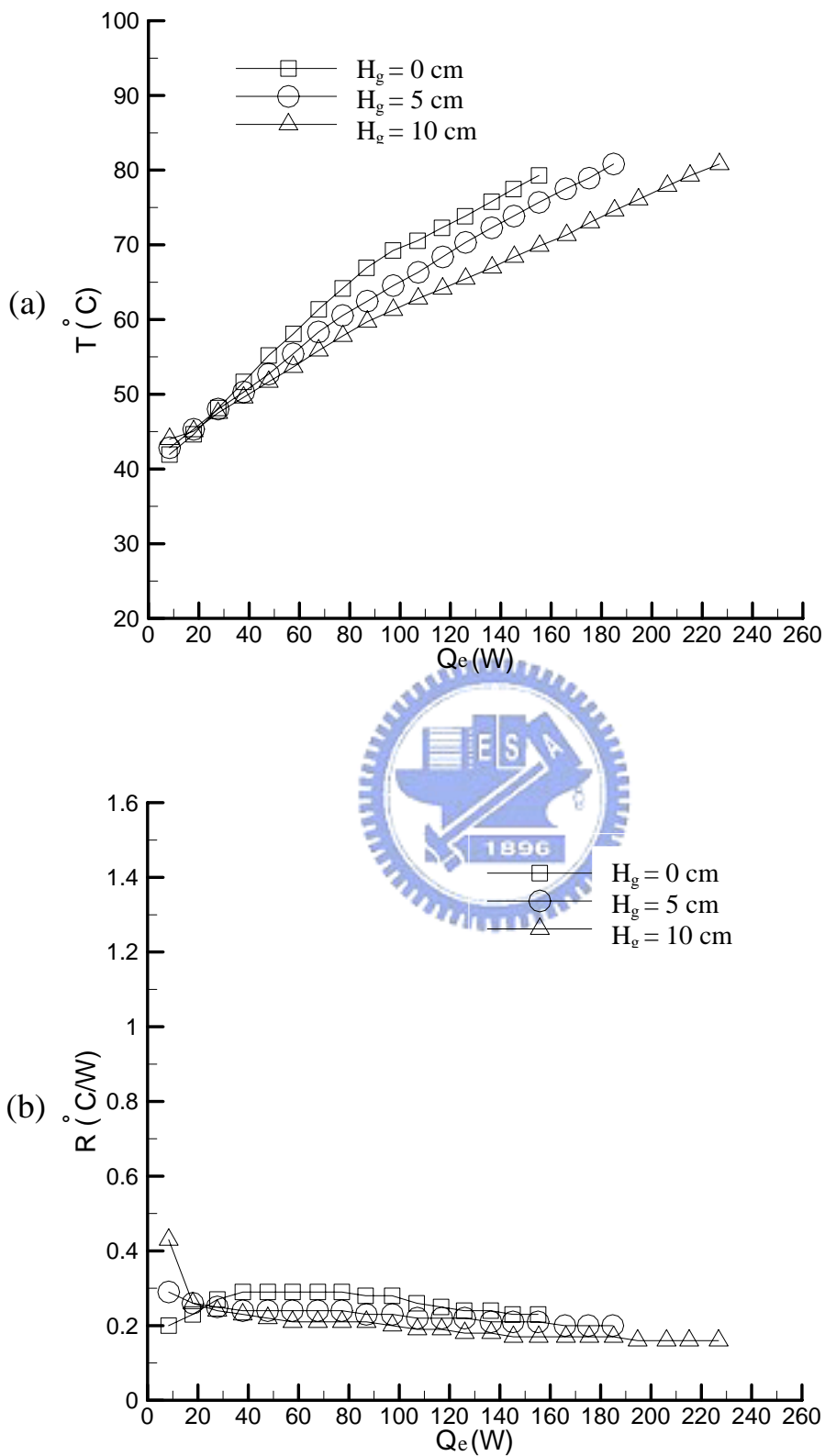


Fig. 4.30 Variations of the mean evaporator temperature (a) and thermal resistance of the CPL (b) with the input power to the evaporator for various relative condenser-evaporator height for cooling water temperature in the condenser  $T_{\text{cold}} = 40$  and liquid inventory of 62%.

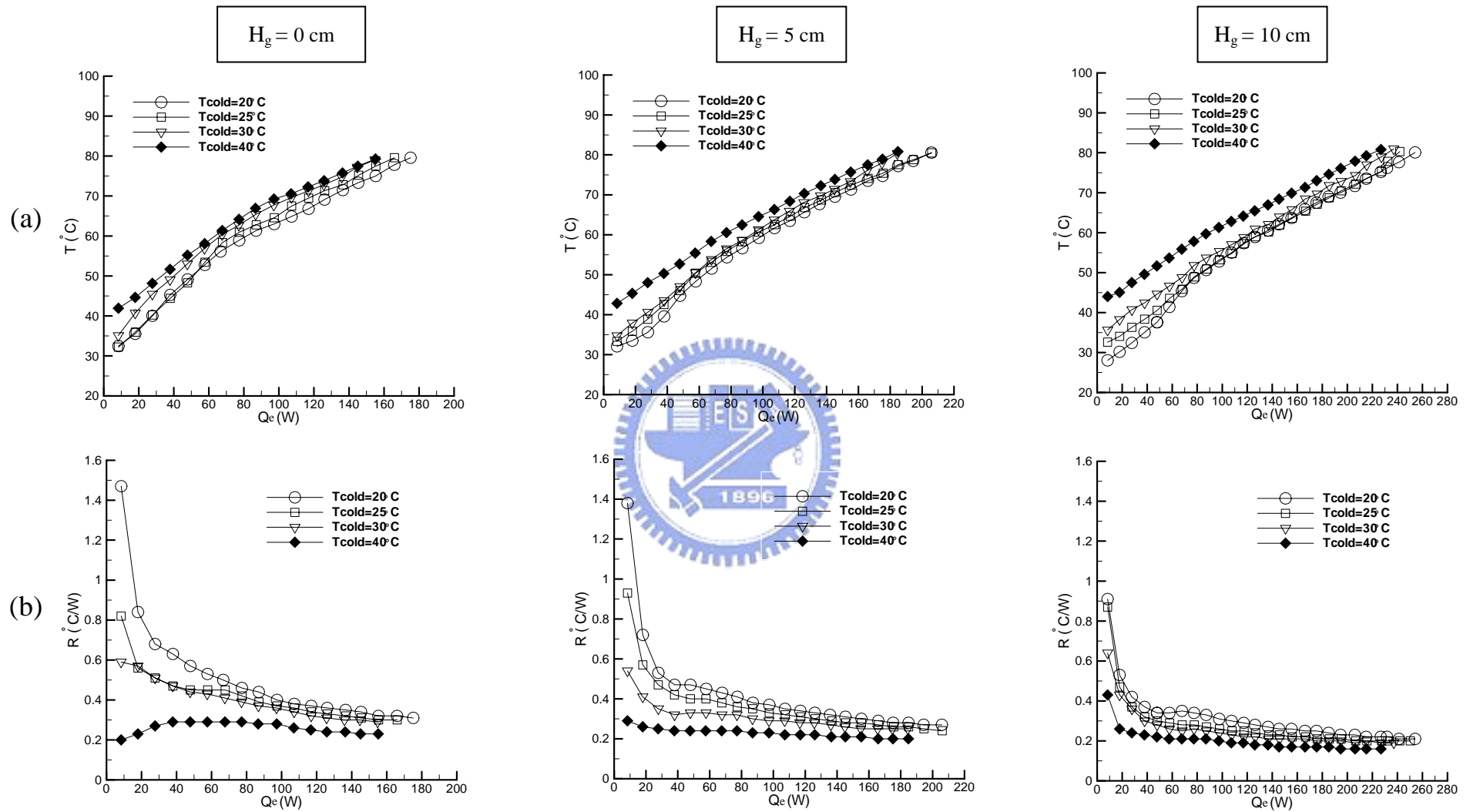


Fig. 4.31 Variations of the mean evaporator temperature (a) and thermal resistance of the CPL (b) with the input power to the evaporator for various cooling water temperatures in the condenser and various relative condenser-evaporator heights for the liquid inventory of 62%.

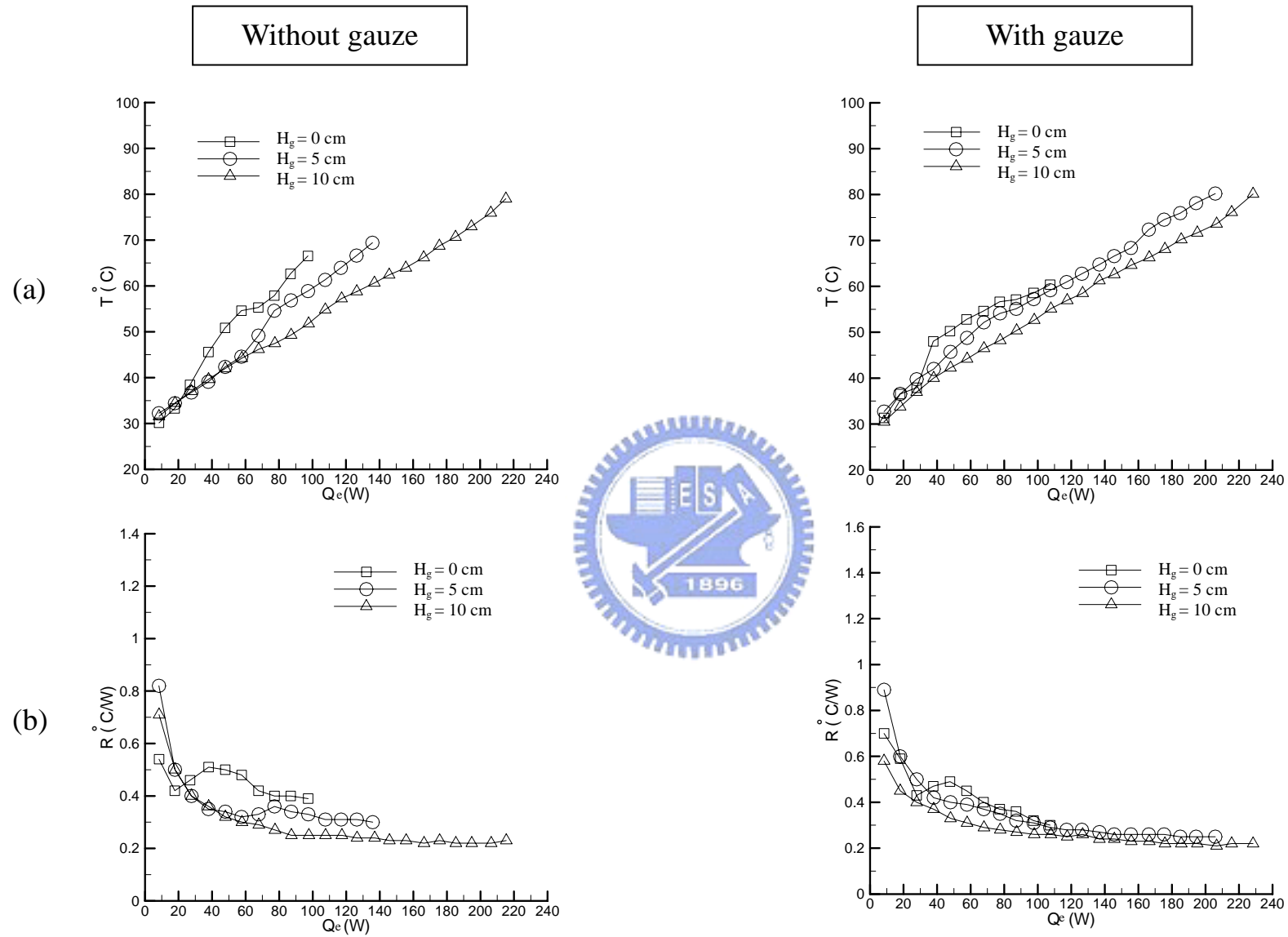


Fig. 4.32 Variations of the mean evaporator temperature (a) and thermal resistance of the CPL (b) with the input power to the evaporator for the CPL with and without cotton gauze covering for various relative condenser-evaporator heights for cooling water temperature in the condenser  $T_{\text{cold}} = 25$  and liquid inventory of 50%.

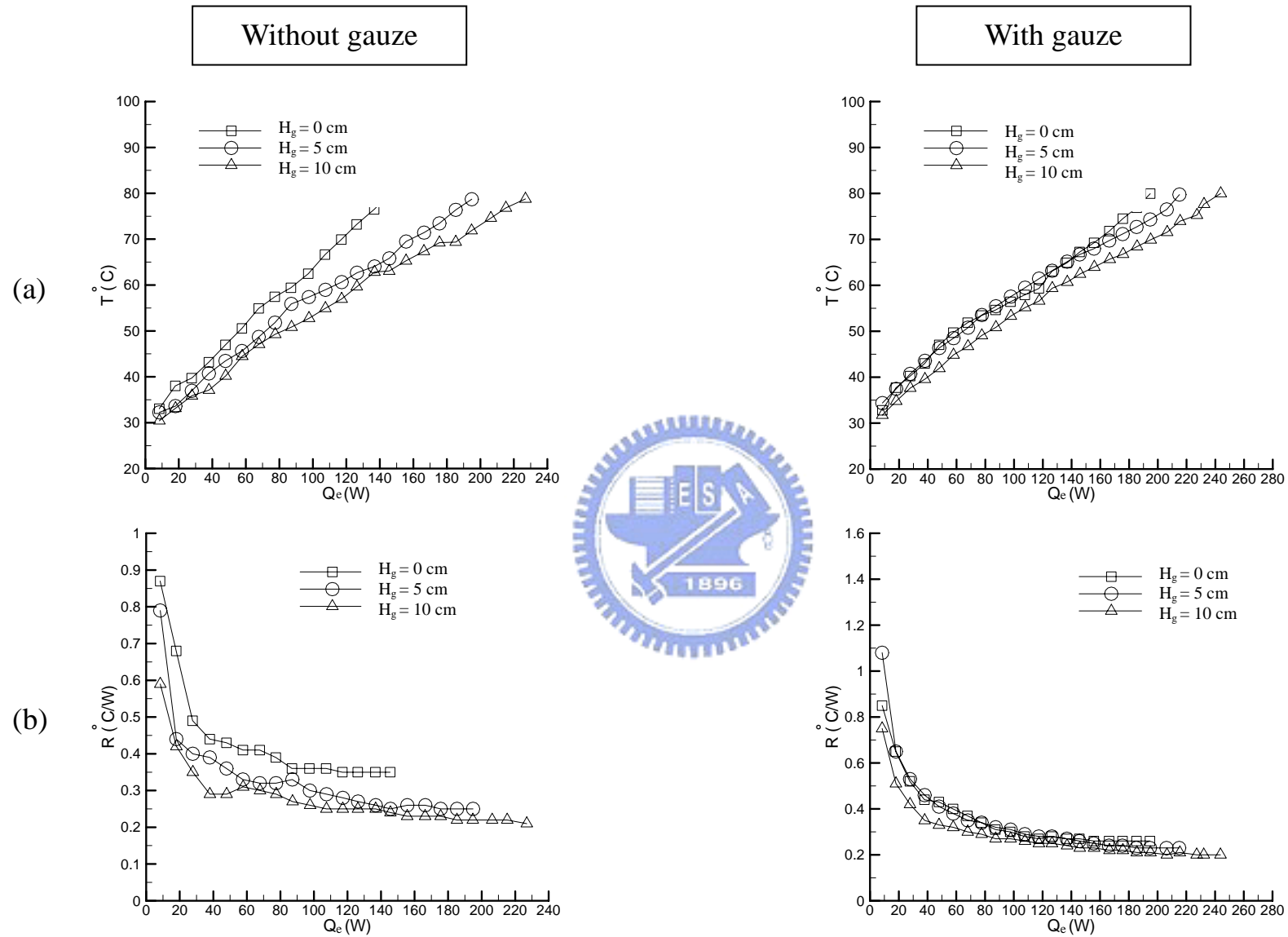


Fig. 4.33 Variations of the mean evaporator temperature (a) and thermal resistance of the CPL (b) with the input power to the evaporator for the CPL with and without cotton gauze covering for various relative condenser-evaporator heights for cooling water temperature in the condenser  $T_{\text{cold}} = 25$  and liquid inventory of 57%.



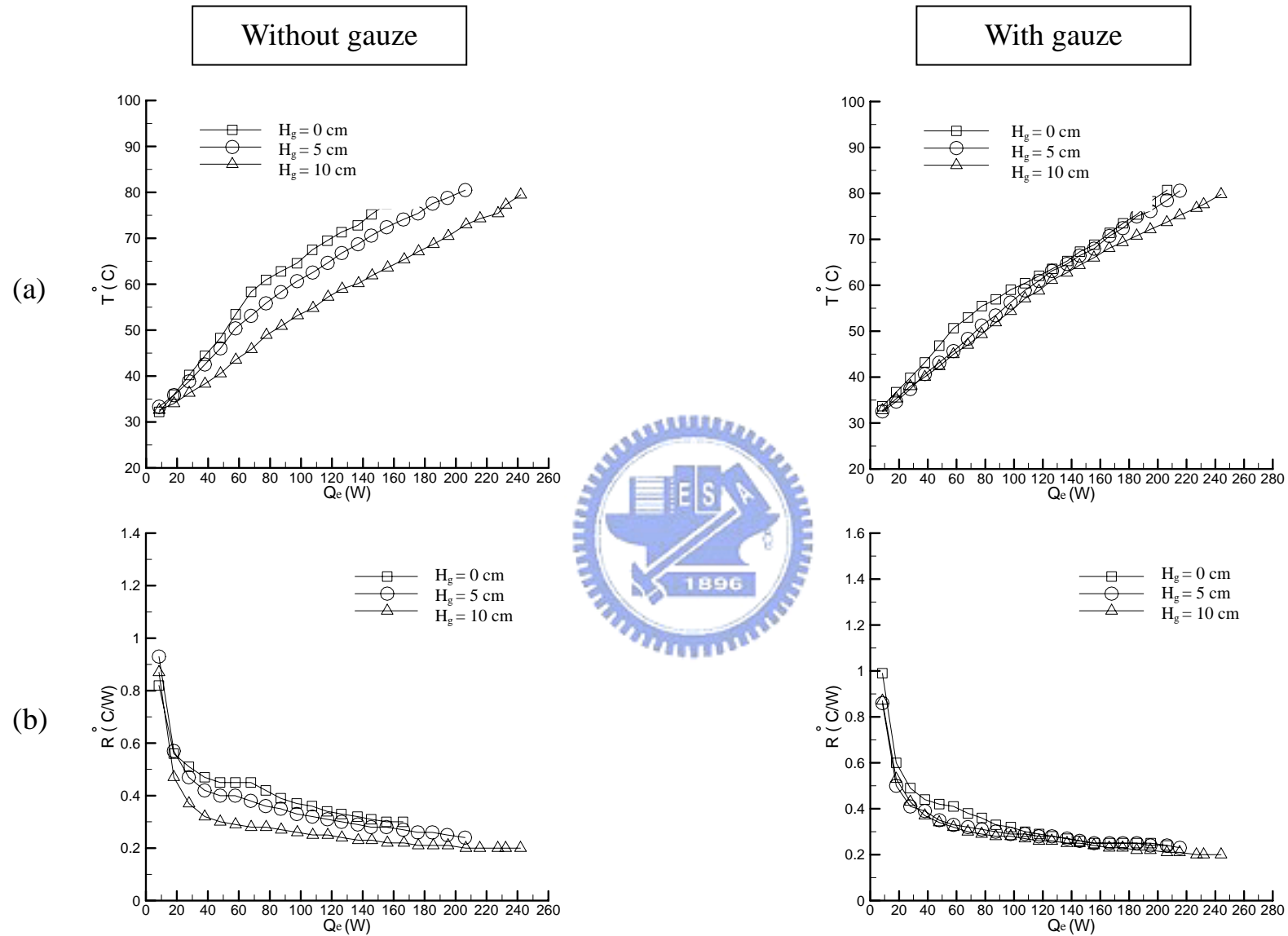


Fig. 4.34 Variations of the mean evaporator temperature (a) and thermal resistance of the CPL (b) with the input power to the evaporator for the CPL with and without cotton gauze covering for various relative condenser-evaporator heights for cooling water temperature in the condenser  $T_{\text{cold}} = 25$  and liquid inventory of 62%.

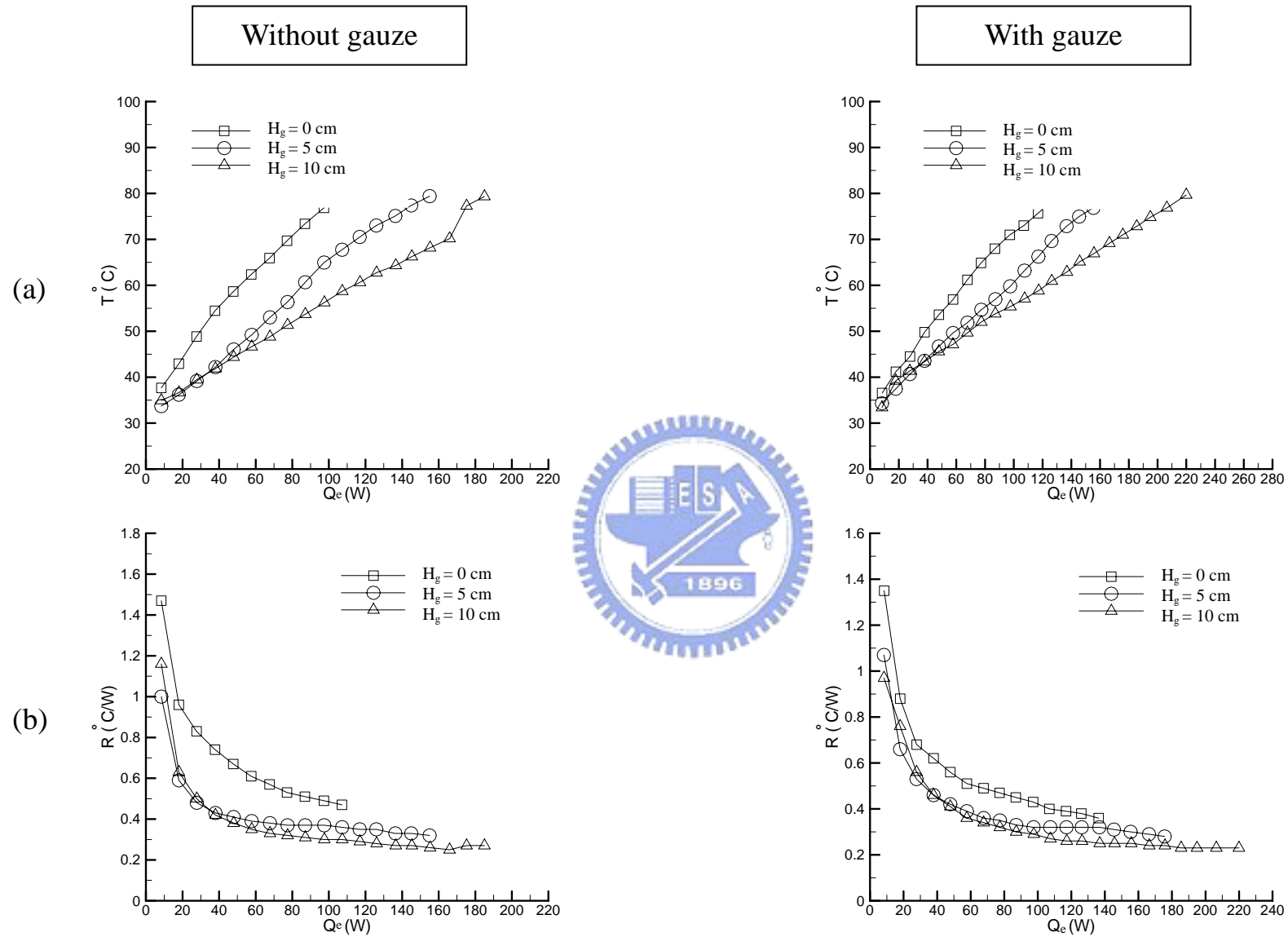


Fig. 4.35 Variations of the mean evaporator temperature (a) and thermal resistance of the CPL (b) with the input power to the evaporator for the CPL with and without cotton gauze covering for various relative condenser-evaporator heights for cooling water temperature in the condenser  $T_{\text{cold}} = 25$  and liquid inventory of 70%.

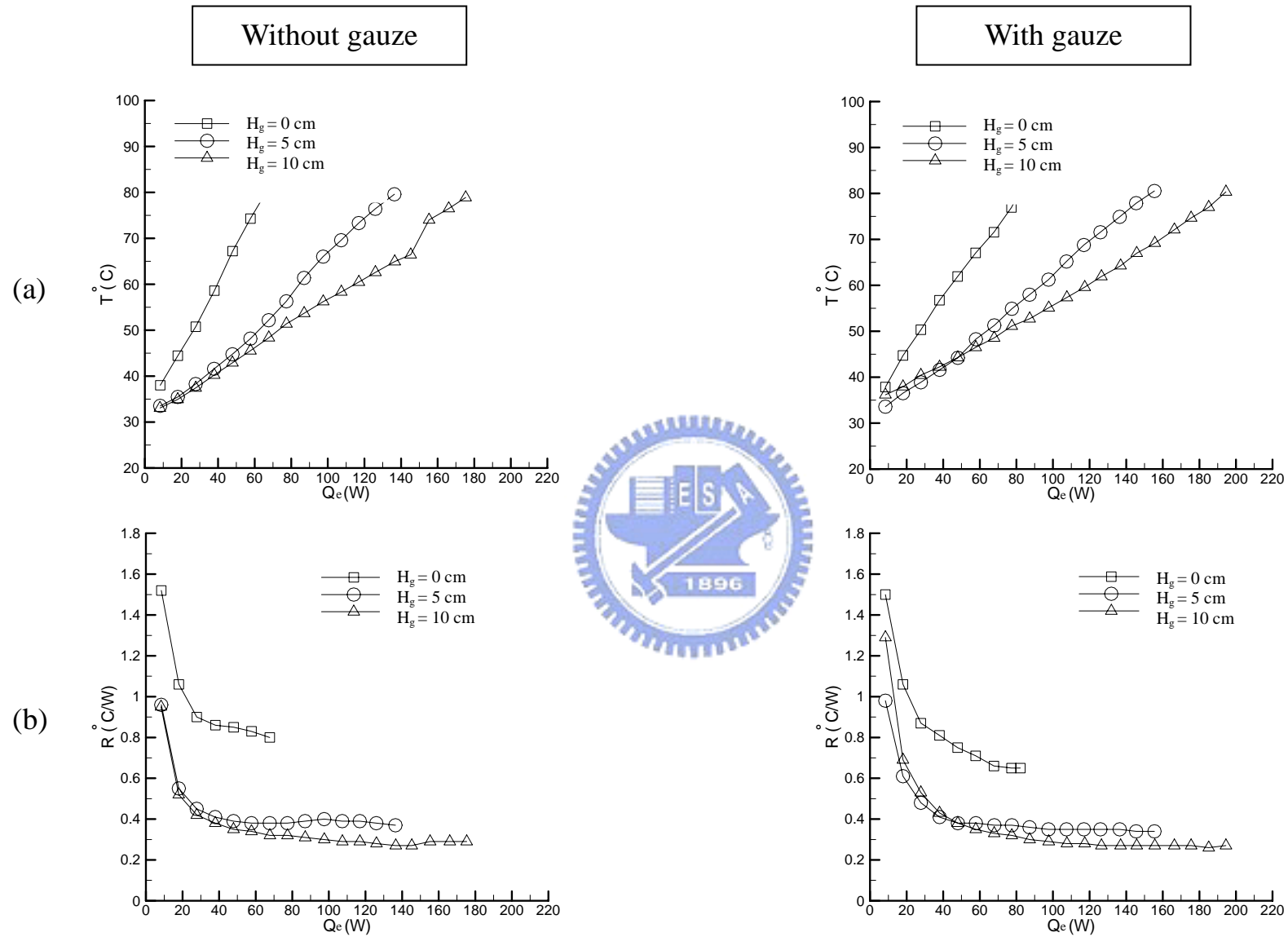


Fig. 4.36 Variations of the mean evaporator temperature (a) and thermal resistance of the CPL (b) with the input power to the evaporator for the CPL with and without cotton gauze covering for various relative condenser-evaporator heights for cooling water temperature in the condenser  $T_{\text{cold}} = 25$  and liquid inventory of 75%.

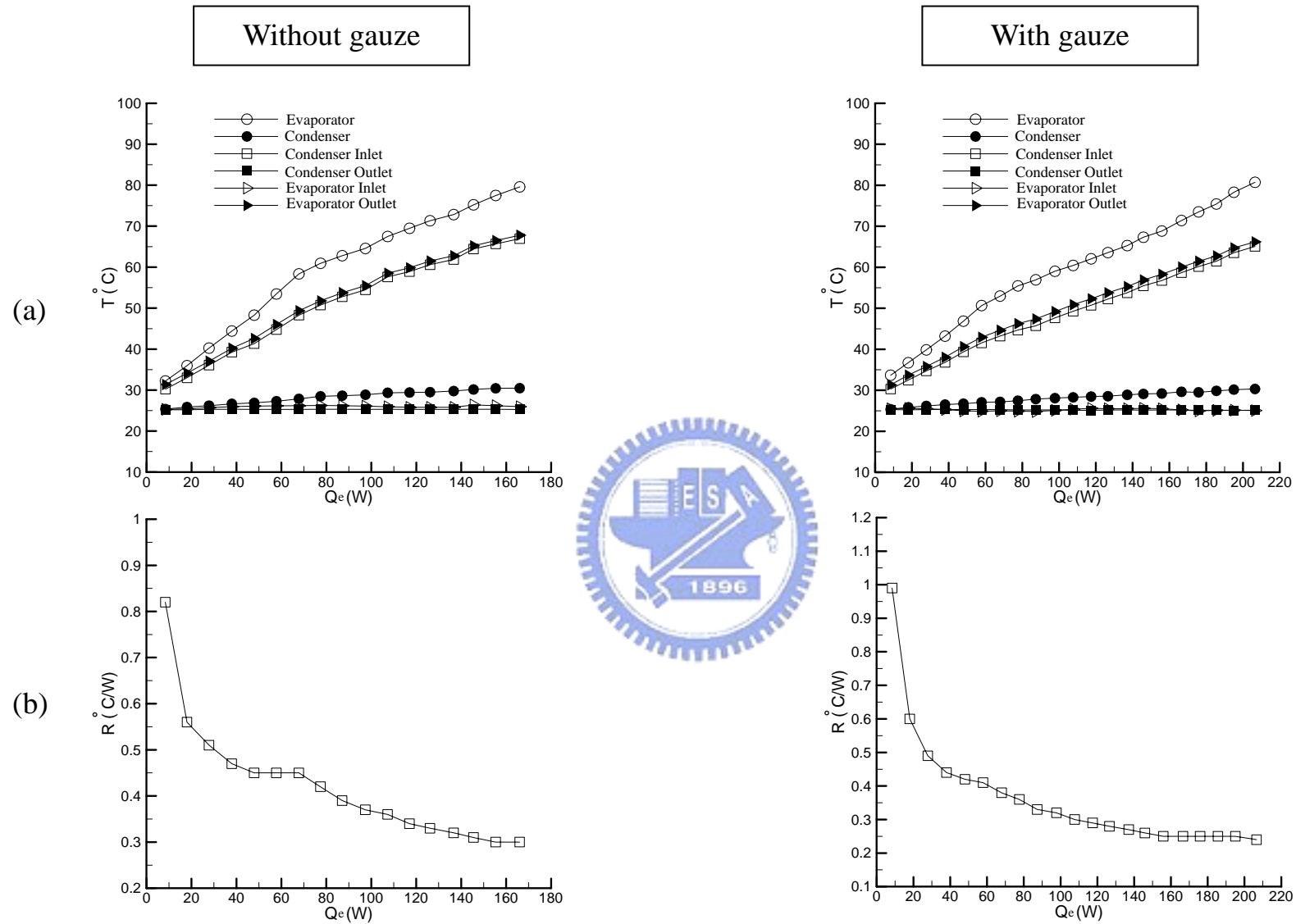


Fig. 4.37 Variations of the temperature at various locations in the CPL (a) and thermal resistance of the CPL (b) with the input power to the evaporator for the CPL with and without cotton gauze covering for cooling water temperature in the condenser  $T_{\text{cold}} = 25$  , liquid inventory of 62% and relative condenser-evaporator height of 0 cm.

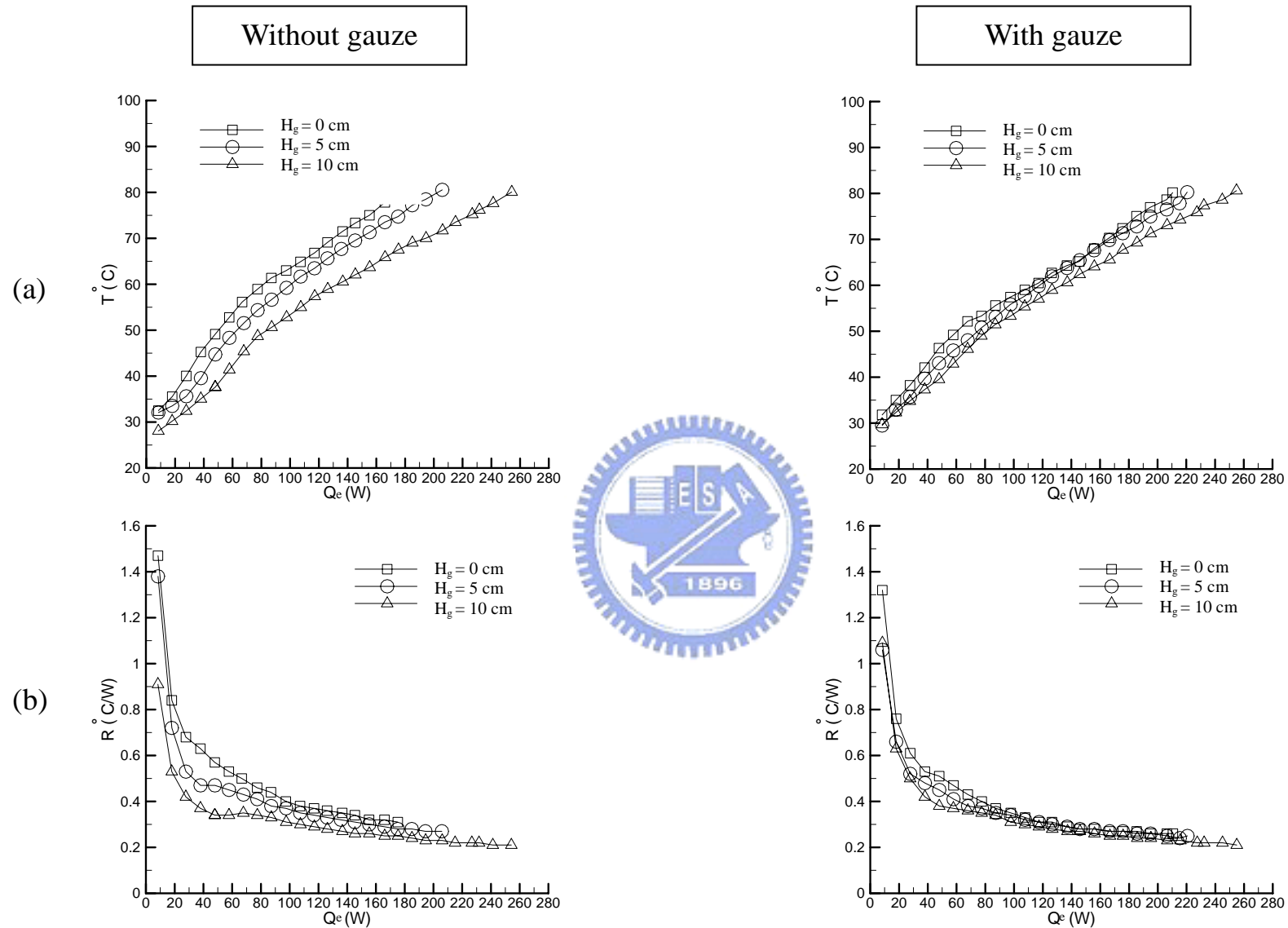


Fig. 4.38 Variations of the mean evaporator temperature (a) and thermal resistance of the CPL (b) with the input power to the evaporator for the CPL with and without cotton gauze covering for various relative condenser-evaporator heights for cooling water temperature in the condenser  $T_{\text{cold}} = 20$  and liquid inventory of 62%.

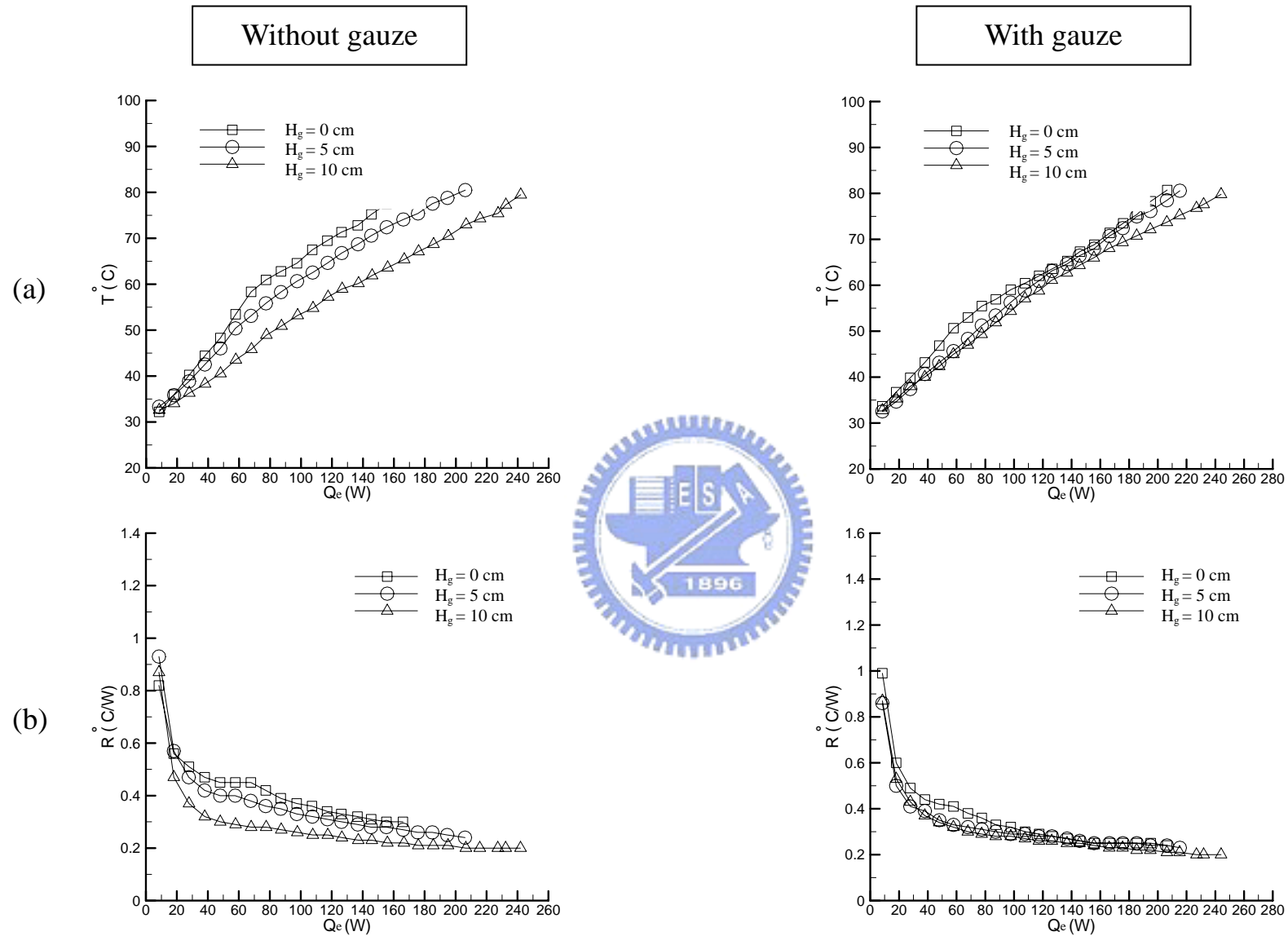


Fig. 4.39 Variations of the mean evaporator temperature (a) and thermal resistance of the CPL (b) with the input power to the evaporator for the CPL with and without cotton gauze covering for various relative condenser-evaporator heights for cooling water temperature in the condenser  $T_{\text{cold}} = 25$  and liquid inventory of 62%.

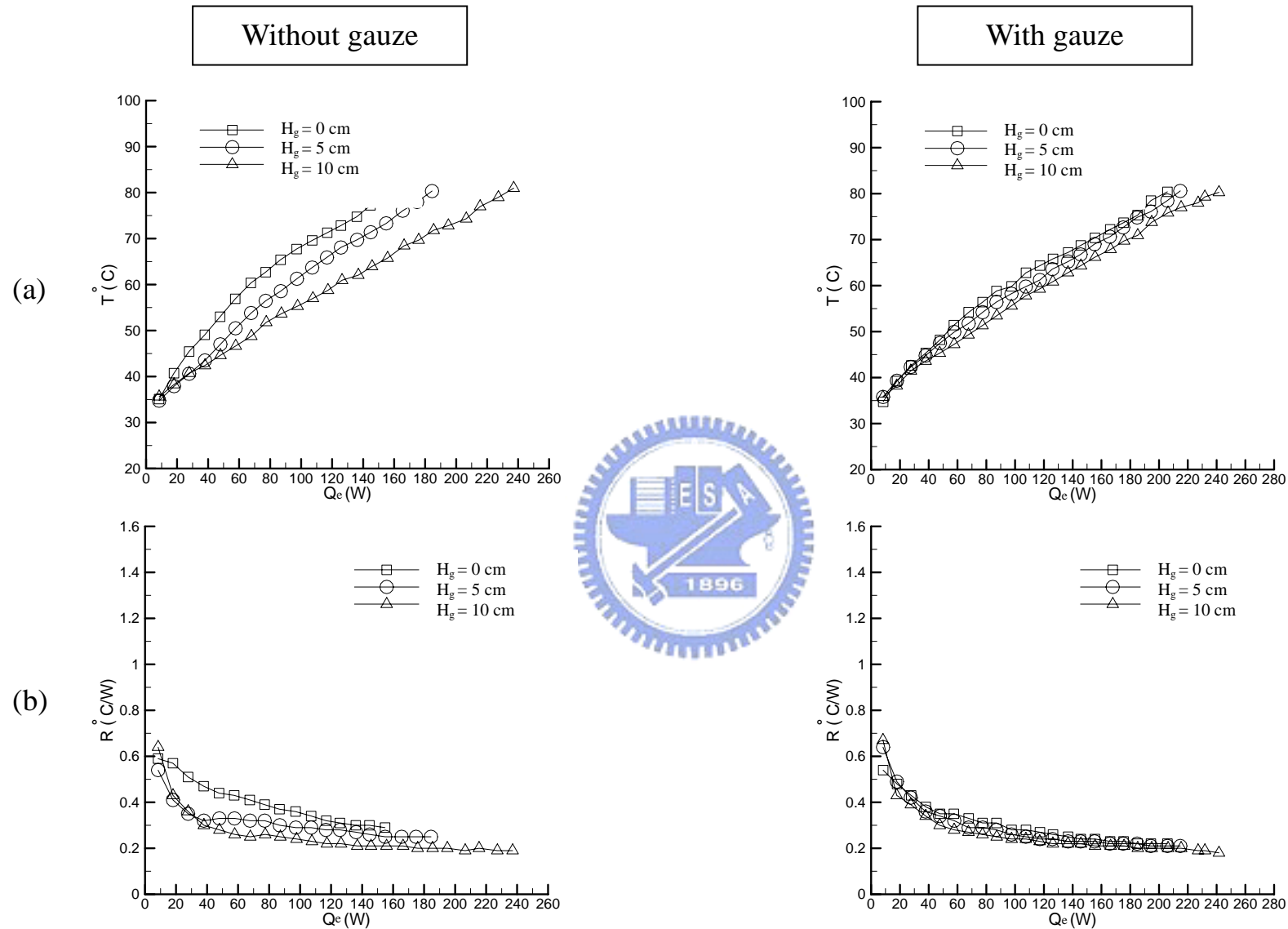


Fig. 4.40 Variations of the mean evaporator temperature (a) and thermal resistance of the CPL (b) with the input power to the evaporator for the CPL with and without cotton gauze covering for various relative condenser-evaporator heights for cooling water temperature in the condenser  $T_{\text{cold}} = 30$  and liquid inventory of 62%.

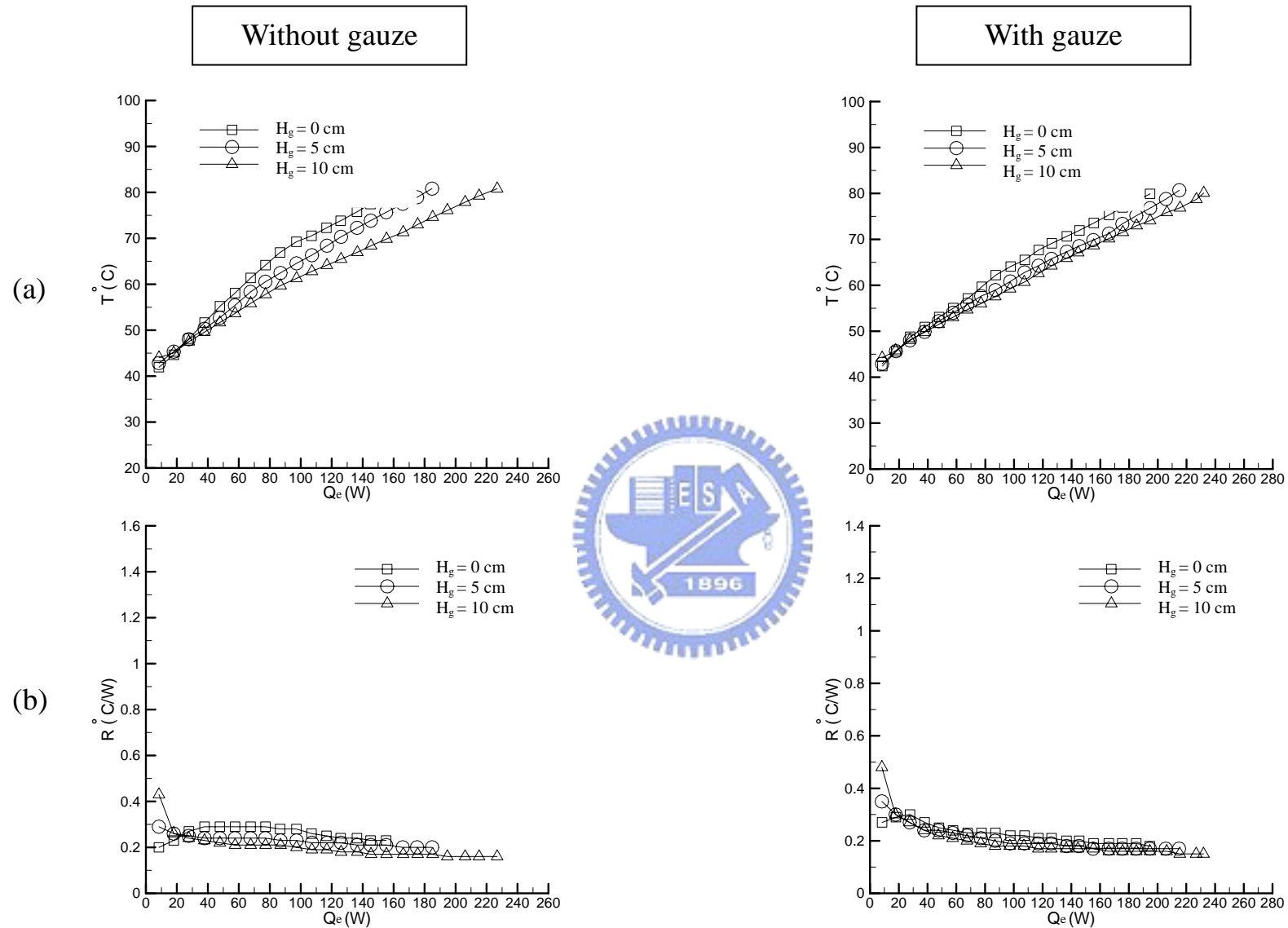


Fig. 4.41 Variations of the mean evaporator temperature (a) and thermal resistance of the CPL (b) with the input power to the evaporator for the CPL with and without cotton gauze covering for various relative condenser-evaporator heights for cooling water temperature in the condenser  $T_{\text{cold}} = 40$  and liquid inventory of 62%.



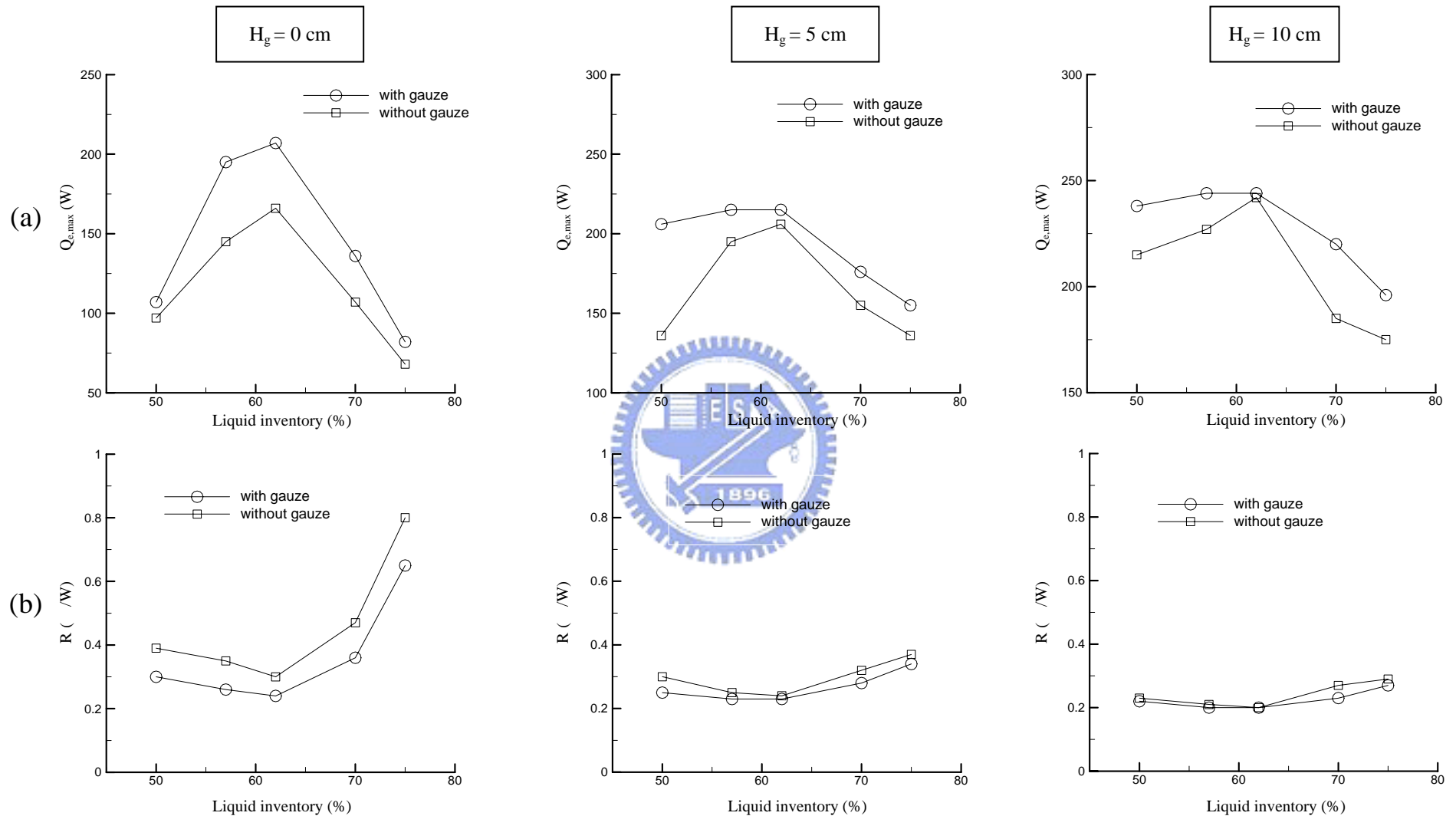


Fig. 4.42 Variations of the maximum obtainable power input to the evaporator (a) and thermal resistance of the CPL (b) with the liquid inventory for the CPL with and without cotton gauze covering for various relative condenser-evaporator heights for cooling water temperature in the condenser  $T_{\text{cold}} = 25$  .

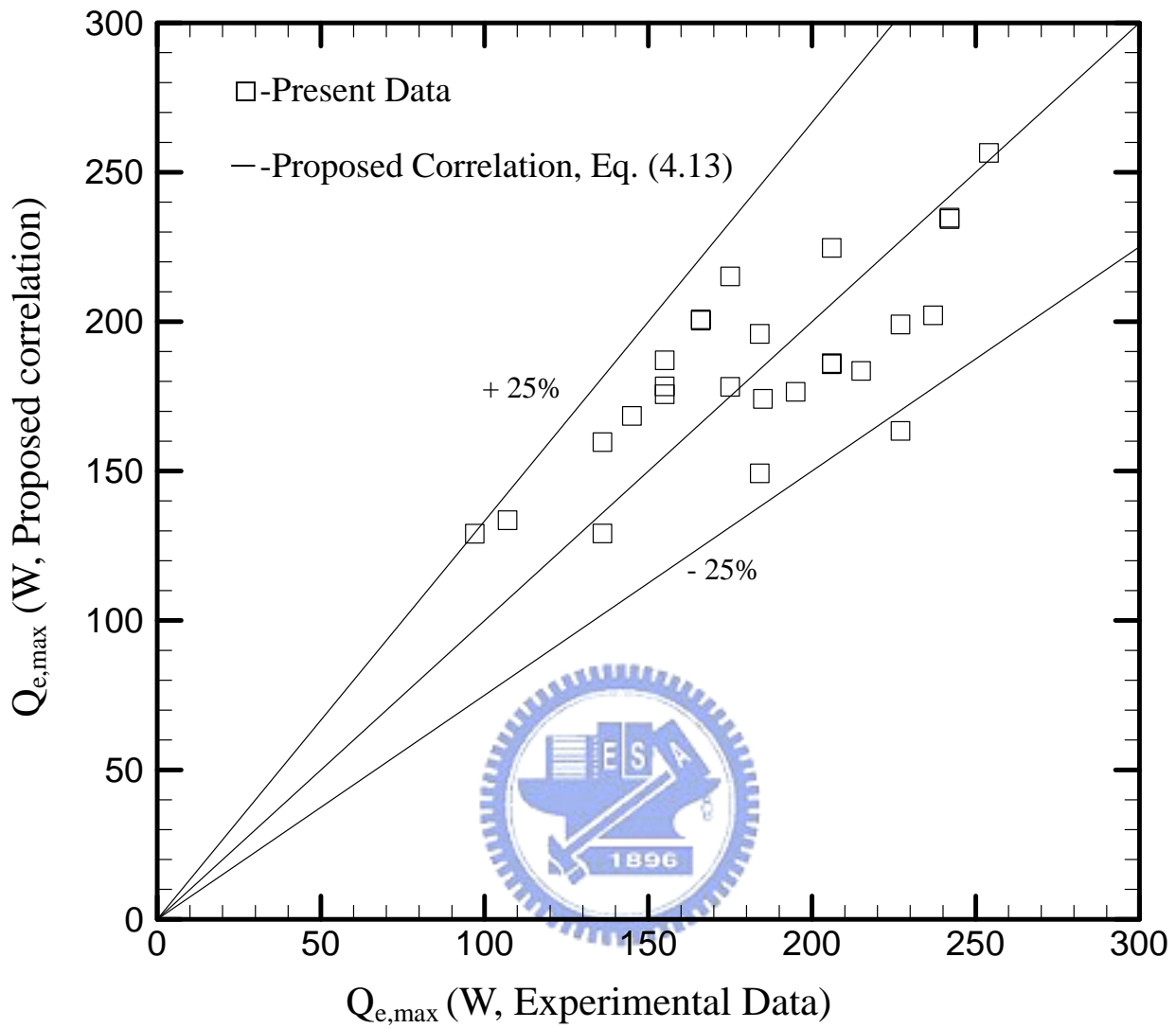


Fig. 4.43 Comparison of the measured data for maximum power input to the evaporator without the cotton gauze layer covering with the proposed correlation.

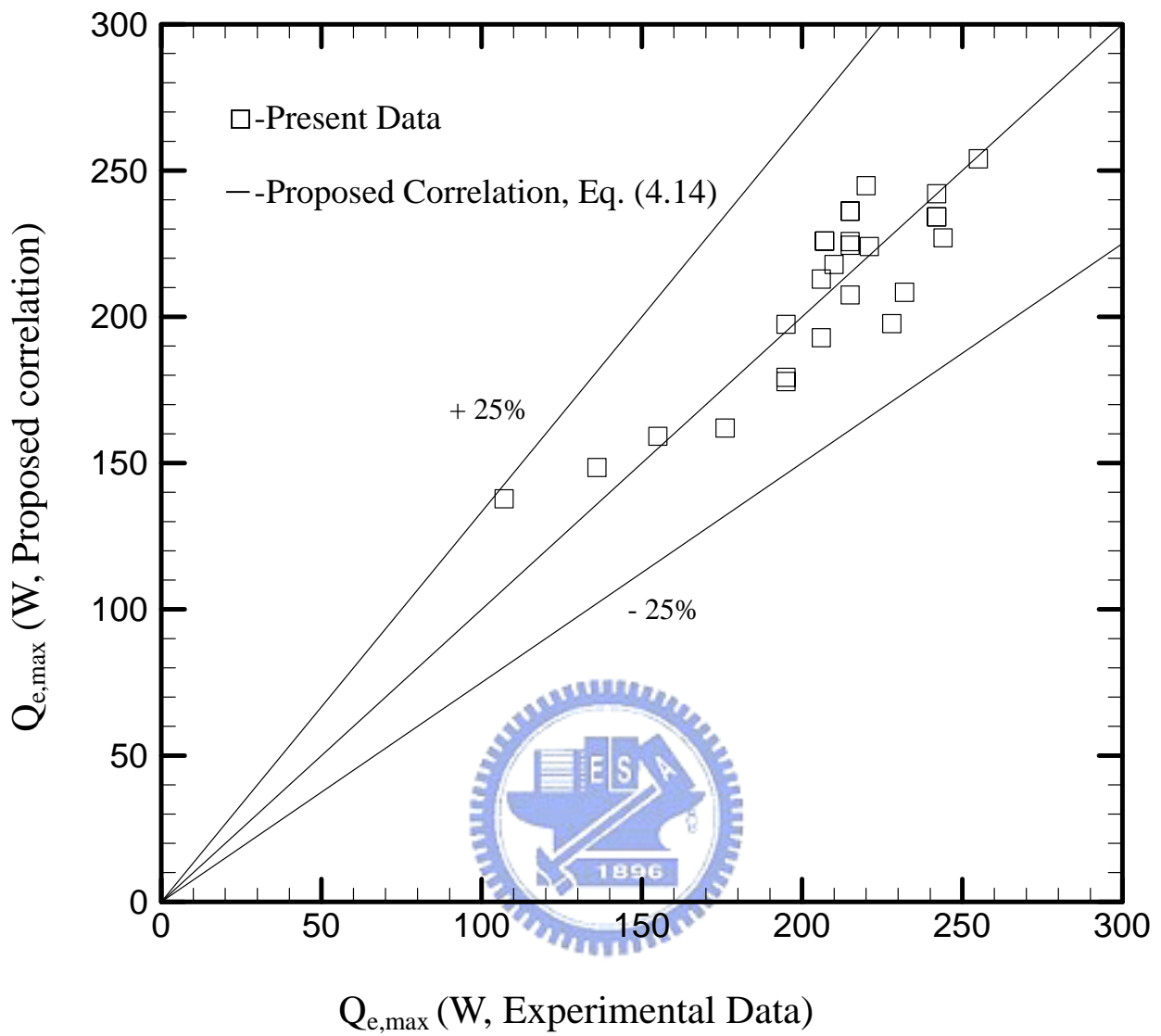


Fig. 4.44 Comparison of the measured data for maximum power input to the evaporator with the cotton gauze layer covering with the proposed correlation.

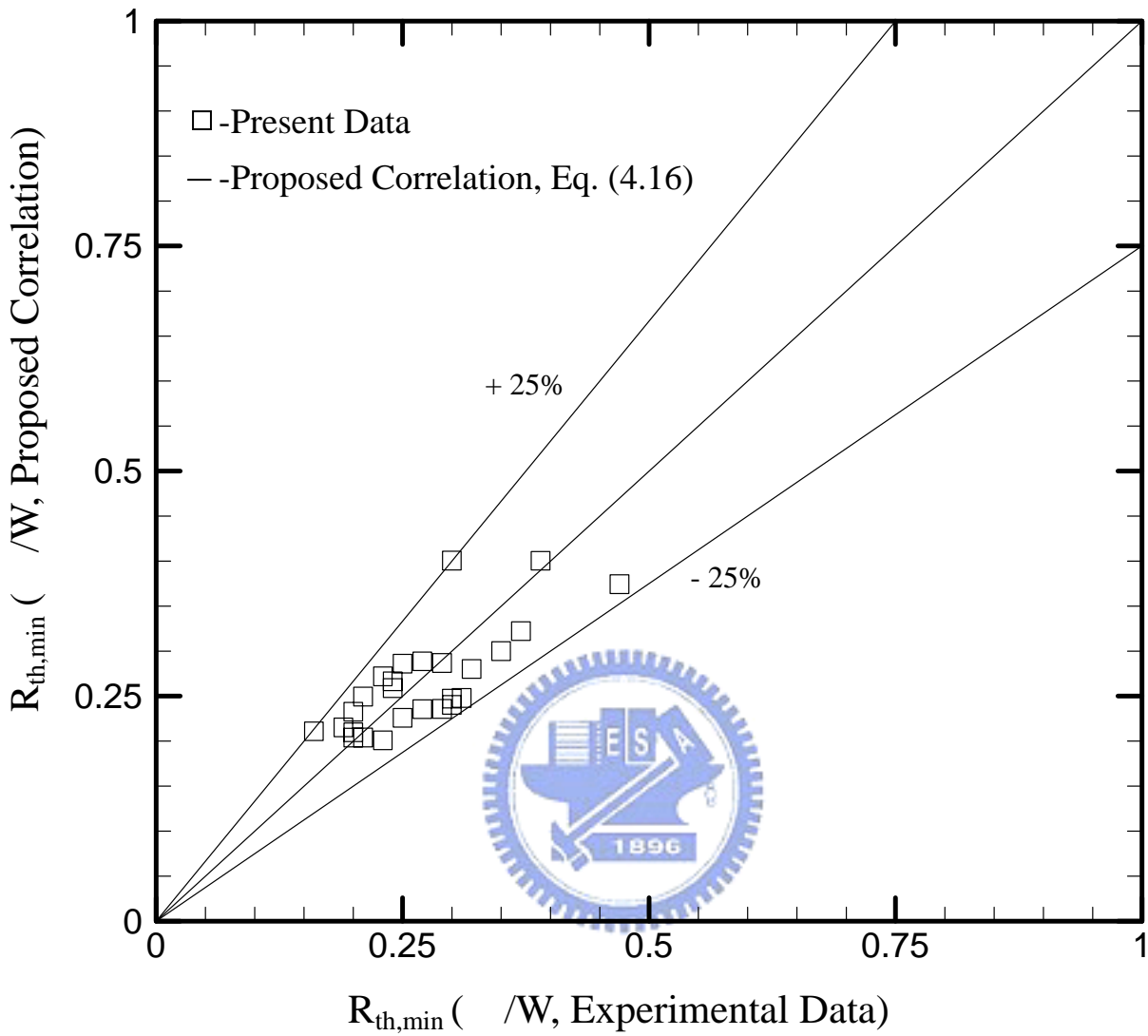


Fig. 4.45 Comparison of the measured data for minimum thermal resistance to the CPL without the cotton gauze layer covering with the proposed correlation.

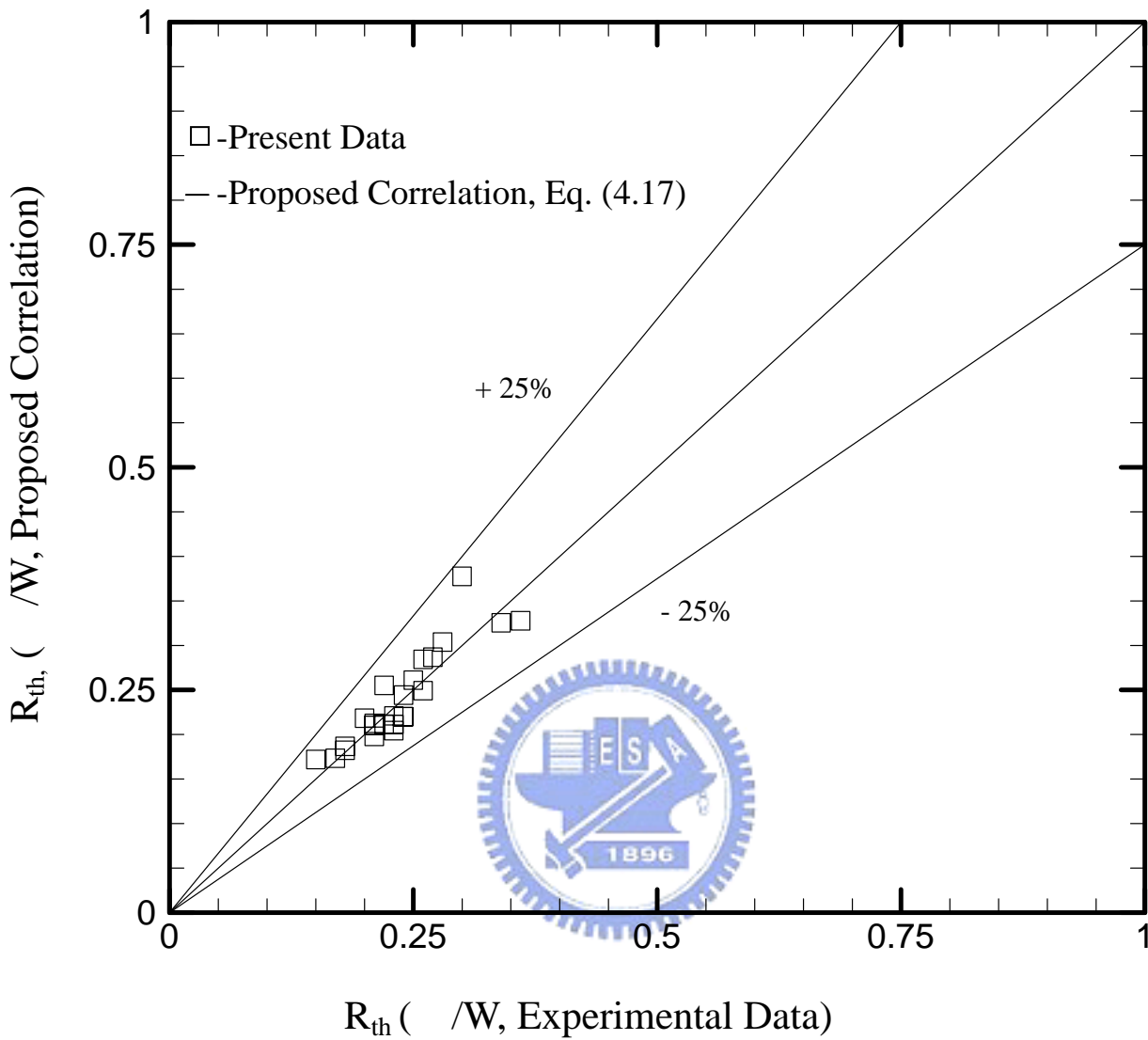


Fig. 4.46 Comparison of the measured data for minimum thermal resistance to the CPL with the cotton gauze layer covering with the proposed correlation.

## CHAPTER 5

### CONCLUDING REMARKS

In this study experimental tests are conducted to investigate an improved CPL design for high power density CPU cooling through covering a thin cotton gauze layer on the vertical and bottom walls of the grooved channels for vapor flow to provide more surface area for liquid vaporization. The effects of the liquid inventory, cooling water temperature in the condenser, and relative height between the condenser and evaporator, and cotton gauze layer covering on the heat transfer performance of the CPL have been examined in detail. The major results obtained here can be briefly summarized as follows:

- (1) An optimal liquid inventory exists at which  $Q_{e,max}$  is the highest and  $R_{th}$  is the lowest for given  $T_{cold}$  and relative condenser-evaporator height for the CPL with and without cotton gauze layer covering on the side and bottom walls of the grooved channel. Moreover, increasing or decreasing the liquid inventory from this optimal value causes a reduction in  $Q_{e,max}$  and a raise in  $R_{th}$ .
- (2) The CPL heat transfer capability is only slightly affected by the cooling water temperature in the condenser. But the evaporator temperature is noticeably higher for a higher  $T_{cold}$ .
- (3) An increase in the relative height between the condenser and evaporator results in a significant improvement in the CPL performance with a much higher  $Q_{e,max}$  and a much lower  $R_{th}$ . Besides, for a larger relative condenser-evaporator height the influences of the liquid inventory on the performance of the CPL are milder.
- (4) Covering a thin cotton gauze layer on the vertical and bottom walls of the grooved channels can substantially improve the heat transfer performance of the CPL

system under certain conditions. For other conditions the improvement is comparatively smaller.

- (5) Empirical correlations for  $Q_{e,max}$  and  $R_{th,min}$  are proposed for the present CPL system to facilitate thermal design of CPU cooling units.



## REFERENCES

1. F. J. Stenger, "Experimental feasibility study of water-filled capillary-pumped heat-transfer loops," NASA TM-X-1310, NASA Lewis Research Center, Cleveland, Ohio, (1966).
2. J. T. Ku, "Overview of Capillary Pumped Loop Technology," HTD-Vol. 236, Heat Pipes and Capillary Pumped Loops ASME (1993).
3. Y. Maldanik, Y. Fershtater, V. G. Pastukhov, and M. Chernysheva, "Experimental and theoretical investigation of startup regimes of two-phase capillary pumped loops," Society of Automotive Engineers, Paper 932305, (1993).
4. R. Meyer, R. Muller, K. Beckmann, "Investigation of the Heat Transfer Performance of a Capillary Pumped Ammonia Loop Under Gravity," Society of Automotive Engineers, Paper 932304, (1993).
5. B. Mo, M.M. Ohadi, and S. V. Dessiatoun, "Startup time reduction in an electrohydrodynamically enhanced capillary pumped loop," Journal of Thermosphysics and Heat Transfer, Vol. 13, (1999), 134-139.
6. B. Mo, M.M. Ohadi, and S. V. Dessiatoun, "Capillary pumped-loop thermal performance improvement with electrohydrodynamic technique," Journal of Thermosphysics and Heat Transfer, Vol. 14, (2000), 103-108.
7. K. R. Kolos and K. E. Herold, "Low frequency temperature and fluid oscillations in capillary pumped loops," AIAA Paper No. 97-3872, (1997).
8. T. O'Connell and J. T. Ku, "Effects of transport line diameters on pressure oscillations in capillary pumped loop," AIAA Paper No.96-1833, (1996).
9. T. O'Connell and T. Hoang, "Effects of wick properties on pressure oscillations in a capillary pumped loop," Society of Automotive Engineers, Paper 961434, (1996).
10. E. Pouzet, J.-L. Joly, V. Platel, J.-Y. Grandpeix, and C. Butto, "Dynamic response



- of a capillary pumped loop subjected to various heat load transients,”  
International Journal of Heat and Mass Transfer, Vol. 47, (2004), 2293-2316.
11. E. Bazzo and R.R. Riehl, “Operation characteristics of a small-scale capillary pumped loop,” Applied Thermal Engineering, Vol. 23, (2003), 687-705.
  12. J. T. Ku, “Thermodynamic aspects of capillary pumped loop operation,” AIAA Paper No.94-2059, (1994).
  13. J. T. Dickey and G. P. Peterson, “Experimental and analytical investigation of a capillary pumped loop,” Journal of Thermophysics and Heat Transfer, Vol. 8, (1994), 602-607.
  14. Q. Liao and T. S. Zhao, “Evaporative heat transfer in a capillary structure heated by a grooved block,” Journal of Thermophysics and Heat Transfer, Vol. 13, (1999), 126-133.
  15. Q. Liao and T. S. Zhao, “A visual study of phase-change heat transfer in a two dimensional porous structure with a partial heating boundary,” Journal of Heat and Mass Transfer, Vol. 43, (2000), 1089-1102.
  16. T. S. Zhao and Q. Liao, “On capillary-driven flow and phase-change heat transfer in a porous structure heated by a finned surface: measurements and modeling,” Journal of Heat and Mass Transfer, Vol. 43, (2000), 1141-1155.
  17. P. C. Chen and W. K. Lin, “The application of capillary pumped loop for cooling of electronic components,” Applied Thermal Engineering, Vol. 21, (2001), 1739-1754.
  18. A. Miyasaka, K. Nakajima, and H. Tsunoda, “Experimental results for capillary looped pipe applied to direct cooling method,” Journal of Thermophysics and Heat Transfer, Vol. 9, (1995), 96-100.
  19. J. Pohner and D. Antoniuk, “Recent enhancements to capillary pumped loop systems,” AIAA Paper No.91-1375, (1991).

20. I. Muraoka, F. M. Ramos, and V. V. Vlassov, "Experimental and theoretical investigation of a capillary pumped loop with a porous element in the condenser," *Int. Comm. Heat Mass Transfer*, Vol. 25, (1998), 1085-1094.
21. R. Schweickart, L. Ottenstein, B. Cullimore, C. Egan, and D. Wolf, "Testing of a controller for a hybrid capillary pumped loop thermal control system," *AIAA Paper No.89-9476*, (1989).
22. J. Kirshberg and K. Yerkes, "Cooling effect of a MEMS based micro capillary pumped loop for chip-level temperature control," *International Mechanical Engineering Congress & Exposition*, Orlando, Florida. Recipient of the Agilent Technologies Best Student Paper Award of the MEMS Symposium, (2000).
23. K. Pettigrew and J. Kirshberg, "Performance of a MEMS based micro capillary pumped loop for chip-level temperature control," *Proceedings of the 14th IEEE International Conference on Micro Electro Mechanical Systems*, Interlaken, Switzerland, (2001), 427-430.
24. L. Meyer, S. Dasgupta, D. Shaddock, J. Tucker, and R. Fillion, "A silicon-carbide micro-capillary pumped loop for cooling high power devices," *Semiconductor Thermal Measurement and Management Symposium*, Ninteenth Annual IEEE11-13 March (2003), 364 - 368.
25. F. W. Holm and S. P. Goplen, "Heat transfer in the meniscus thin-film region," *ASME J. Heat transfer* Vol. 101, (1979), 543-547.
26. K. Park, K. J. Noh, and K. S. Lee, "Transport phenomena in the thin-film region of a micro-channel, " *International Journal of Heat and Mass Transfer*, Vol. 46, (2003), 2381-2388.
27. K. Park, K. J. Noh, and K. S. Lee, "Evaporative modeling in a thin-film region of micro-channel," *Ninth International Refrigeration and Air Conditioning Conference at Purdue*, (2002), 16-19,

28. Y. Cao and A. Faghri, "Analytical solutions of flow and heat transfer in a porous structure with partial heating and evaporation on the upper surface," *International Journal of Heat and Mass Transfer*, Vol. 37, (1994), 1525-1533.
29. Y. Cao and A. Faghri, "Conjugate analysis of a flat-plate type evaporator for capillary pumped loops with three-dimensional vapor flow in the groove," *International Journal of Heat and Mass Transfer*, Vol. 37, (1994), 401-409.
30. T. S. Zhao and Q. Liao, "Rapid vaporization of subcooled liquid in a capillary structure," *International Journal of Heat and Mass Transfer*, Vol. 45, (2002), 165-172.
31. T. S. Zhao, P. Cheng, and C. Y. Wang, "Buoyancy-induced flow and phase-change heat transfer in a vertical capillary structure with symmetric heating," *Chemical Engineering Science*, Vol. 55, (2000), 2653-2661.
32. M. A. Hanlon and H. B. Ma, "Evaporation heat transfer in sintered porous media," *ASME J. Heat transfer* Vol. 125, (2003), 644-652.
33. C. Figus, L. Ounougha, P. Bonzom, W. Supper, and C. Puillet, "Capillary fluid loop developments in Astrium," *Applied Thermal Engineering*, Vol. 23, (2003), 1085-1098.
34. J. P. Holman, "Heat Transfer," 7d ed., McGraw-Hill Book Company, New York, c1990, 355-357.
35. V. Gnielinski, New equations for heat and mass transfer in turbulent pipe and channel flow, *International Chemical Engineering* 16 (2) (1976) 359-368
36. R. W. Fox and A. T. McDonald, "Introduction to Fluid Mechanics," New York, Wiley, c1978, 357-361.
37. S. J. Kline and F. A. McClintock, "Describing Uncertainties in Single-sample Experiments," *Mech. Engng*, Vol. 75, (1953), 3-8
38. NASA Jet propulsion Laboratory, [www.jpl.nasa.gov](http://www.jpl.nasa.gov)

39. M. C. Tsai, C. S. Yu, and S. W. Kang, "Flat plate loop heat pipe with a novel evaporator structure," Semiconductor Thermal Measurement and Management Symposium, IEEE Twenty First Annual, (2005), 187-191.
40. Y. F. Maydanik, S. V. Vershinin, M. A. Korukov, and J. M. Ochterbeck, "Miniature loop heat pipes-a promising means for cooling electronics," IEEE Transactions on Components and Packaging Technologies, Vol. 28, (2005), 290-296.

